nagra.

Arbeitsbericht NAB 16-54

Corrosion Study of FEBEX-DP Components

September 2016

Virginia Madina

TECNALIA

National Cooperative
for the Disposal of
Radioactive Waste

Hardstrasse 73
P.O. Box 280
5430 Wettingen
Switzerland
Tel. +41 56 437 11 11

www.nagra.ch

nagra.

Arbeitsbericht NAB 16-54

Corrosion Study of FEBEX-DP Components

September 2016

Virginia Madina

TECNALIA

KEYWORDS

FEBEX/FEBEX-DP, corrosion, carbon steel, titanium, copper, microbiology, bentonite

National Cooperative
for the Disposal of
Radioactive Waste

Hardstrasse 73
P.O. Box 280
5430 Wettingen
Switzerland
Tel. +41 56 437 11 11

www.nagra.ch

Nagra Arbeitsberichte ("Working Reports") present the results of work in progress that have not necessarily been subject to a comprehensive review. They are intended to provide rapid dissemination of current information.
This report was prepared on behalf of Nagra. The viewpoints presented and conclusions reached are those of the author(s) and do not necessarily represent those of Nagra.

tecnalia Inspiring Business

www.tecnalia.com

PROJECT Nº: 043170

CLIENT: National Cooperative for the Disposal of radioactive Waste (NAGRA)

CONTACT PERSON: Dr. Florian Kober

AUTHOR: Virginia Madina

TITLE: CORROSION STUDY OF FEBEX –DP COMPONENTS

DATA: 05/05/2016

Signed:

Dr. Virginia Madina, Ph. D

Responsible for the work in Tecnalia

TECNALIA
Materials for Energy and Environment
Parque Tecnológico de San Sebastián
Mikeletegi Pasealekua, 2
E-20009 Donostia-San Sebastián (Spain)
T +34 667115986
T +34 946 430 850
virginia.madina@tecnalia.com
www.tecnalia.com

INDEX

1. INTRODUCTION

NAGRA requested TECNALIA to carry out the tasks laid down in Tecnalia´s quotation nº 043170: *Corrosion study of FEBEX-DP components,* dated on 08/05/2014, consisting of a study of the corrosion suffered by different components of the FEBEX experiment carried out at the Grimsel Test Site. Heating started in 1997, and since then, a constant temperature of 100°C has been maintained, while the bentonite buffer has been hydrating in a natural way for 18 years, under partly aerobic conditions. A partial dismantling and sampling of the EBS was carried out during 2002.

The list of samples under study in Tecnalia is summarized in Table 1.1. Photographs of the samples upon reception at TECNALIA are contained in Annex I.

Table 1.1 gives a relation and brief description of the elements studied by Tecnalia.

SAMPLE TYPE	SAMPLE CODE	SAMPLING SECTION	DESCRIPTION
SENSORS	SHSD2-01 (S-S-54-14A)	54	Extensometer type sensors used to measure the displacement of the heaters (Key SH). The active element is protected by an austenite alloy tube (sheath).
	SHSD2-02 (S-S-54-15A)	54	
	SHSD2-03 (S-S-54-15)	54	
BENTONITE	BM-S-54-2	54	Bentonite in contact with sensor SHSD2-01
	BM-S-54-3	54	Bentonite in contact with sensor SHSD2-02
COUPONS	2A (316L) M-S-48-2	48	Coupons of different candidate metals placed in the bentonite barrier. Coupons are made of the following alloys: TStE355 carbon steel, AISI 316L austenitic stainless steel, titanium alloys grade 2, 7 and 12, Cu-ETP copper and the 70/30 and 90/10 cupro-nickel alloys.
	3A (Titanium) M-S-48-3	48	
	4A (Copper) M-S-48-4	48	
LINER	ML-45-1 ML-45-2 ML-45-3 ML-45-4	45	Perforated steel tube 970 mm in diameter and 15 mm thick, used to facilitate the insertion of the container in its storage position
	ML-52-1 ML-52-2 ML-52-3 ML-52-4	52	
HEATER	MH		Carbon steel cylinder with welded lids, approximately 4,54 m long, 0,9 m in diameter and a wall thickness of 100 mm

Table 1.1: List of components under study by Tecnalia

The activities relates to TECNALIA comprise of the following:

- Examination of components on receipt. Cutting of test pieces
- Optical and scanning electron microscope study. Metallographic study
- Chemical characterization of the corrosion products and deposits
- Chemical and microbiological analysis of the bentonite
- Reporting

REFERENCE DOCUMENTS

1) Bárcena, I., García-Siñeriz, J.-L..(2015): FEBEX-DP (GTS) Full Dismantling Test Plan R7. Nagra Arbeitsbericht NAB 15-014.

2) Kober, F.(2015): FEBEX-DP Sample Log Book. Nagra Aktennotiz. AN 15-578.

3) Kober, F.(2015): FEBEX-DP Summary of Extra Reports (1-13). Nagra Aktennotiz. AN 15-619.

2. STUDIES CARRIED OUT

The study carried out by TECNALIA covers the following:

SAMPLE TYPE	SAMPLE CODE	STUDIES CARRIED OUT
SENSORS	SHSD2-01 (S-S-54-14A) SHSD2-02 (S-S-54-15A) SHSD2-03 (S-S-54-15)	1. Visual examination of the sensors on receipt. Identification of the sections to be studied. Dry cut is used in this first stage. 2. These sections are studied in two ways: - SEM/EDS analysis on dry cut, non-embedded sections. The surface of the sections is examined in detail by scanning electron microscopy (SEM). Corrosion products and/or deposits on the samples are chemically analysed by Energy Dispersive X-ray Spectroscopy (EDX), using a microanalyser coupled to the SEM microscope. - The molecular formula of said products is determined by means of X-ray diffraction spectroscopy (XRD). 3. Metallographic study: Metallographic probes are studied by optical and SEM microscopy in order to analyse the microstructure, morphology and extent of the corrosion-derived damage. 3-5 metallographic probes have been prepared for each sensor/extensometer.
COUPONS	2A M-S-48-2 3A M-S-48-3 4A M-S-48-4	1. Visual examination of the coupons on receipt. 2. The analyses proceed in the same way as for the sensors.
BENTONITE	BM-S-54-2 BM-S-54-3	1. Chemical analysis of the leachate obtained. 2. Microbiological characterization of the bentonite samples.
LINER	ML-45-1 ML-45-2 ML-45-3 ML-45-4 ML-52-1 ML-52-2 ML-52-3 ML-52-4	Visual examination of the 2 sections of the liner on receipt. Identification of the sections to be studied (dry cut). The analyses proceed in the same way as for the sensors. 1-3 metallographic probes have been prepared from each quarter of the liner.
HEATER	MH-02-F9C MH-01-F3C MH-03-ET	Visual examination of the heater in AITEMIN premises. 3 sections were taken by dry cut (radial), two of them from the Front (F): references MH-01-F3C and MH-02-F9C, and the third one from the End (E): (reference MH-03-ET. Where 3C means 3 o´clock position, 9C: 9 o´clock and T = Top. The analyses proceed in the same way as for the sensors. 2-3 metallographic probes have been prepared from each of the three sections

Table 2.1: Studies carried out on the different components

3. SENSORS

The sensors studied are three extensometer type sensors identified as SHSD2-01 (S-S-54-14A), SHSD2-02 (S-S-54-15A) and SHSD2-03 (S-S-54-15).

The picture in Figure 3.1 shows the initial location of the 3 extensometers in sampling section 54.

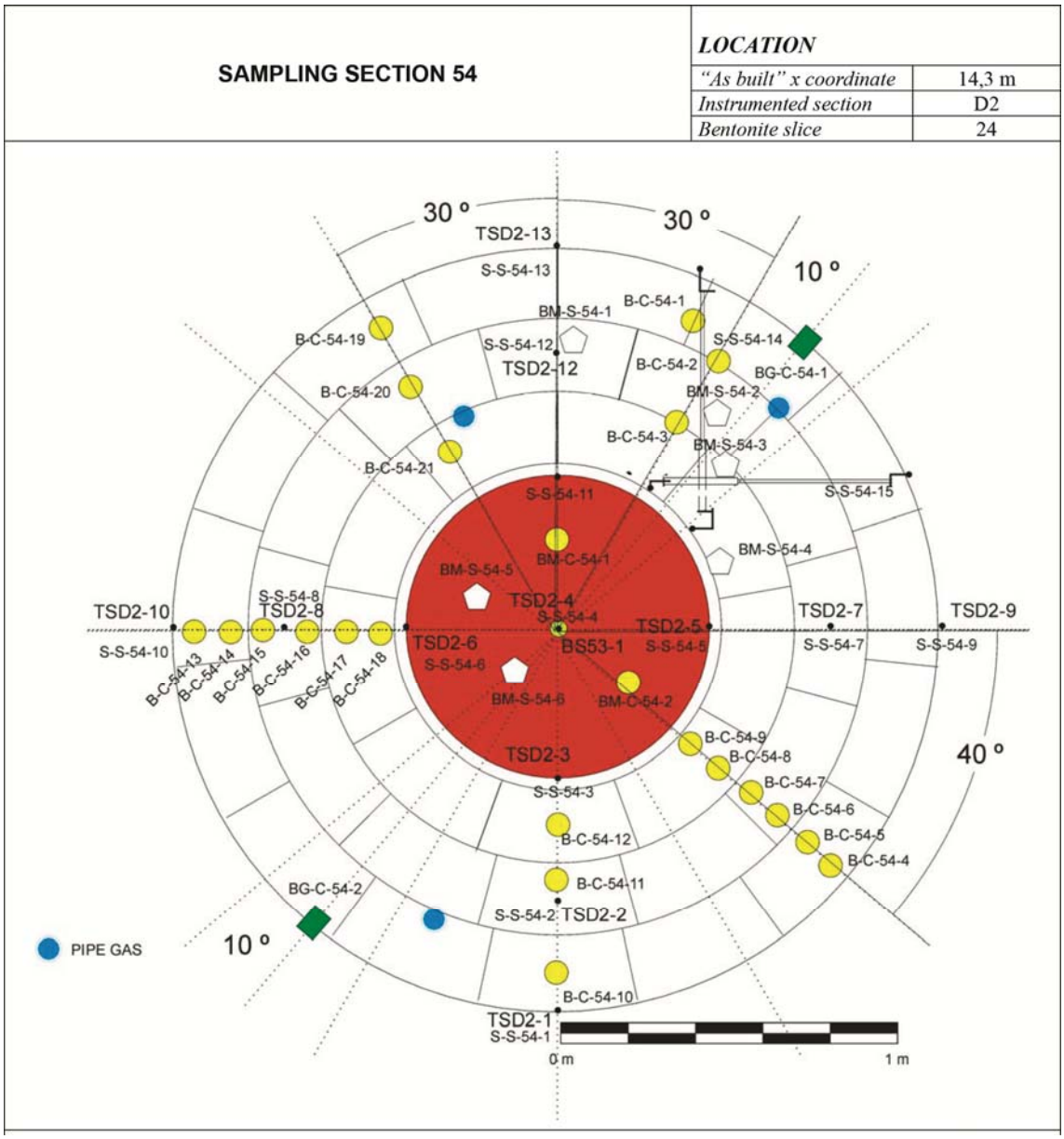

Figure 3.1: Location of extensometers in sampling section 54 (Bárcena & García-Siñeriz, 2015)

3.1 Visual inspection

Macrographs in Figures 3.2 to 3.11 show the overall appearance of the 3 sensors.

The corrosion damage observed on sensor ref. SHSD2-01 is very similar with that observed for sensors SHSD2-02 and SHSD2-03. The corrosion damage is defined in three zones: R (close to the rock), L (close to the Liner), and C (central zone of the extensometer). Zones R and L coincide with the zones of greatest corrosion and diffusion of corrosion products, as it can be seen in the above mentioned photographs.

The corrosion damage observed on the devices for anchoring the sensors to the rock and liner is shown in Figures 3.2 to 3.34. Significant corrosion damage can be seen on the plats, bolts, screws and other items making up the anchoring device. It is a generalized extensive corrosion mode, with an important generation of reddish corrosion products.

Reddish corrosion products are not observed on the central zone of the extensometers.

Apparently the brownish-red corrosion products observed on the surface of the extensometer tubes in areas close to the rock and close to the liner, are due to the corrosion of components parts of the anchoring devices made from carbon steel. In order to verify this issue, some sections extracted from the tubes have been chemically cleaned, with the intention of removing the adhered corrosion products. One of the cleaning solutions proposed for stainless steels in ASTM G1[1] standard, has been used. This chemical solution removes all the corrosion products with negligible attack of the underlying metal. Photographs in Figures 3.14 and 3.15 show the aspect of the extensometer tubes, on reception and after removing the tightly adhered corrosion products. Areas of mechanical damage are observed on the surface of the stainless steel tube, but pitting or other kind of localized corrosion is not detected.

[1] *ASTM G1: Standard Practice for Preparing, Cleaning, and Evaluating Corrosion Test Specimens*

Figure 3.2: Macrograph showing general appearance of sensor ref. SHSD2-01 and bentonite surrounding it

Figure 3.3: Detail of sensor ref. SHSD2-01 close to the rock

Figure 3.4: Detail of bentonite sourrounding sensor ref. SHSD2-01 close to the rock

Figure 3.5: Detail of sensor ref. SHSD2-01 close to the liner

Figure 3.6: Detail of sensor ref. SHSD2-01 close to the rock

Figure 3.7: Macrograph showing general appearance of sensor ref. SHSD2-02 and bentonite surrounding it

Figure 3.8: Detail of sensor ref. SHSD2-02 close to the rock

Figure 3.9: Detail of sensor ref. SHSD2-02 close to the liner

Figure 3.10: Detail of central zone in sensor ref. SHSD2-02 and bentonite surrounding it

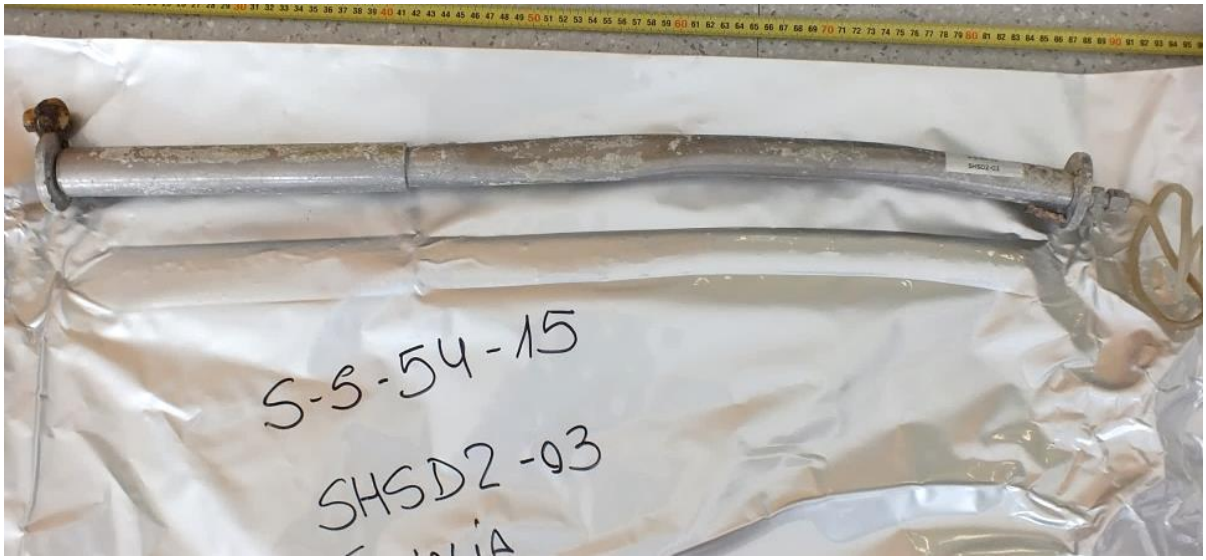

Figure 3.11: Macrograph showing general appearance of sensor ref. SHSD2-03

Figure 3.12: Detail of sensor ref. SHSD2-03 close to the rock

Figure 3.13: Details of sensor ref. SHSD2-03 close to the liner

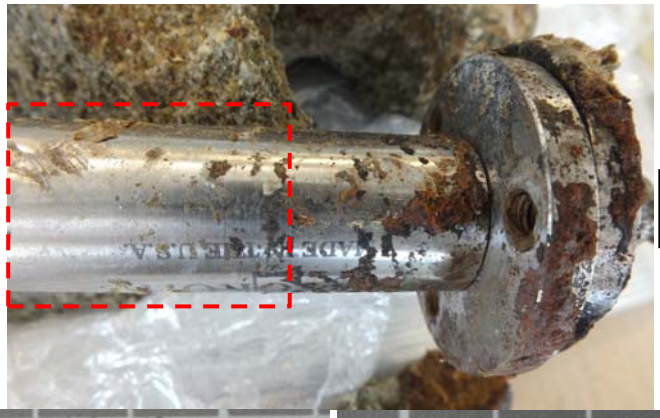

Photograph shown in Fig. 3.3

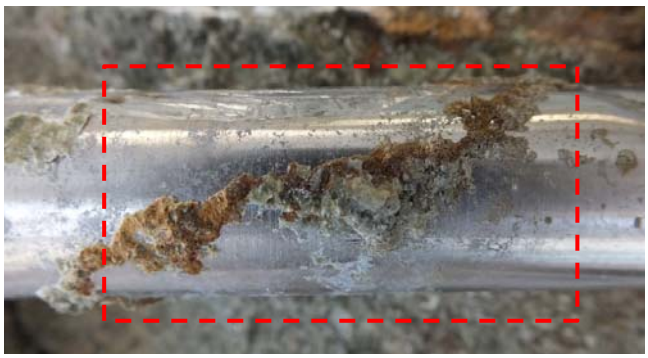

Photograph shown in Fig. 3.6

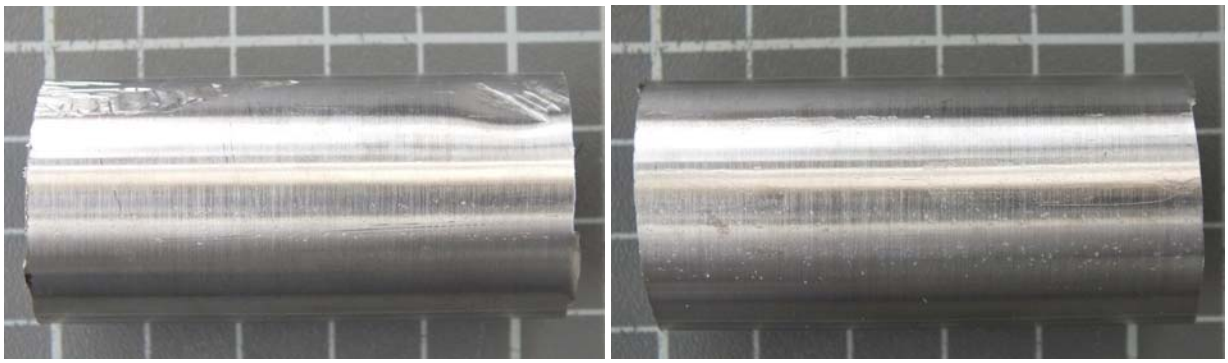

Figure 3.14: Sections of sensor ref. SHSD2-02 (close to the rock) before and after removing the adhered corrosion products. One side and the other

Photograph shown in Fig. 3.8

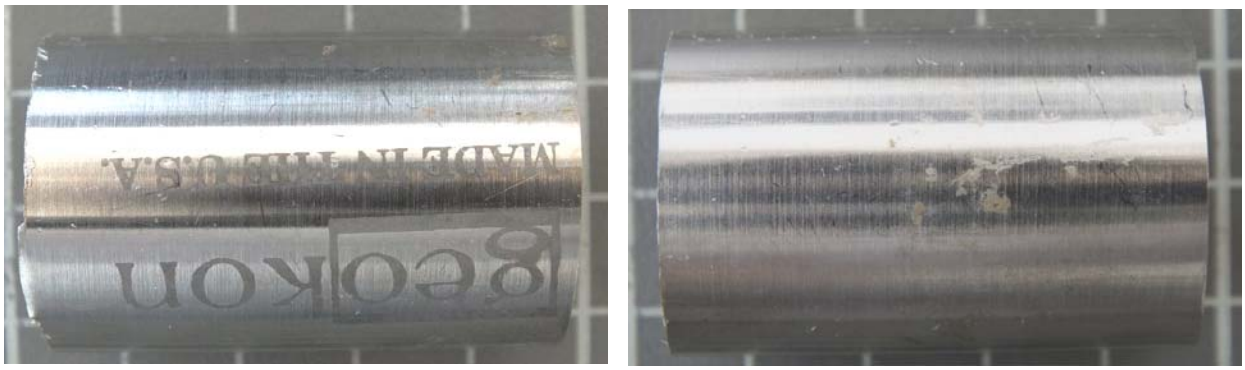

Figure 3.15: Section of sensor ref. SHSD2-01, close to the rock, before and after removing the adhered corrosion products. One side and the other

3.2 Corrosion products analysis: SEM/ EDS and XRD

In order to chemically characterize the corrosion products and /or deposits generated in the three sensors, energy dispersive spectroscopy (EDX-OXFORD INCA-act) analyses were carried out using a microanalyser coupled to a scanning electron microscope (SEM-JEOL 5910-LV). Some of the spectra obtained are shown in Figures 3.16 to 3.25.

Analyses of the reddish corrosion products show that they are mainly constituted of iron and oxygen, as well as silicon, calcium, magnesium and aluminum, as elements making up the bentonite surrounding the samples.

The EDS analyses carried out on the black corroded area of the joints close to the rock from sensors ref. SHSD2-01 and SHSD2-02, Figures 3.16 and 3.21, respectively, show a significant presence of sulphur. There is not detected sulphur in such significant way in other zones of the sensors. It should be noted also in the electron micrograph shown in Figure 3.16, the dendritic skeletons observed in the weld joint. This corrosion morphology is sometimes associated with microbiologically influenced corrosion (MIC).

Chloride is only detected in the EDS analyses carried out on the shallow “pits” observed on stainless steel joints close to the liner in sensors ref. SHSD2-02 and SHSD2-03, shown in Figures 3.22, 3.23 and 3.27.

Table 3.1 lists the semi-quantitative elemental chemical composition obtained in the EDS analyses.

In order to stoichiometrically characterise some of the corrosion products generated on the three sensors, X-ray diffraction analyses were carried out using a Brucker D8-Advance X-ray-Diffractometer. The spectra obtained and the identification of the main peaks is shown in Figure 3.20 and Figure 3.25. The most significant results are detailed below:

- The black brilliant oxide layer generated in screw from sensor ref. SHSD2-02 close to the rock, shown in Figure 3.19, corresponds principally to magnetite (Fe_3O_4)
- Corrosion products generated in the nut from sensor ref. SHSD2-02 close to the liner, shown in Figure 3.24, correspond principally to magnetite (Fe_3O_4) and siderite ($FeCO_3$)
- It is important to point out that in the XRD spectrum only the crystalline species (diffracting ones) are shown.

SENSOR SH SD2-01

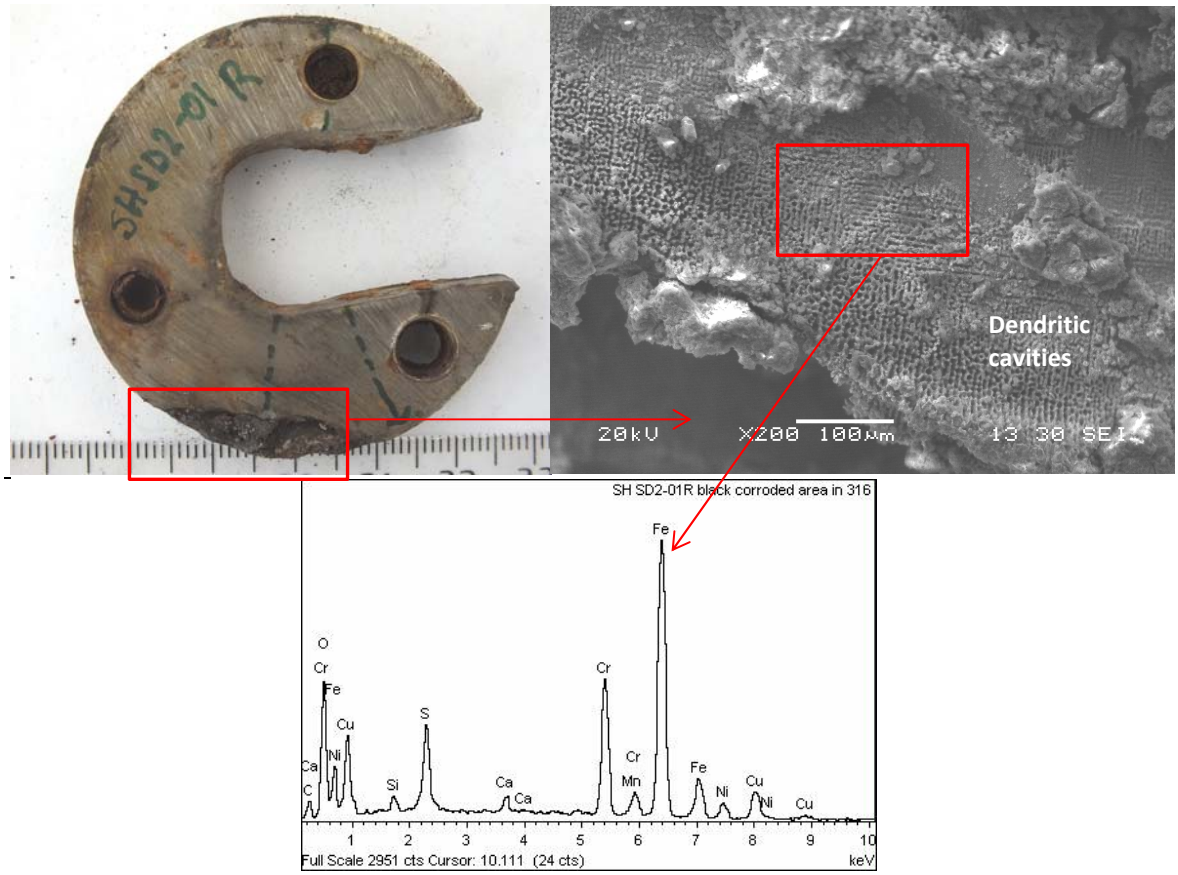

Figure 3.16: Macrograph showing corroded zone of joint from sensor ref. SHSD2-01 close to the rock, and electron micrograph and EDS spectrum corresponding to this zone

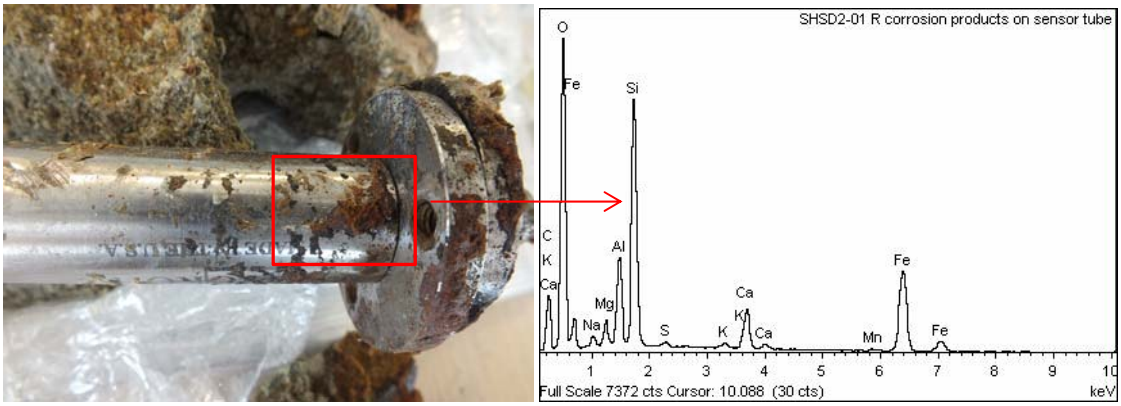

Figure 3.17: Macrograph of sensor ref. SHSD2-01 close to the rock, and EDS spectrum corresponding to this zone

Figure 3.18: Macrograph of sensor ref. SHSD2-01 close to the liner

SENSOR SH SD2-02

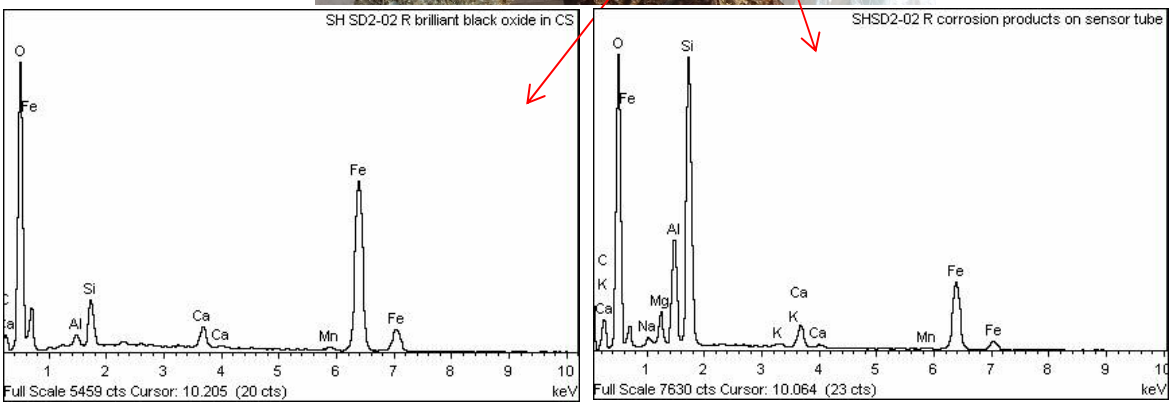

Figure 3.19: Macrograph of sensor ref. SHSD2-02, close to the rock, and corresponding EDS spectra

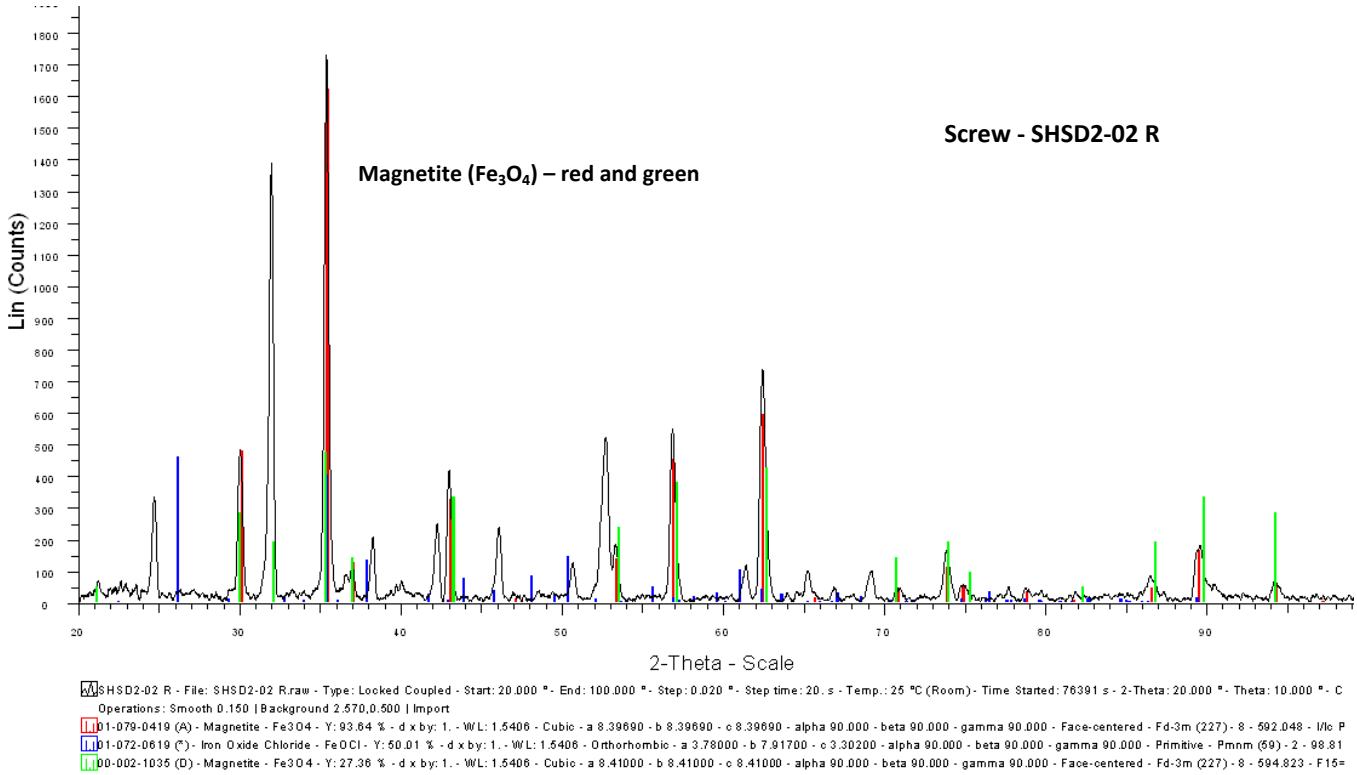

Figure 3.20: XRD spectrum of oxide layer on component shown in Figure 3.19

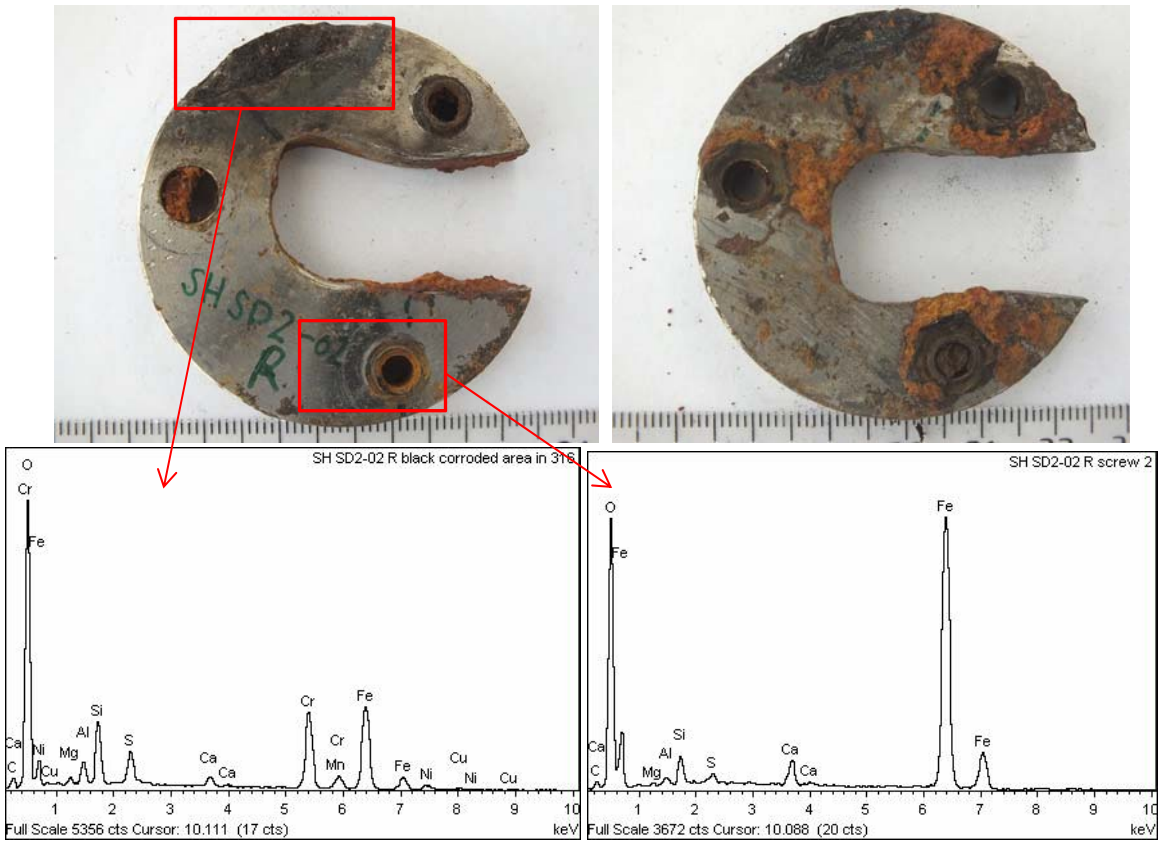

Figure 3.21: Macrographs showing corroded zone of stainless steel joint section (one side and the other) from sensor ref. SHSD2-02 close to the rock, and the corresponding EDS spectra

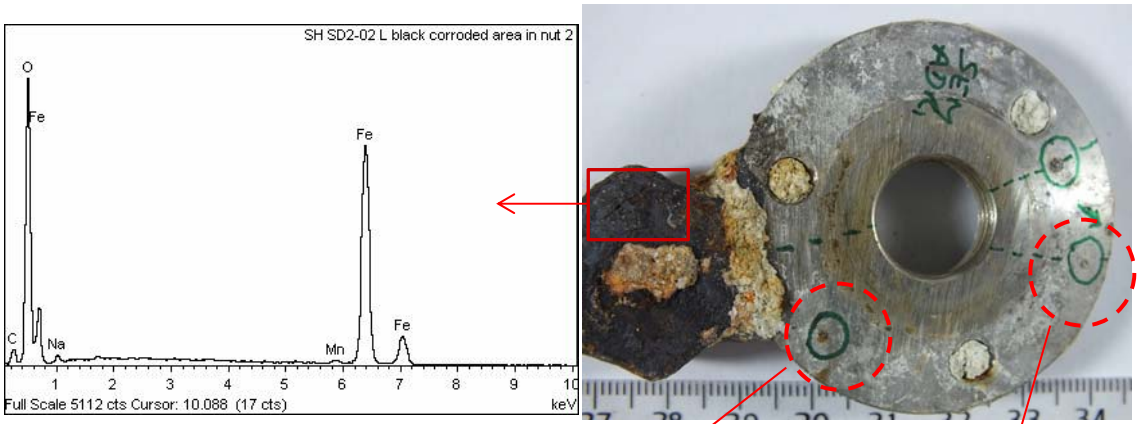

Figure 3.22: Macrograph showing corroded zone of joint from sensor ref. SHSD2-02 close to the liner, and EDS spectrum corresponding to carbon steel corroded nut

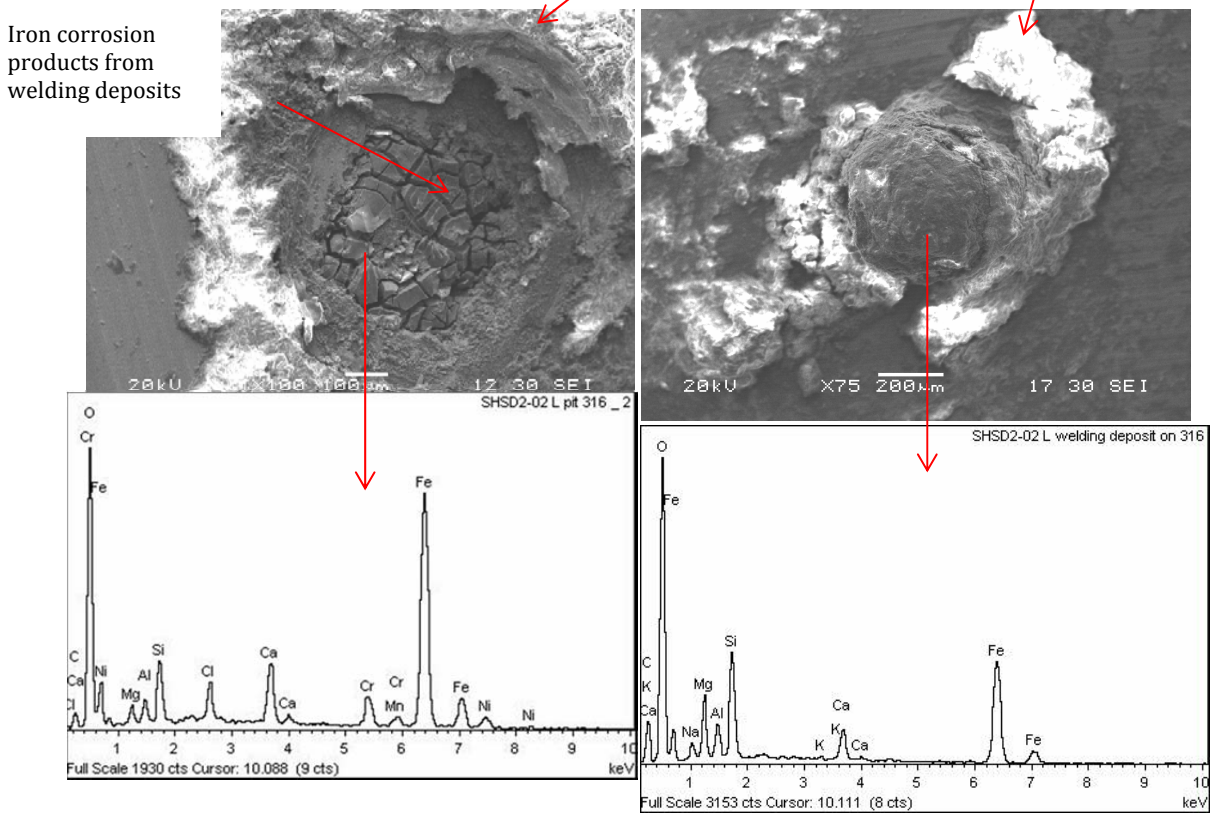

Figure 3.23: Electron micrographs of iron weld deposits on stainless steel joint from sensor ref. SHSD2-02 close to the liner

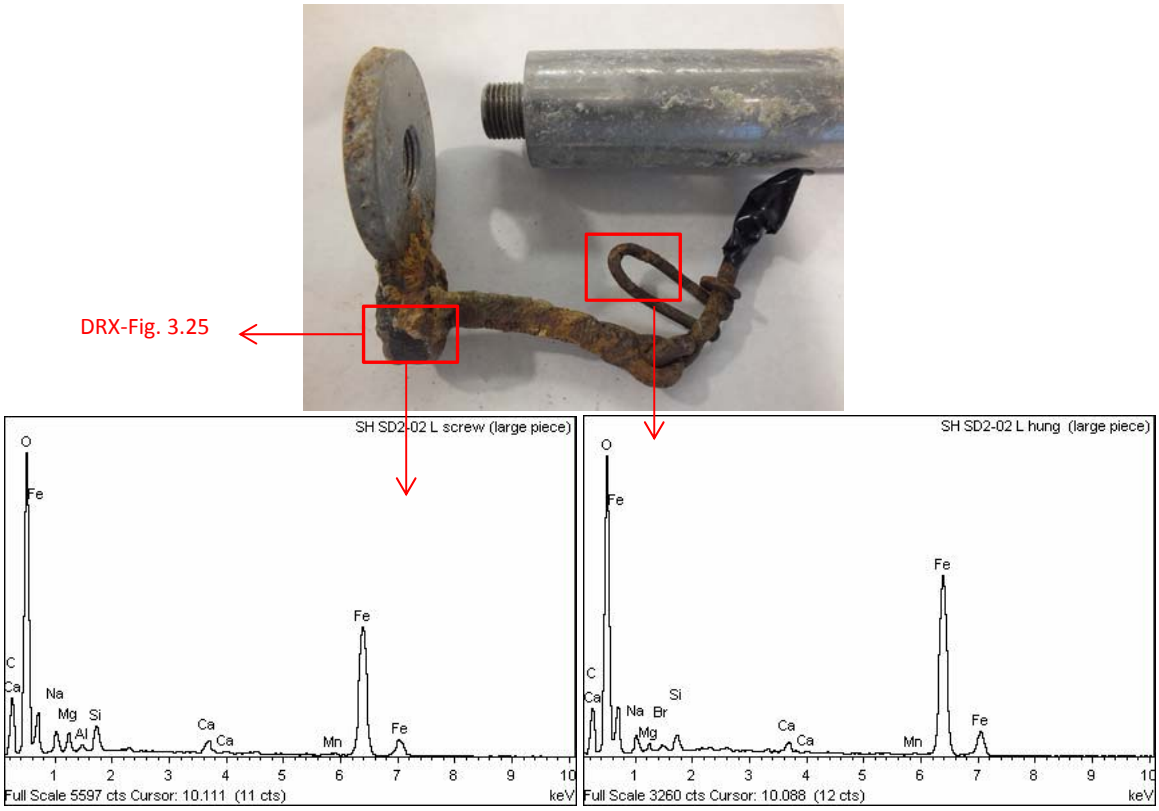

Figure 3.24: EDS spectra of corroded surface of carbon steel components in sensor ref. SH-SD2-02 close to the liner

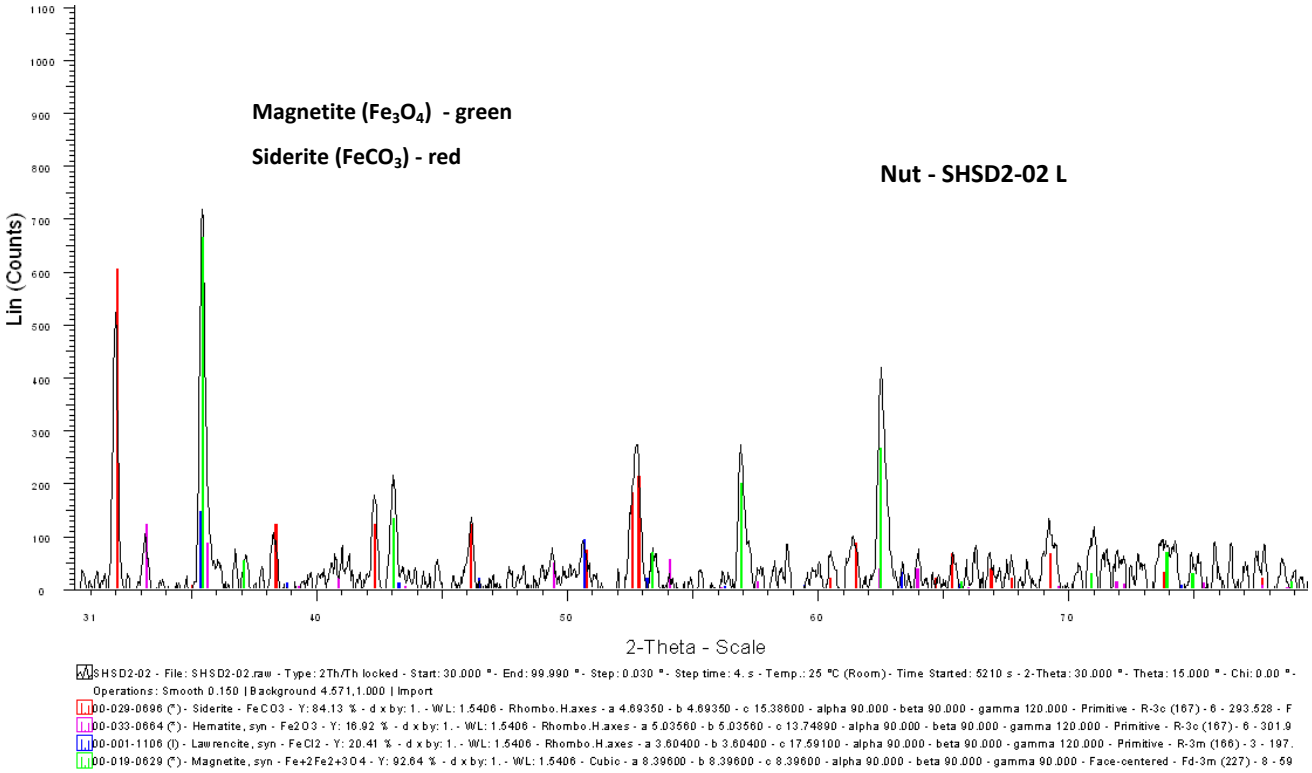

Figure 3.25: XRD spectrum of corrosion products on component shown in Figure 3.24

SENSOR SH SD2-03

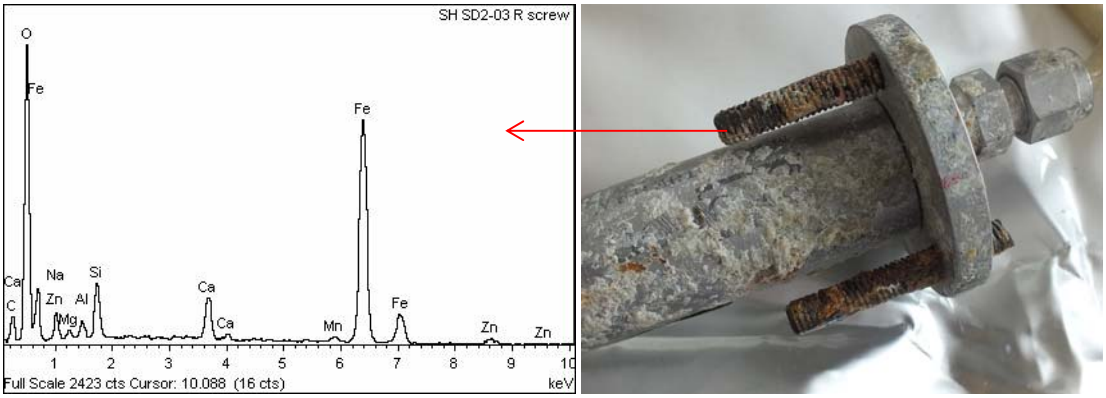

Figure 3.26: EDS spectrum of corroded surface of carbon steel screw in sensor ref. SH-SD2-03 close to the liner

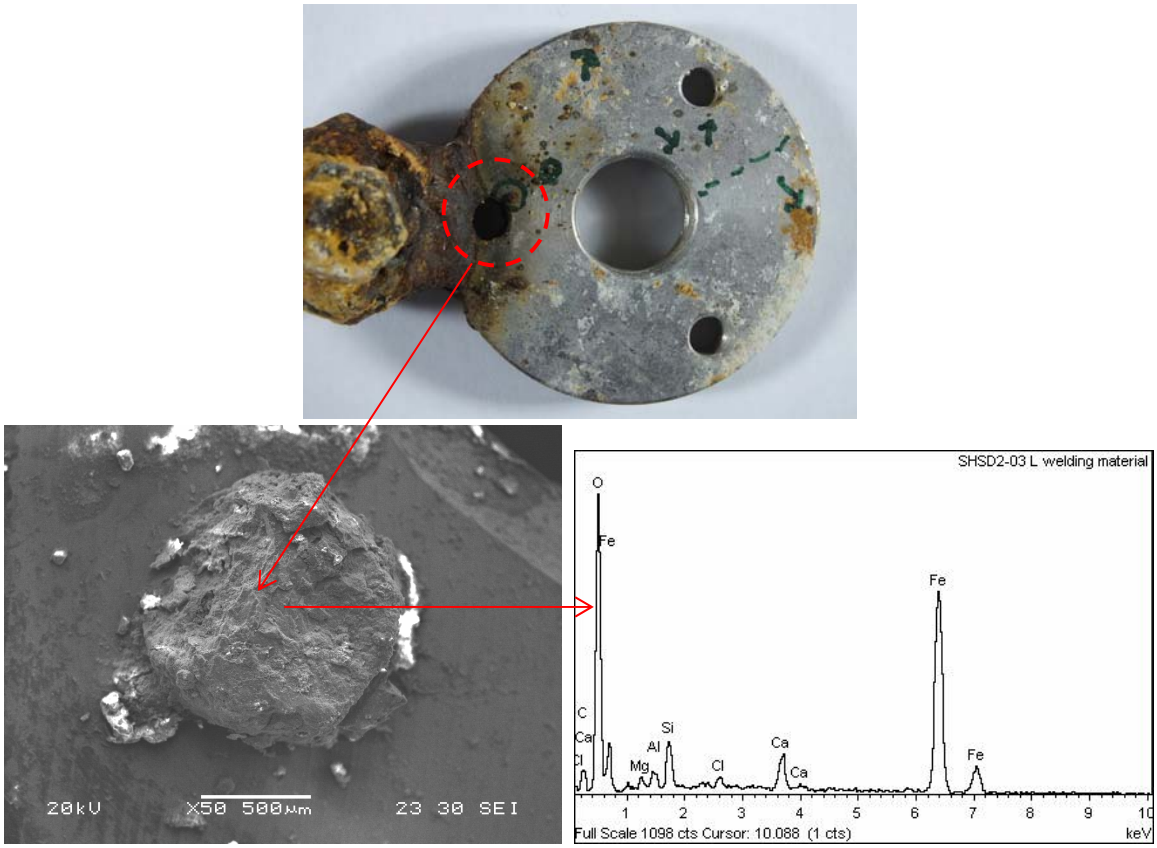

Figure 3.27: Photograph showing corroded zone of joint from sensor ref. SHSD2-03 close to the liner, and electron micrograph and EDS spectrum corresponding to this zone

EDS analysis	Element (%w/w)																	
	O	Na	Mg	Al	Si	S	Cl	K	Ca	Cr	Mn	Fe	Ni	Cu	Zn	Br	Hg	Total
SH SD2-02 R screw	49.05		1.05		0.77	0.71			2.48		0.73	45.21						100.00
SH SD2-02 R screw 2	35.58		0.44	0.48	1.89	0.45			1.93			59.22						100.00
SH SD2-02 R black corroded area in 316	45.99		0.84	1.93	5.18	2.42			1.04	14.59	1.03	24.47	1.79	0.70				100.00
SH SD2-01R black corroded area in 316	15.39				0.91	3.91			0.95	15.30	1.07	48.57	4.21	9.68				100.00
SH SD2-02 R brilliant black oxide in CS	45.41			0.97	3.78				1.98		0.66	47.20						100.00
SH SD2-02 L black corroded area in nut	37.75	0.73	0.71		0.74	1.00			1.12	0.61		50.93					6.42	100.00
SH SD2-02 L black corroded area in nut 2	38.91	1.27									0.59	59.23						100.00
SH SD2-02 L screw (large piece)	49.12	3.84	2.63	0.52	2.31				1.35		0.44	39.77						100.00
SH SD2-02 L hung (large piece)	43.51	3.04	0.80		1.30				0.87		0.48	48.92				1.08		100.00
SH SD2-03 R screw	39.91	2.24	0.76	1.15	3.48				3.29		0.84	45.81			2.52			100.00
SHSD2-01 L corr. products on sensor tube	45.12	0.51	1.42	2.67	7.96				1.45		0.65	40.22						100.00
SHSD2-01 R corr. products on sensor tube	52.99	1.07	1.89	5.41	15.42	0.23		0.37	3.37		0.35	18.89						100.00
SHSD2-02 R corr. products on sensor tube	52.08	0.72	2.47	6.69	18.84			0.30	1.96		0.43	16.52						100.00
SHSD2-03 L welding material	43.87		1.20	1.25	3.32		0.80		2.99			46.57						100.00
SHSD2-02 L welding deposit on 316	51.49	2.14	6.25	2.61	7.88			0.28	2.80			26.56						100.00
SHSD2-02 L pit 316	40.59		2.01	3.57	10.59		1.23	0.23	2.85	5.80	1.01	28.84	3.28					100.00
SHSD2-02 L pit 316 _ 2	36.30		1.39	1.30	3.41		2.28		4.27	3.63	1.06	43.34	3.01					100.00

Table 3.1: EDS semi-quantitative elemental composition of corroded products on sensors ref. SHSD2-01, SHSD2-02 and SHSD2-03

3.3 Metallographic study

In order to analyse the microstructure, morphology and extent of the corrosion-derived damage, metallographic probes were prepared from sections extracted from the components under study. These probes were then analysed using optical microscopy.

Anchoring devices

Optical micrographs in Figures 3.28 to 3.35 show some details of the devices for attaching the sensors to the liner and to the rock in sensors ref. SHSD2-01 and SHSD2-02. These micrographs clear indicate that:

- Carbon steel components: screws, nuts and iron welding deposits, show significant corrosion damage.
- The corrosion damage observed in the stainless steel parts of the anchoring devices is due to the corrosion of the carbon steel filler welding material.
- The stainless steel making up the anchor device sections shows a non-sensitized austenitic microstructure, Figure 3.30. Sensitization refers to the precipitation of chromium carbides at grain boundary.

Stainless steel tube

The optical micrographs in Figures 3.36 and 3.37 show no signs of localized or generalized corrosion in the 316 stainless steel tubes from sensors ref. SHSD2-01 and SHSD2-02. Chemical etching reveals a non-sensitized austenitic microstructure.

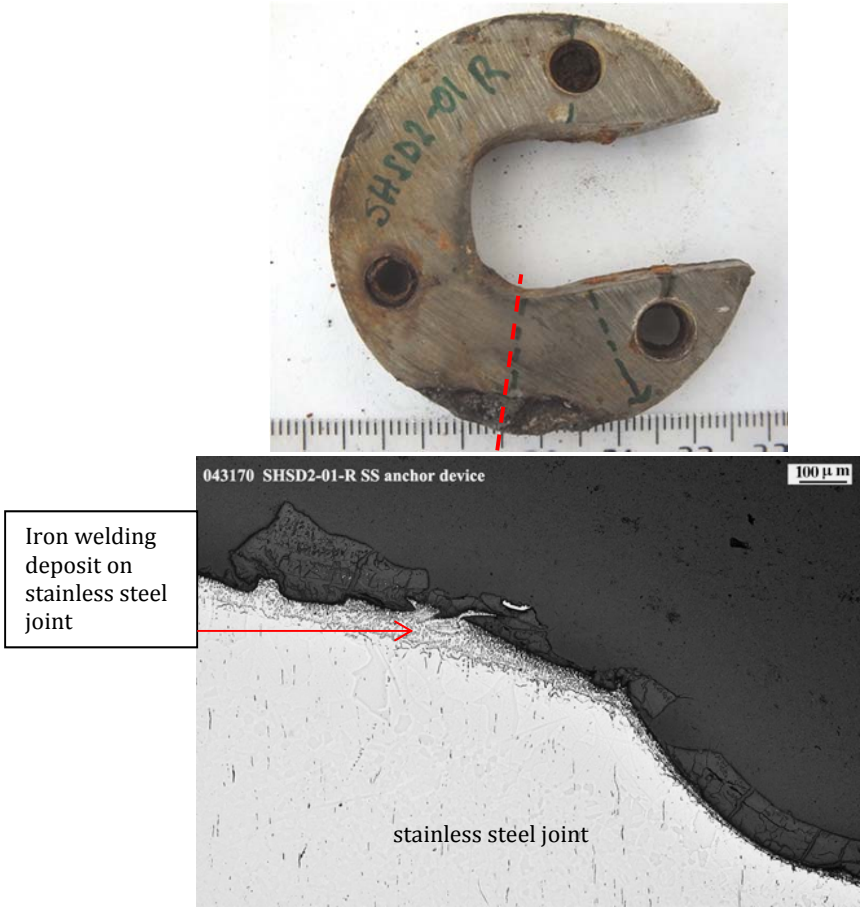

Figure 3.28: Optical micrograph of stainless steel anchoring section from sensor ref. SHSD2-01, close to the rock

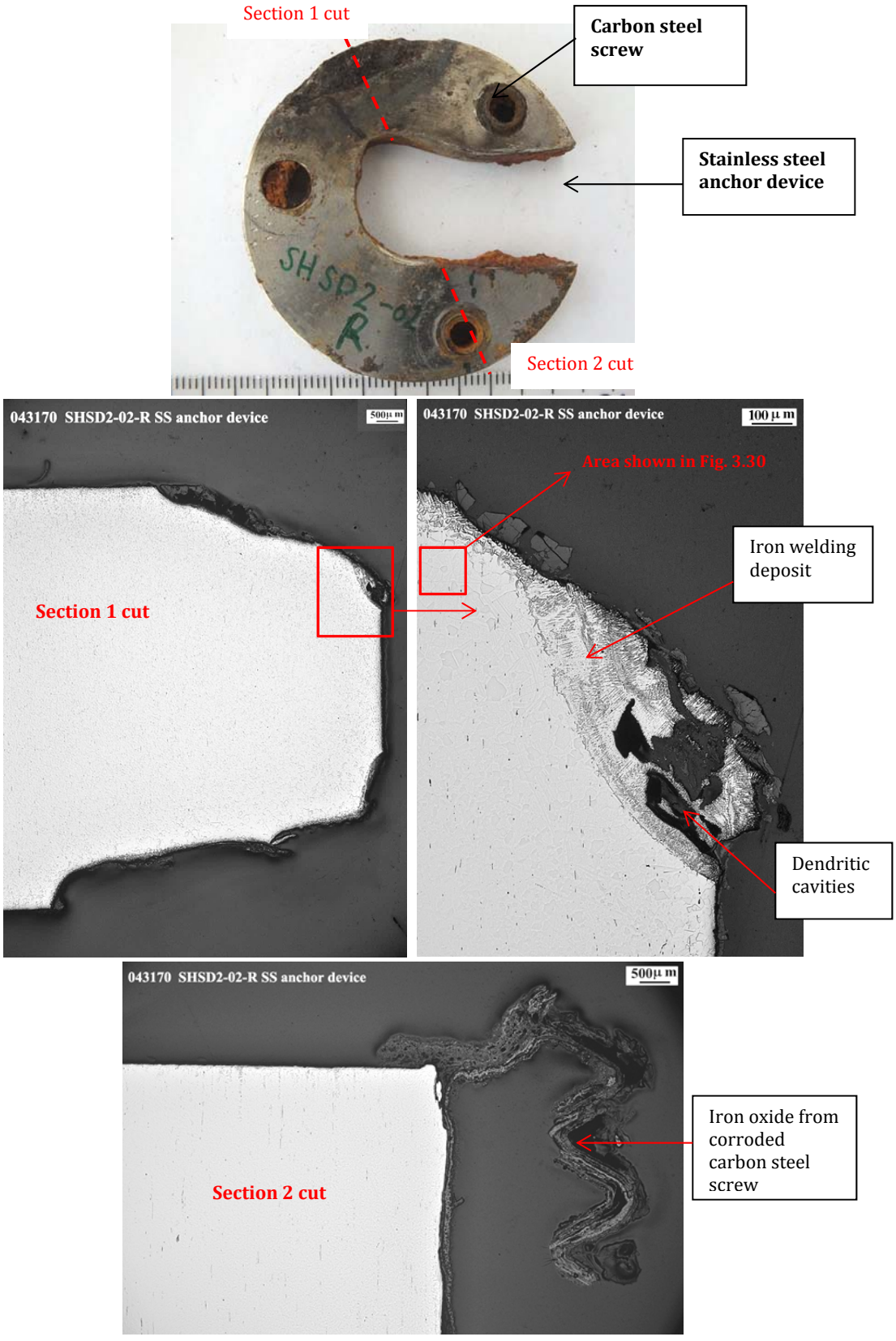

Figure 3.29: Optical micrographs of stainless steel anchoring section from sensor ref. SHSD2-02, close to the rock

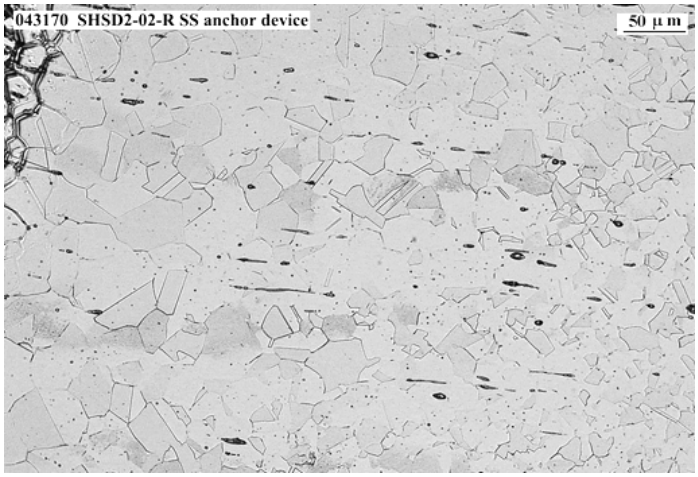

Figure 3.30: Optical micrograph detail of Figure 3.29, with metallographic etching

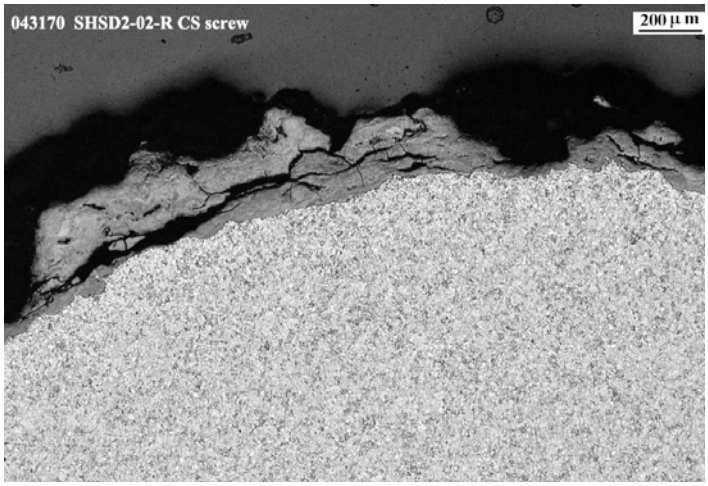

Figure 3.31: Optical micrograph of carbon steel (CS) screw in sensor ref. SHSD2-02-R, with metallographic etching

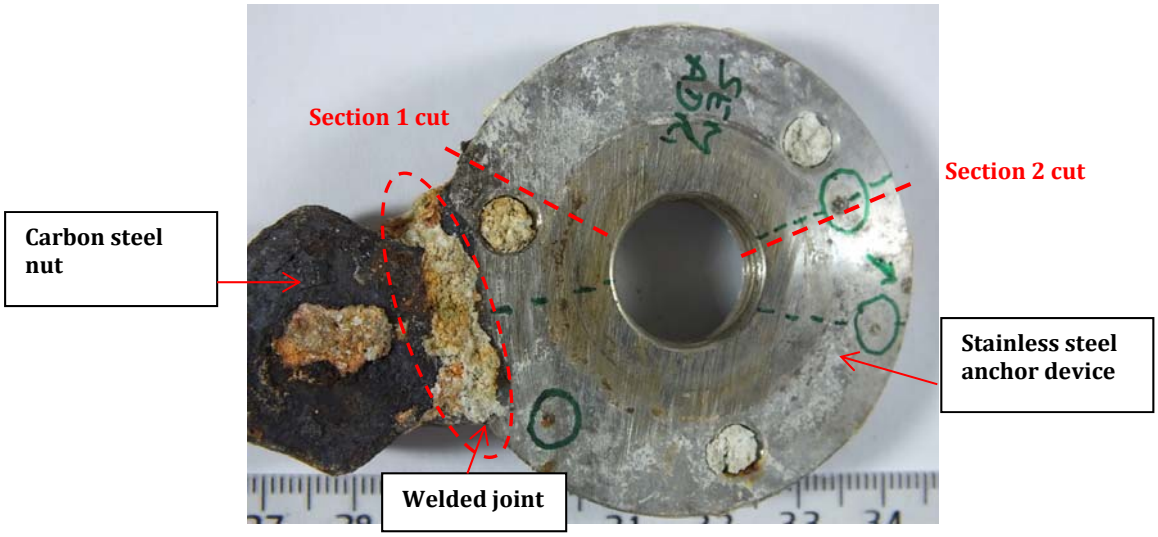

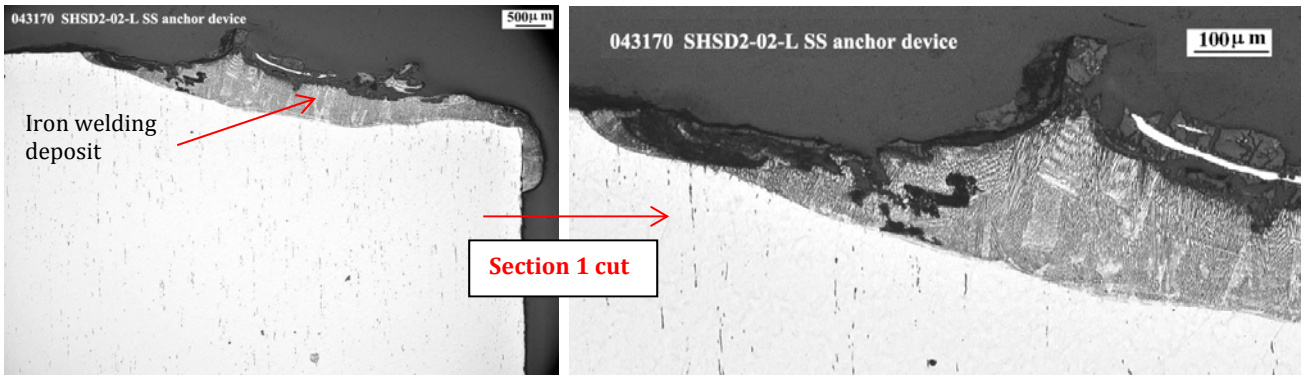

Figure 3.32: Optical micrographs of stainless steel anchoring section 1, from sensor ref. SHSD2-02, close to the liner, with carbon steel metallographic etching

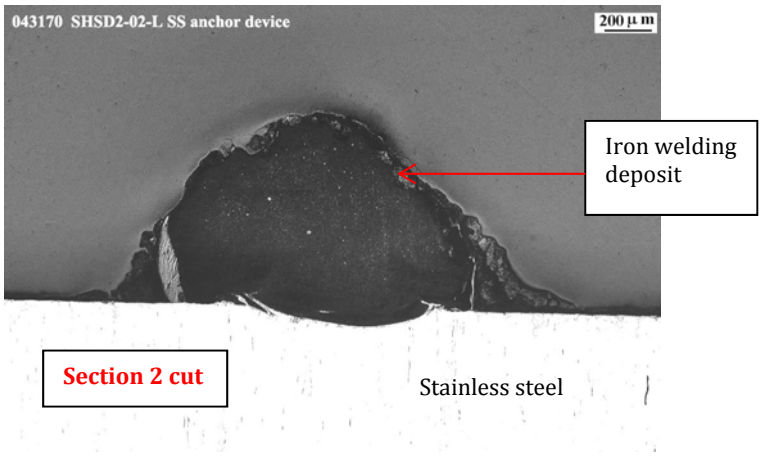

Figure 3.33: Optical micrograph of section 2 from sensor ref. SHSD2-02, close to the liner, showing an iron welding deposit, with carbon steel metallographic etching

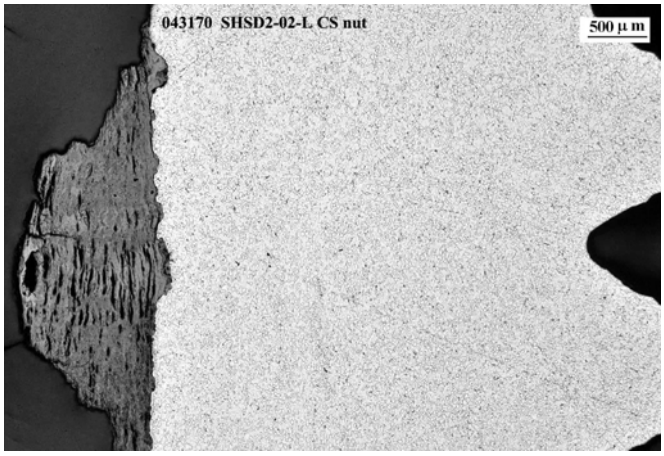

Figure 3.34: Optical micrograph of carbon steel nut section of liner-sensor ref. SHSD2-02, with metallographic etching

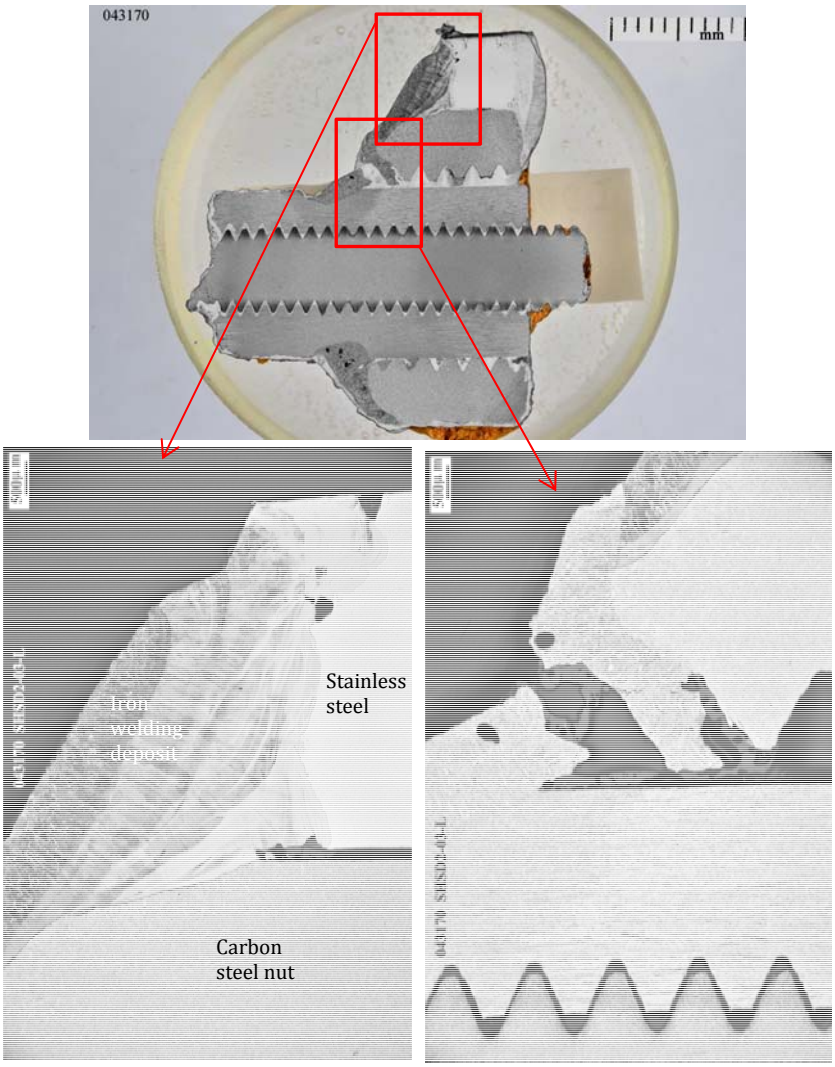

Figure 3.35: Photograph showing metallographic probe with cross section of liner-sensor fixing plate, and optical micrographs of details examined, with metallographic etching

Stainless steel tubes

Figure 3.36: Photograph of metallographic probe and optical micrographs of stainless steel tube from sensor ref. SHSD2-01 close to the rock, with metallographic etching

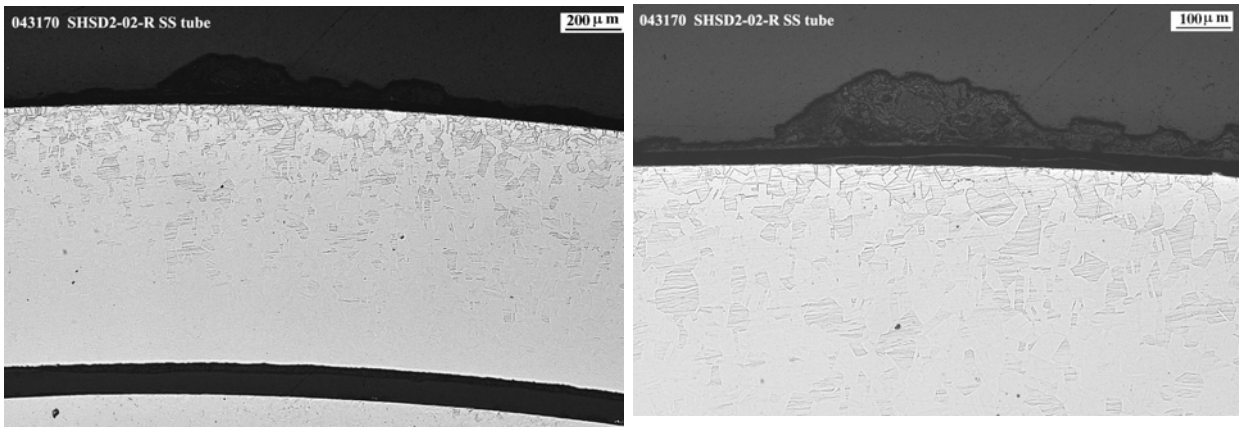

Figure 3.37: Optical micrographs of stainless steel tube close to the rock, from sensor ref. SHSD2-02, with metallographic etching

4. BENTONITE ANALYSIS

4.1 Visual Inspection

Bentonite samples code BM-S-54-2 (in contact with sensor SHSD2-01) and BM-S-54-3 (in contact with sensor SHSD2-02) are analysed. The studies carried out include the chemical analyses of the leached obtained, and the determination of the presence or aerobic and anaerobic bacteria.

Figure 4.1 shows the appearance of the bentonite samples surrounding sensors SHSD2-01 and SHSD2-02. The bentonite located around the attaching devices of the sensors to the rock and to the liner, shows a brownish-red color, due to the diffusion of corrosion products. There is not detected significant diffusion of corrosion products in the bentonite located around the central part of the extensometers. Bentonite samples are identified with L (liner), R (rock) and C (center) based on their location (see Figure 4.1).

The bentonite samples looked highly hydrated.

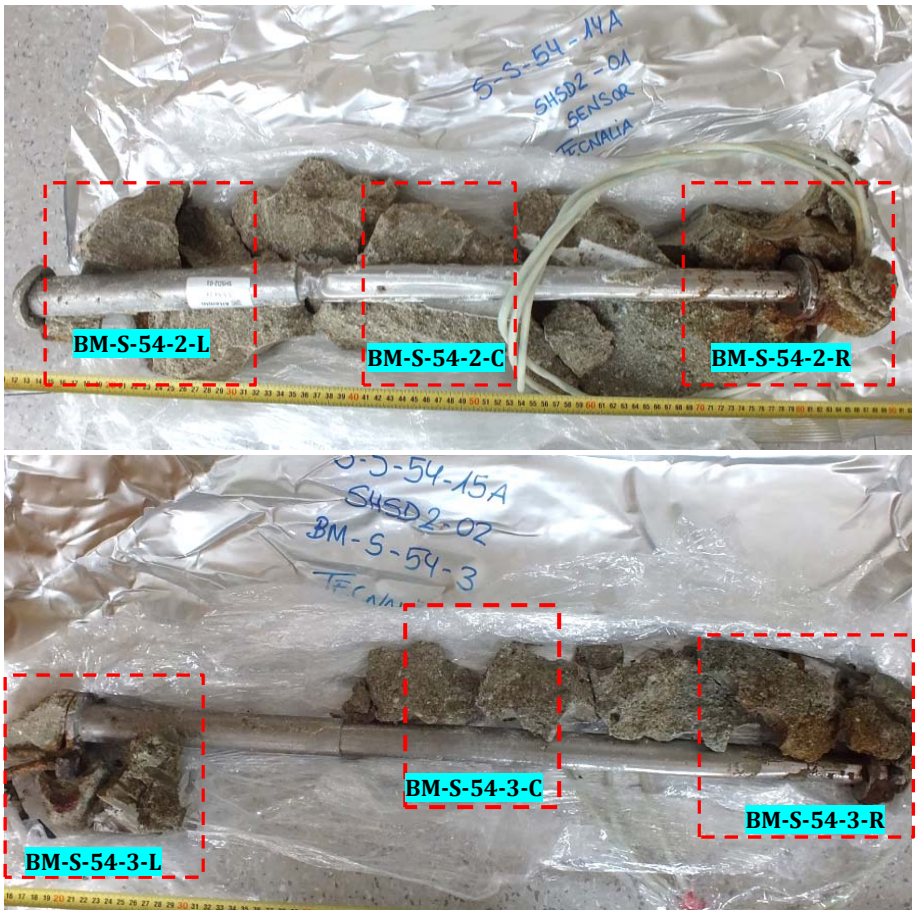

Figure 4.1: Macrographs showing location of the bentonite samples reference BM-S-54-2 (up) and BM-S-54-3 (down)

Figure 4.2: Macrograph showing samples of bentonite for chemical characterization

4.2 Chemical analysis

Bentonite samples ref. BM-S-54-2-R, BM-S-54-2-C, BM-S-54-2-L, BM-S-54-3-R, BM-S-54-3-C, BM-S-54-3-L, were leached using de-ionized water. The leached solution was analyzed in order to determine the concentration of Cl^-, S^{2-}, HCO_3^-, NO_3^{2-}, SO_4^{2-}, Ca^{2+}, Mg^{2+}, K^+ and Na^+. The amount of chromium and iron was also evaluated, in addition to the pH, conductivity and moisture content of the bentonite. The amount of Cr and Fe and the moisture content was determined on a solid waste portion.

The results and methods used in the determination of the different parameters are shown in Table 4.1. Chemical analysis shows a significant percentage of iron in the bentonite samples due to the diffusion of the reddish corrosion products from the corroded sensors.

The analysis of the leached was carried out according standard UNE-EN 12457-4:2003: *Characterization of waste-leaching. Compliance test for leaching of granular waste materials and sludges. Part 4: One stage batch test at a liquid to solid ratio of 10 l/kg for materials with particle size below 10 mm (without or with size reduction).*

	SAMPLE REF.					
	BMS-54-2-R	**BMS-54-2-C**	**BMS-54-2-L**	**BMS-54-3-R**	**BMS-54-3-C**	**BMS-54-3-L**
PARAMETERS /units						
Electrical Conductivity (20ºC) µS/cm	322	543	761	421	556	380
pH value (20.5 ºC)	8.0	9.4	8.3	8.7	9.5	8.3
Chloride mg/kg d.m*	399	310	475	429	262	304
Sulfide mg/kg d.m.	4.0	4.0	<3	10	4.0	6.0
Hydrogen carbonate mg/kg d.m.	1269	2245	1513	1660	2002	1171
Nitrate mg/kg d.m.	<50	<50	81,4	<50	<50	<50
Sulfate mg/kg d.m.	490	577	2280	764	536	545
Calcium mg/kg d.m.	28.9	34.2	55.2	19.0	19.5	24.8
Magnesium mg/kg d.m.	11.5	<10	21.2	22.8	<10	<10
Potassium mg/kg d.m.	11.6	20.1	29.3	15.2	15.2	12.3
Sodium mg/kg d.m.	705	957	1420	672	891	738
Chromium** mg/kg d.m.	51.0	6.31	6.55	6.89	7.26	12.8
Iron** mg/kg d.m.	34600	23600	25800	27700	23800	34200
Moisture content** % dried mass	29.2	23.7	23.3	25.2	23.4	24.0

PARAMETERS	**METHODS**
Conductivity, pH	Electrometric
Sulfide	Redox volumetric
Ca, Mg, K, Na, Cr, Fe:	ICP-OES (Plasma Optical Emission Spectrometry)
Hydrogen carbonate	Volumetric
Chloride, Nitrate, Sulfate	Ion Chromatography
Moisture content	Gravimetric

Table 4.1: Chemical analysis of the leachate from the bentonites

* dry mass (d.m.)

** Cr, Fe and moisture content was determined on solid waste portion

4.3 Microbiological analysis

Aerobic and anaerobic bacteria density was determined by the agar pour plate method. Plates were incubated at 28 °C for 72-120 hours. The final colonies were counted as Colony Forming Units (CFU). During all the process the equipment, reagents and media that came in contact with the cells were sterilized. The anaerobic culture plates were manipulated in an O_2 free environment, and incubated in an anaerobic jar.

The presence of SRB was determined after extraction with phosphate buffer. This media was anaerobically incubated (under oxygen free N_2 gas) at 28ºC, in specific medium (API RP-38). Growth of bacteria was monitored by periodic counts by the Most Probably Number (MPN) method, for periods up to 15-20 days.

The results of the microbiological analysis are shown in Table 4.2.

No viable microbial groups were detected in the bentonite surrounding the sensors ref. SHSD2-01 and SHSD2-02. It should be noted, however, that viable microbes were detected by other laboratories in samples from other parts of the FEBEX experiment (Bengtsson et al. 2016).

c.f.u/ g count of sample	B-SH SD2-02-C	B-SH SD2-02-R	B-SH SD2-02-L
Aerobic bacteria	< 2	< 2	< 2
Anaerobic bacteria	< 2	< 2	< 2
Sulphate-reducing	< 2	< 2	< 2

C.F.U/ g count of sample	B-SH SD2-01-C	B-SH SD2-01-R	B-SH SD2-01-L
Aerobic bacteria	< 2	< 2	< 2
Anaerobic bacteria	< 2	< 2	< 2
Sulphate-reducing	< 2	< 2	< 2

Table 4.2: Microbiological characterization of samples of bentonite

5. CORROSION COUPONS

5.1 Description of the samples studied

The corrosion coupons studied consisted of different sized parallelepipeds manufactured from the following materials: TStE355 type carbon steel (UNE F 6215), AISI 316L (UNS S31603) austenitic stainless steel, titanium alloys Grade 2 (UNS R50400), Grade7 (UNS R52400) and Grade 12 (UNS R53400), pure copper Cu-ETP (UNS C11000) and cupronickel alloys 70/30 (UNS C71500) and 90/10 (UNS C70600). In the case of the steels and the titanium alloys, some of the coupons contained joints welded by EBW (Electron Beam Welding), FCAW (Flux Cored Arc Welding) and MAGW (Metal Active Gas Welding) for the TStE355 steel, EBW and GTAW (Gas Tungsten Arc Welding) for the 316L steel, and EBW and PAW (Plasma Arc Welding) for the titanium.

Coupons of the same material were placed on Teflon supports separated by Teflon spacers. Each material was assigned a number: 1 for the TStE355 steel, 2 for the 316L steel, 3 for the titanium alloys and 4 for the coppers. For each type of material, 3 units or racks were assembled, differentiated by the letters A, B, and C, marked on one of the Teflon supports of each rack. This marked support allowed perfect identification of each corrosion coupon, Figure 5.1.

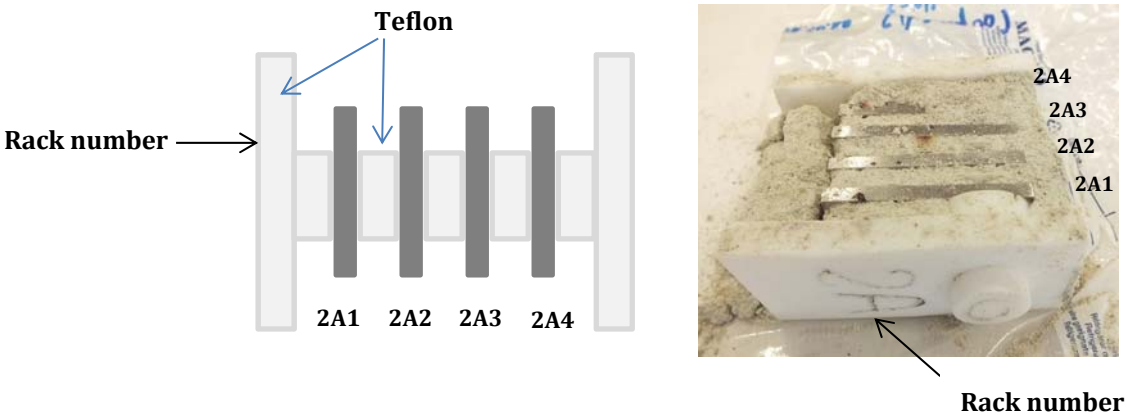

Figure 5.1: Picture and photograph showing identification of corrosion coupons in the test racks

Three racks were delivered to TECNALIA in order to carry out the corrosion study: Rack 2A (316L), 3A (titanium) and 4A (copper). Table 5.1 lists the relation of racks and coupons under study, as well as measured weight of the coupons. The weight measurement was primarily used for identification of coupons in damaged racks, and should not be used for corrosion rate interpretation. Figure 5.2 shows the initial location of the racks in sampling section 48. The coupons were inserted into the bentonite blocks closest to the heater and at the bottom.

Alloy	Rack number	Coupons	Size (mm)	Initial weight (g)	Final weight* (g)
AISI 316L	2A	2A1 base	50x20x4.3	30.3488	30.3475
	M-S-48-2	2A2 base	50x20x4.3	30.2025	30.2027
		2A3 EBW	50x20x4.4	29.9077	29.9070
		2A4 GTAW	50x20x4.6	31.8859	31.8833
Titanium alloys	3A	3A1 Ti2 base	29.7x30x5.9	21.2882	*Missing*
	M-S-48-3	3A2 Ti2 EBW	30x30x5.5	19.6726	19.717
		3A3 Ti7 base	50x20x4.6	17.9093	17.977
		3A4 Ti7 base	50x20x4.6	17.8977	17.600
		3A5 Ti7 EBW	50x20x4.5	17.6395	*Missing*
		3A6 Ti7 PAW	48.5x20x4.6	17.2416	17.158
		3A7 Ti12 base	29.7x30x9.9	36.3886	36.4066
		3A8 Ti12 base	29.8x30x10	36.8666	36.8705
Copper alloys	4A	4A1 Cu (99%)	50x20x4.7	36.5960	36.4974
	M-S-48-4	4A2 Cu (99%)	50x20x4.7	36.0878	36.0900
		4A3 90Cu/10Ni	60x24.4x1.85	14.3551	14.3225
		4A4 90Cu/10Ni	60x24.3x1.85	14.1873	14.1624
		4A5 70Cu/30Ni	60x25x2.1	25.8008	25.8668

Table 5.1: List of racks and coupons under study

*Approximate value. Bentonite is tightly adhered to the surface of certain coupons

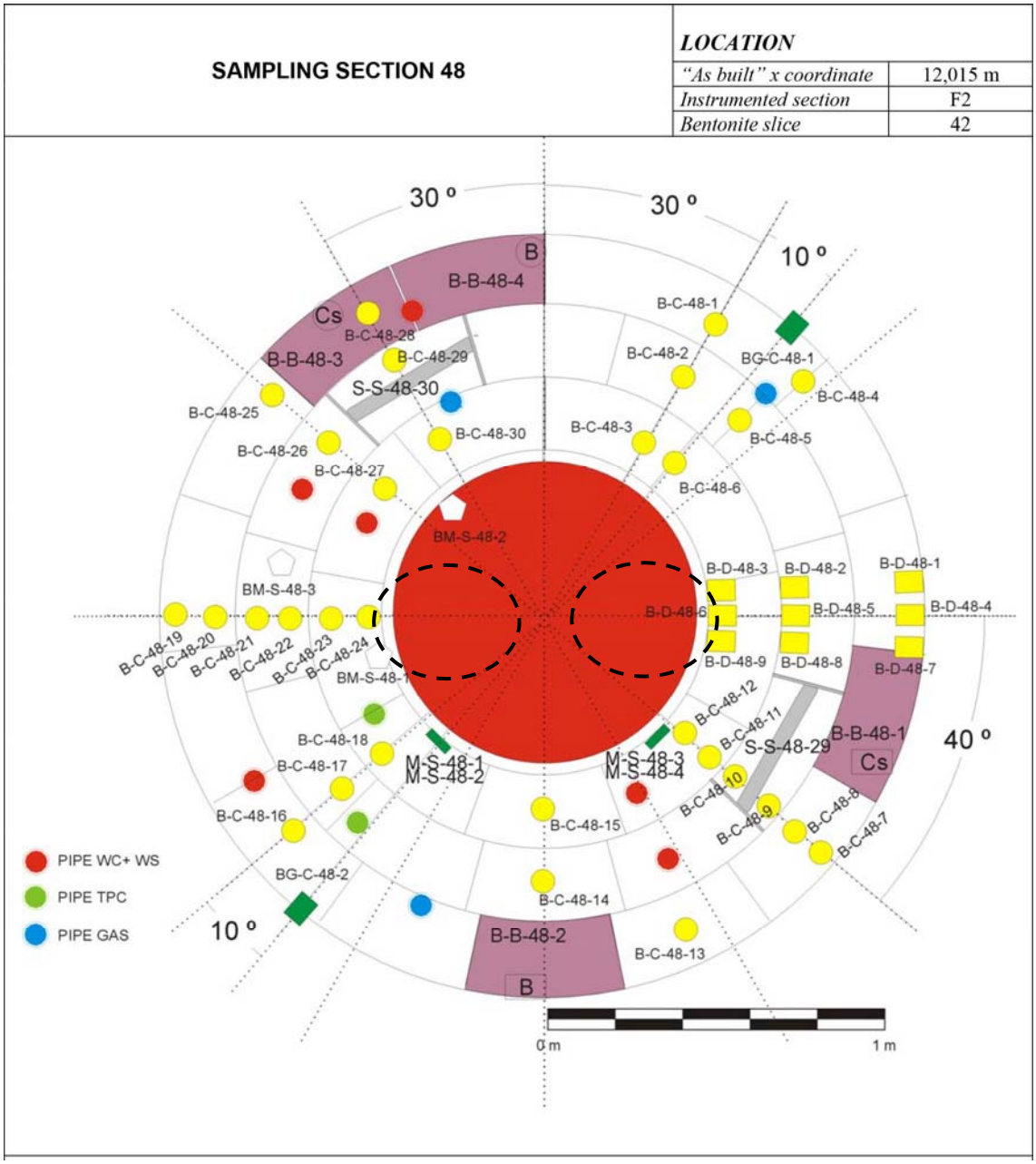

Figure 5.2: Location of corrosion coupons in sampling section 48 (Bárcena & García-Siñeriz, 2015)

All the racks were protected in vacuum packs: one external aluminum foil + 2 plastic bags. No vacuum loss was observed in any of the racks under study. Photographs showing the appearance of the racks as received are given in Annex I of this document.

5.2 Rack 2A: 316L stainless steel

5.2.1 Visual inspection

Figure 5.3 shows the overall appearance of the rack 2A. The photographs in Figures 5.4 to 5.6 show details of the 4 stainless steel coupons. This rack consists of 4 stainless steel coupons: 2 base material coupons identified as 2A1 and 2A2, and 2 test coupons with welded joints: 2A3 (EBW) and 2A4 (GTAW).

The bentonite adhered to these coupons has a much lesser degree of humidity than that observed for the bentonite hosting sensors ref. SHSD2-01 and SHSD2-02.

Corrosion damage in these coupons is manifested as pitting, observed in the four stainless steel coupons, and cracking detected on coupon ref. 2A2. Besides, all the coupons show areas with a little penetration of the corrosion, Figures 5.4, 5.6 and 5.7.

Corrosion products associated to cracking are reddish-brown, and they are poorly adhered. Corrosion products associated to pits are more compact and adherent, being the corrosion products brownish-black. No significant differences in corrosion behaviour are observed between welded and base material samples.

Figure 5.3: Macrographs showing general appearance on reception of rack ref. 2A (stainless steel)

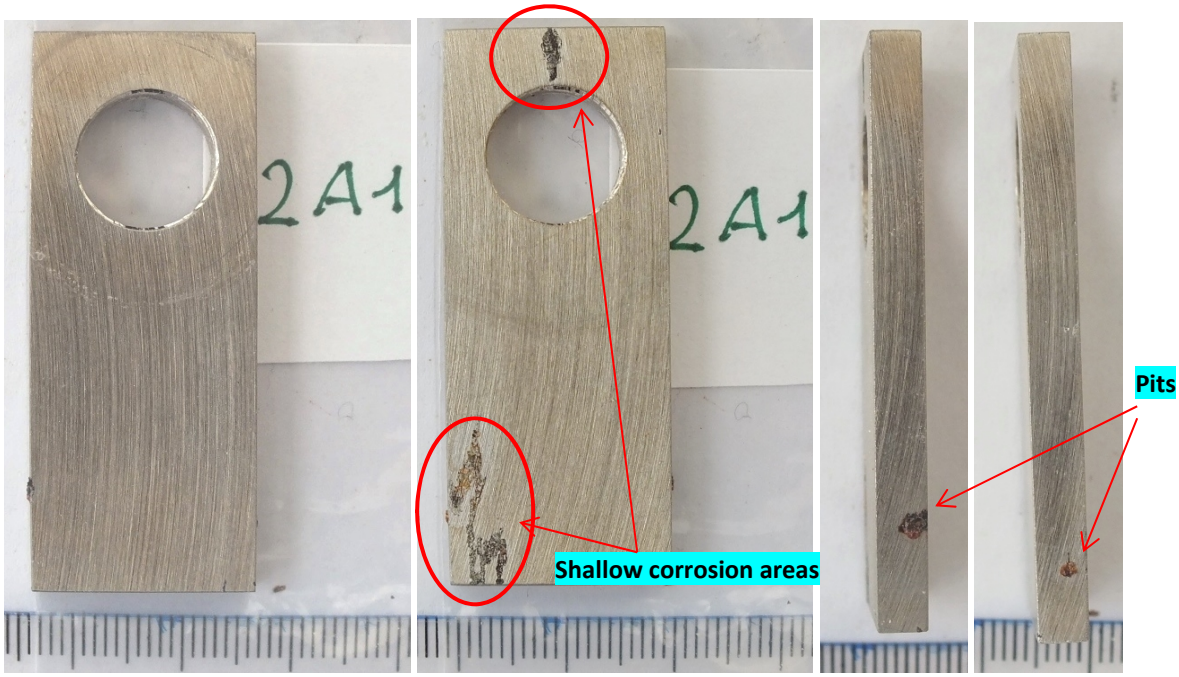

Figure 5.4: Photographs showing corrosion coupon ref. 2A1 (base), one side and the other

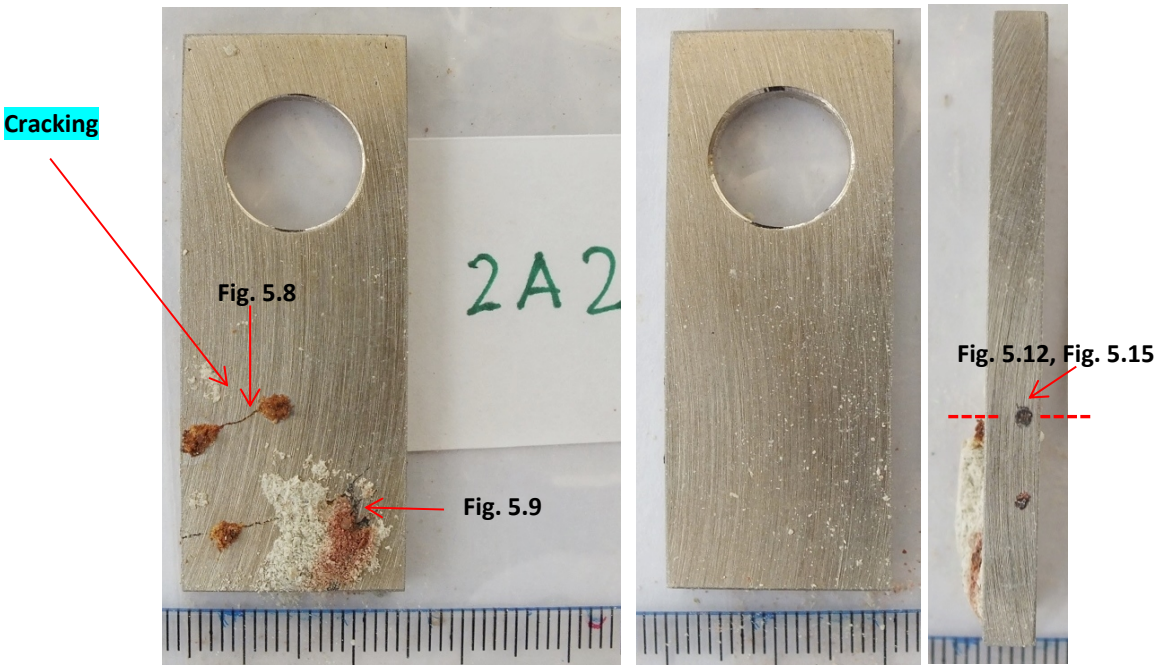

Figure 5.5: Photographs showing corrosion coupon ref. 2A2 (base), one side and the other.

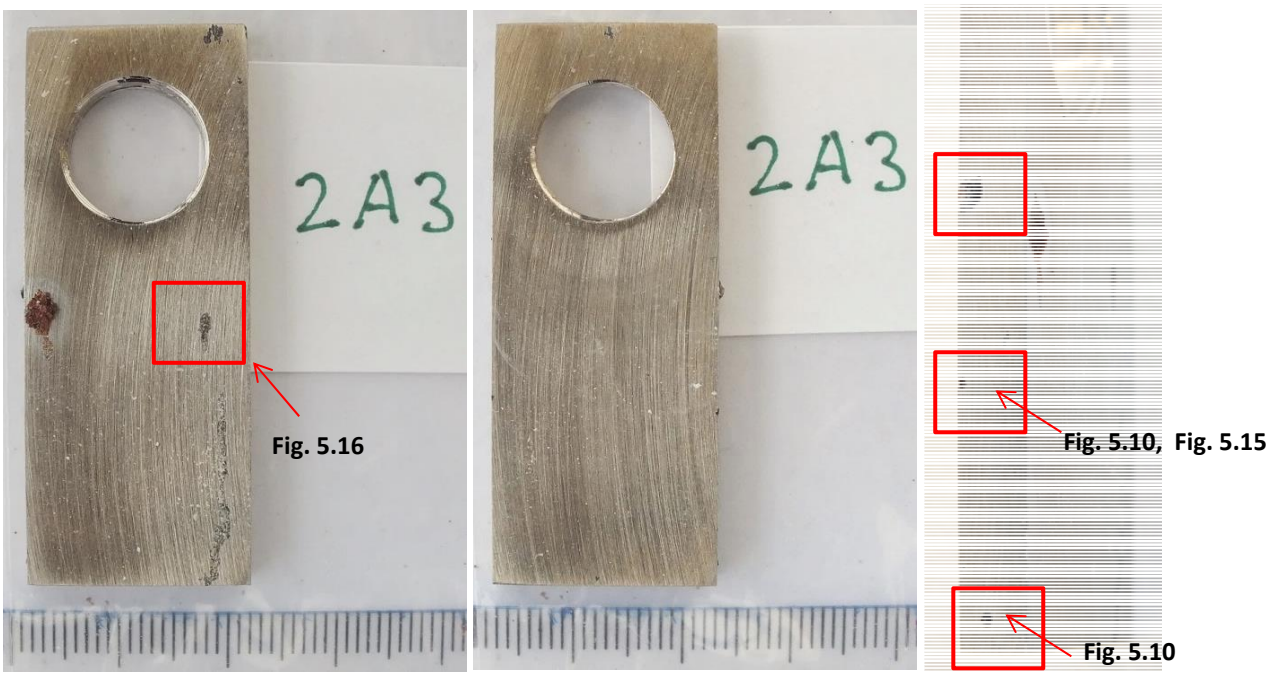

Figure 5.6: Photographs showing corrosion coupon ref. 2A3 (EBW), one side and the other

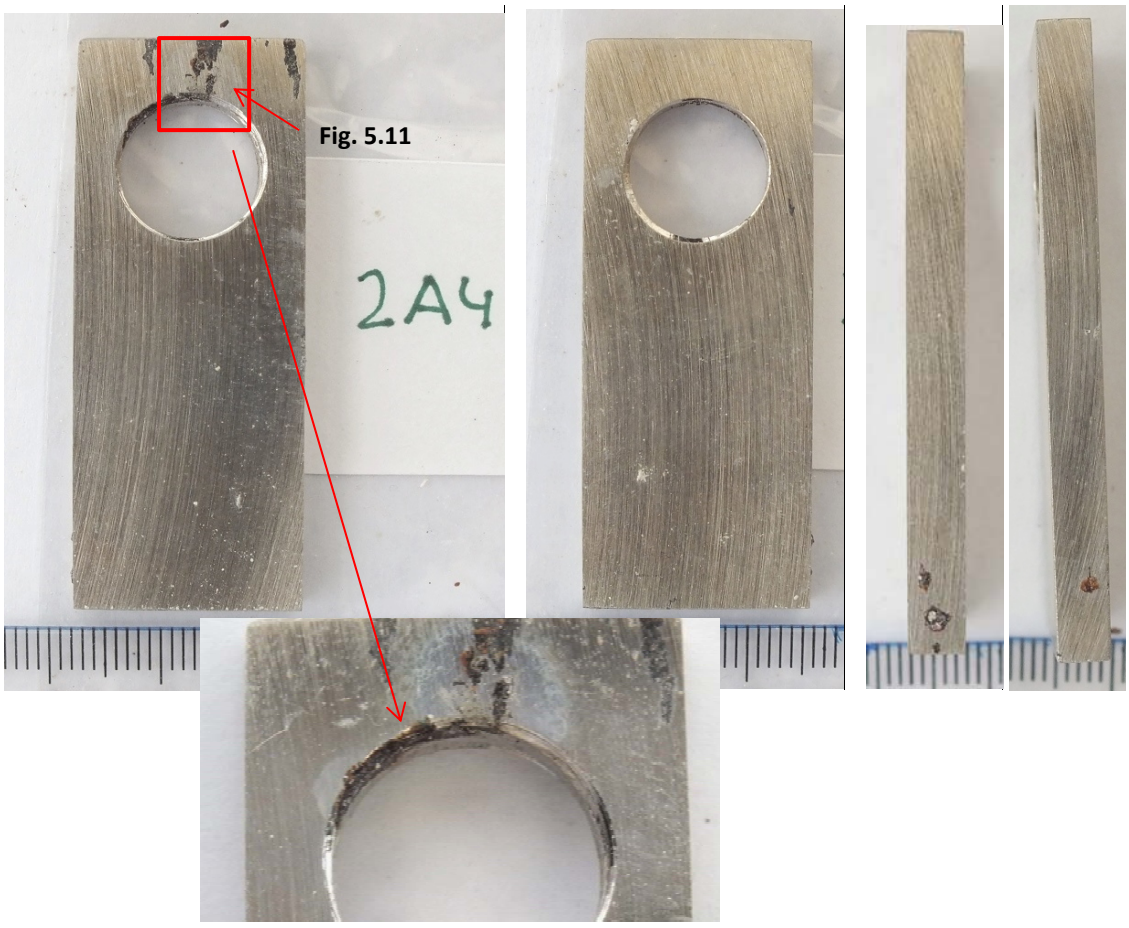

Figure 5.7: Photographs showing corrosion coupon ref. 2A4 (GTAW), one side and the other

5.2.2 Corrosion products analysis: SEM/EDS and RAMAN

The corrosion products and/or deposits generated in the 316L corrosion products are analysed by EDS. Analysis are conducted on the specimens on reception, in order to avoid contamination of samples during cutting steps. The most significant aspects of these analyses are described below.

Analyses of the reddish corrosion products associated to cracking, show them to be enriched with the elements iron and oxygen, Figures 5.8 and 5.9. As well as iron, the analyses identify chrome and nickel, as elements making up the stainless steel, and silicon, calcium, magnesium and aluminum, as elements making up the bentonite surrounding the samples. EDS analysis carried out on the brownish-black pits show them to be more enriched with chromium, Figure 5.10. The EDS analyses carried out in all the corroded areas of the coupons detect a significant chloride peak, sometimes predominant, as in Figure 5.11. Table 5.2 lists the semi-quantitative elemental chemical composition obtained in the EDS analyses carried out.

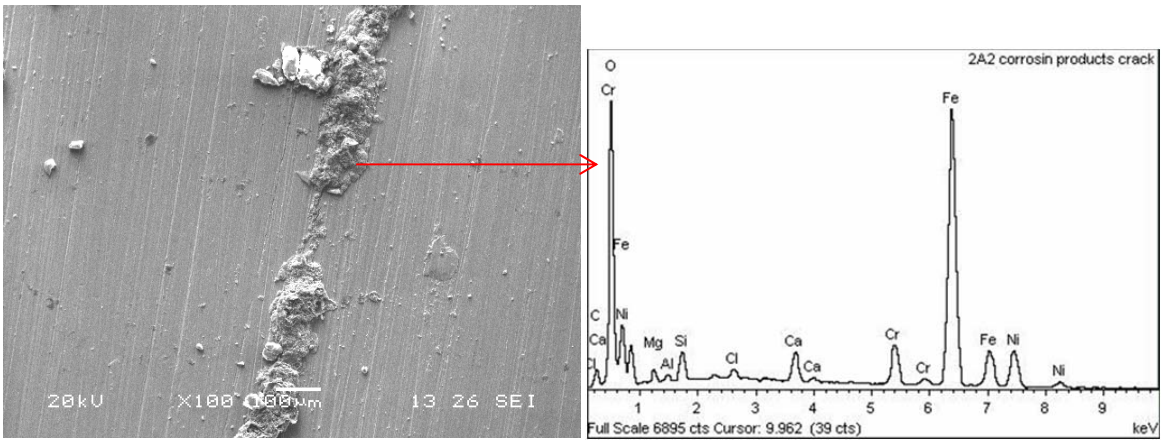

Figure 5.8: Electron micrograph of the surface of coupon ref. 2A2 showing detail of cracking and the corresponding EDS spectrum

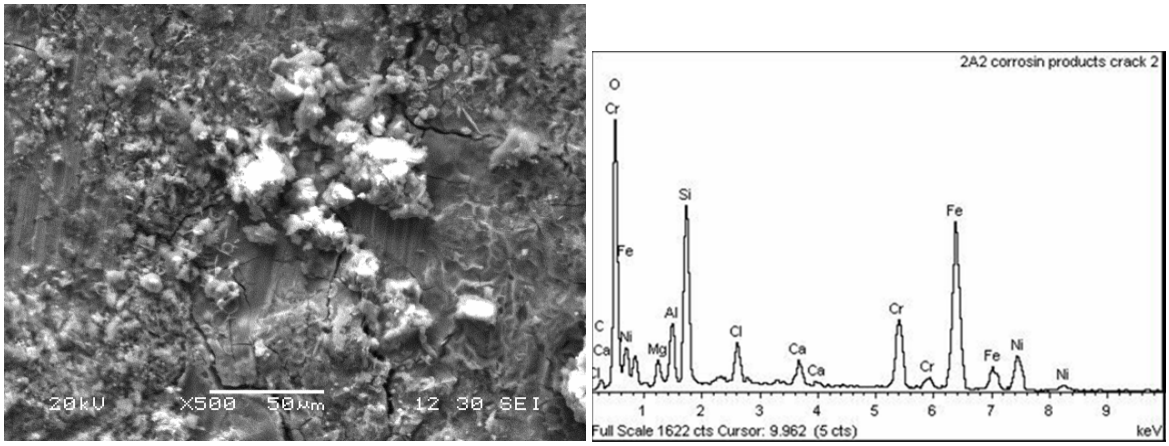

Figure 5.9: Electron micrograph of the surface of coupon ref. 2A2 showing detail of cracking and the corresponding EDS spectrum

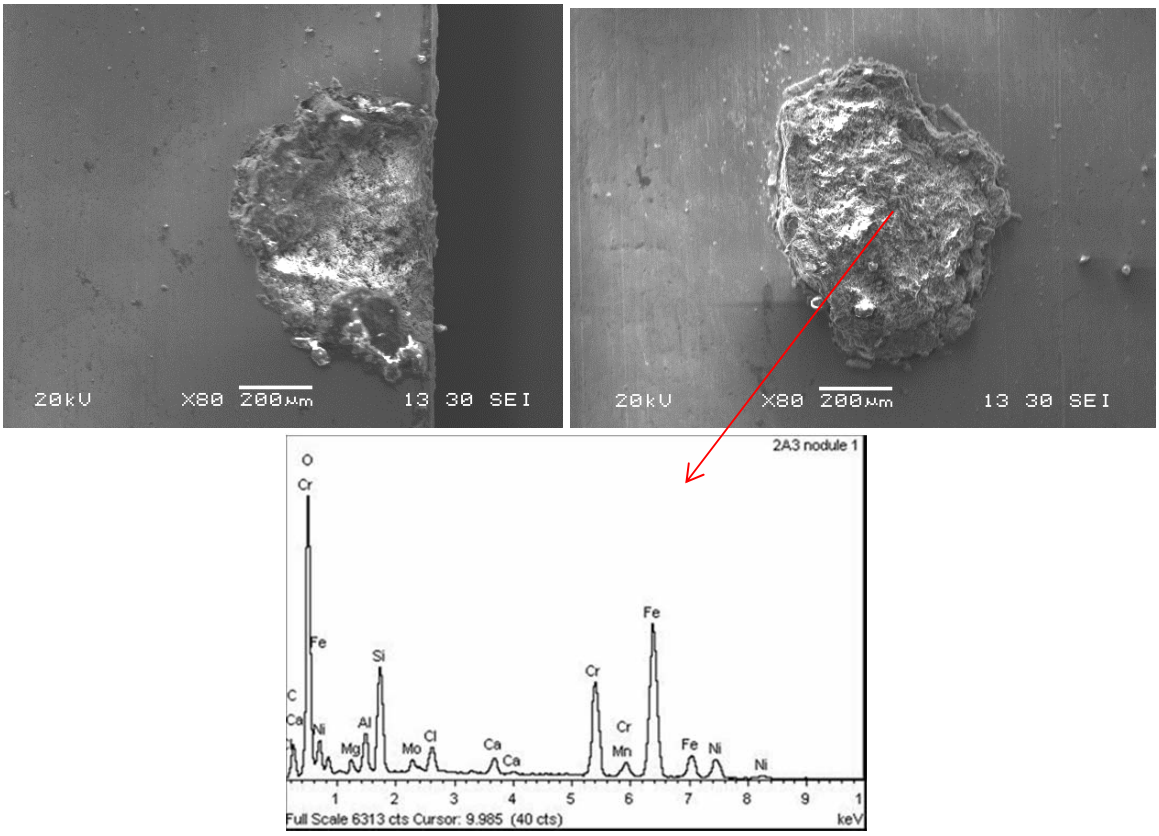

Figure 5.10: Electron micrographs of two pits on coupon ref. 2A3 and the corresponding EDS spectrum

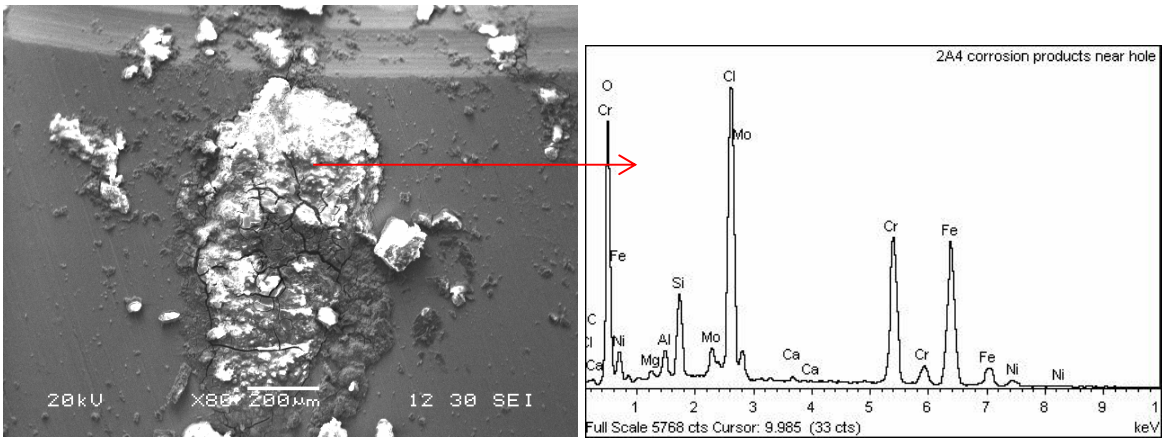

Figure 5.11: Electron micrograph of "shallow" corroded area on coupon ref. 2A4 (see Fig.5.7) and the corresponding EDS spectrum

EDS analysis	Element (wt%)													
	C	O	Mg	Al	Si	Cl	K	Ca	Cr	Mn	Fe	Ni	Mo	Total
2A2 "nodule"		40.79	1.56	5.04	15.12	5.03	0.52		8.05		23.90			100.00
2A2 corrosion products crack	4.94	31.15	1.02	0.37	1.49	0.51		1.76	4.25		45.19	9.33		100.00
2A2 corrosion products crack 2	3.44	34.30	1.63	3.25	9.12	2.21		1.40	7.90		28.00	8.76		100.00
2A4 corrosion products near hole	6.83	34.75	0.47	1.07	3.21	13.37		0.18	14.66		21.46	1.28	2.72	100.00
2A3 "nodule" 1	15.51	35.36	0.81	1.75	4.48	1.20		0.83	9.54	0.51	24.22	4.45	1.35	100.00

Table 5.2: Semi-quantitative elemental chemical composition obtained in the EDS analyses carried out on stainless steel coupons ref. 2A2, 2A3 and 2A4

No valuable results were obtained in the XRD analyses carried out on the cracking areas and pits on coupon ref. 2A2. The XRD spectra of the sample only detect the substrate, given the little amount of corrosion products generated. In order to stoichiometrically characterise the corrosion products generated inside the pits, a micro RAMAN spectroscopy analysis was carried out on a metallographic probe, using a 785 nm laser. Very little information was also obtained in the RAMAN analysis. One of the spectra obtained associates the main peaks to magnetite (Fe_3O_4), Figure 5.12.

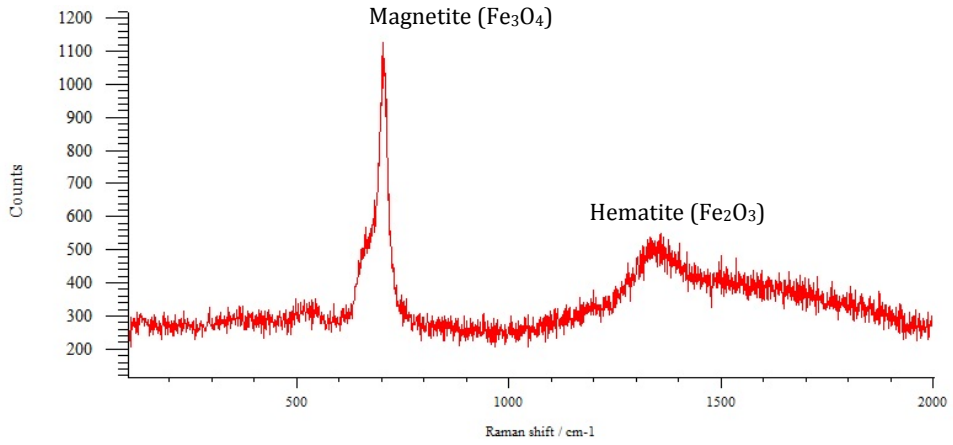

Figure 5.12: Raman spectrum obtained in the analysis of the corrosion products in one pit of sample ref. 2A2 (see Figure 5.16, top)

In order to obtain more information about the composition of the corrosion products generated in the pits, EDS analyses were conducted to determine the spatial distribution of the elements in the corrosion products. Figure 5.13 shows the back-scattered electron micrograph obtained in a pit section from coupon ref. 2A2, together with the maps of the different elements detected in the EDS analyses. The obtained results indicate that:

- Oxygen and chromium are the main constituents of the corrosion products generated inside the pit
- Chlorides are also detected in the corrosion products. Chloride concentration is slightly higher at the bottom of the pit
- Iron oxide (apparently associated to magnetite) is only detected at the top of the pit.

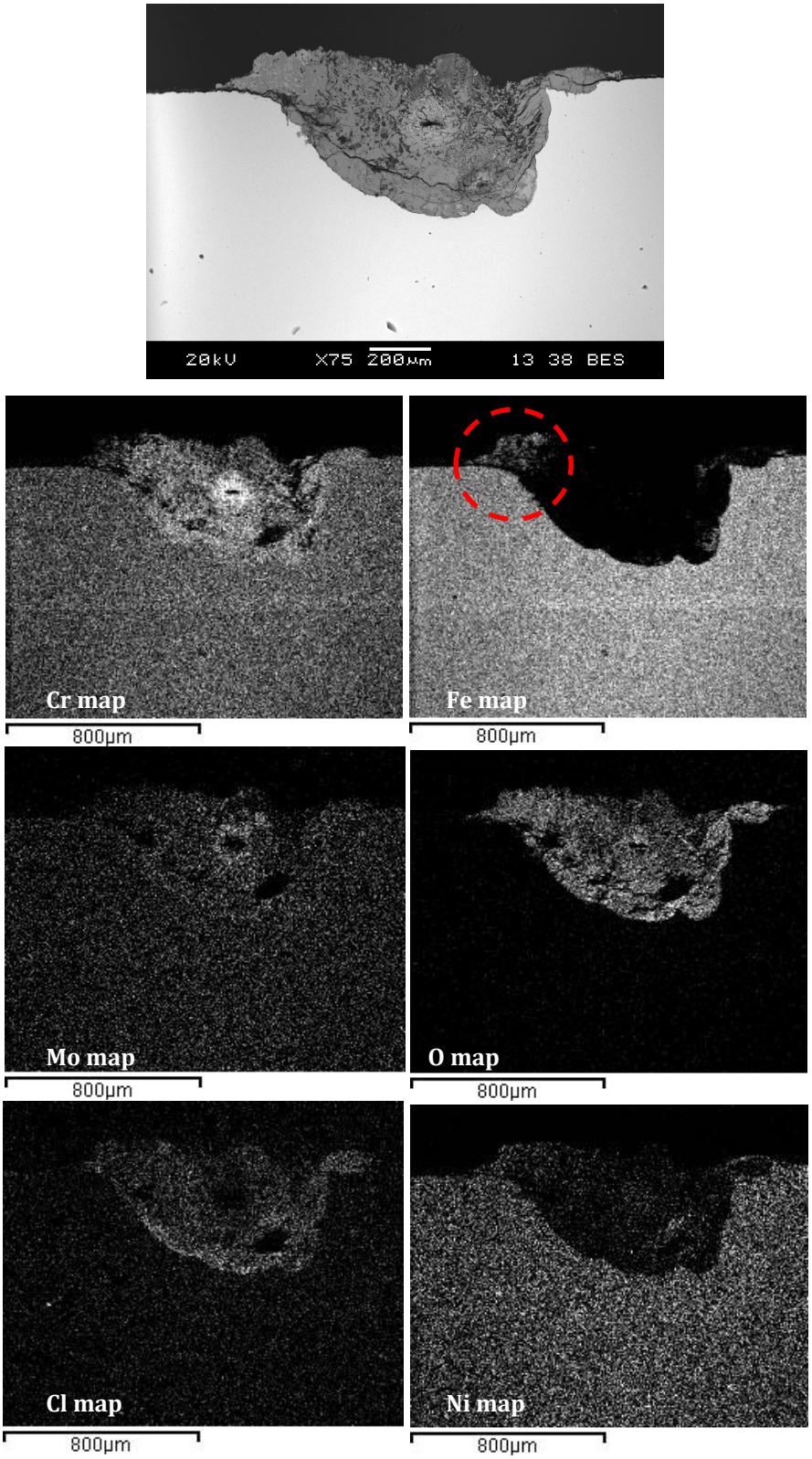

Figure 5.13: Back-scattered electron micrograph of pit section from coupon ref. 2A2, and associated element maps

5.2.3 Metallographic study

In order to analyse the microstructure, morphology and extent of the corrosion-derived damage, metallographic probes were prepared from cross sections extracted from coupons ref 2A2 (base) and 2A3 (EBW). These probes were then investigated under optical microscopy.

Optical micrographs in Figures 5.14 and 5.15 show a detail of the cracking observed on coupon ref. 2A2. Cracks initiate at the outer periphery, with a branched morphology with transgranular progression, typical of stress corrosion cracking (SCC) of stainless steels. Metallographic etching shows a non-sensitized austenitic microstructure for 316L stainless steel. In cracking areas there is observed a preferential corrosion of the ferrite bands.

Optical micrographs in Figure 5.16 show two of the pits observed on coupons ref. 2A2 and 2A3. Pitting cavities are filled with corrosion products forming caps over the pit cavities. The penetration depth for pit in coupon 2A2 is about 300 microns.

Micrograph in Figure 5.17 shows a section of the “shallow” corrosion area observed in coupon ref. 2A3. These areas are characterized by little corrosion penetration, with a preferential corrosion attack of the ferrite bands.

No significant differences are observed between base and welded samples.

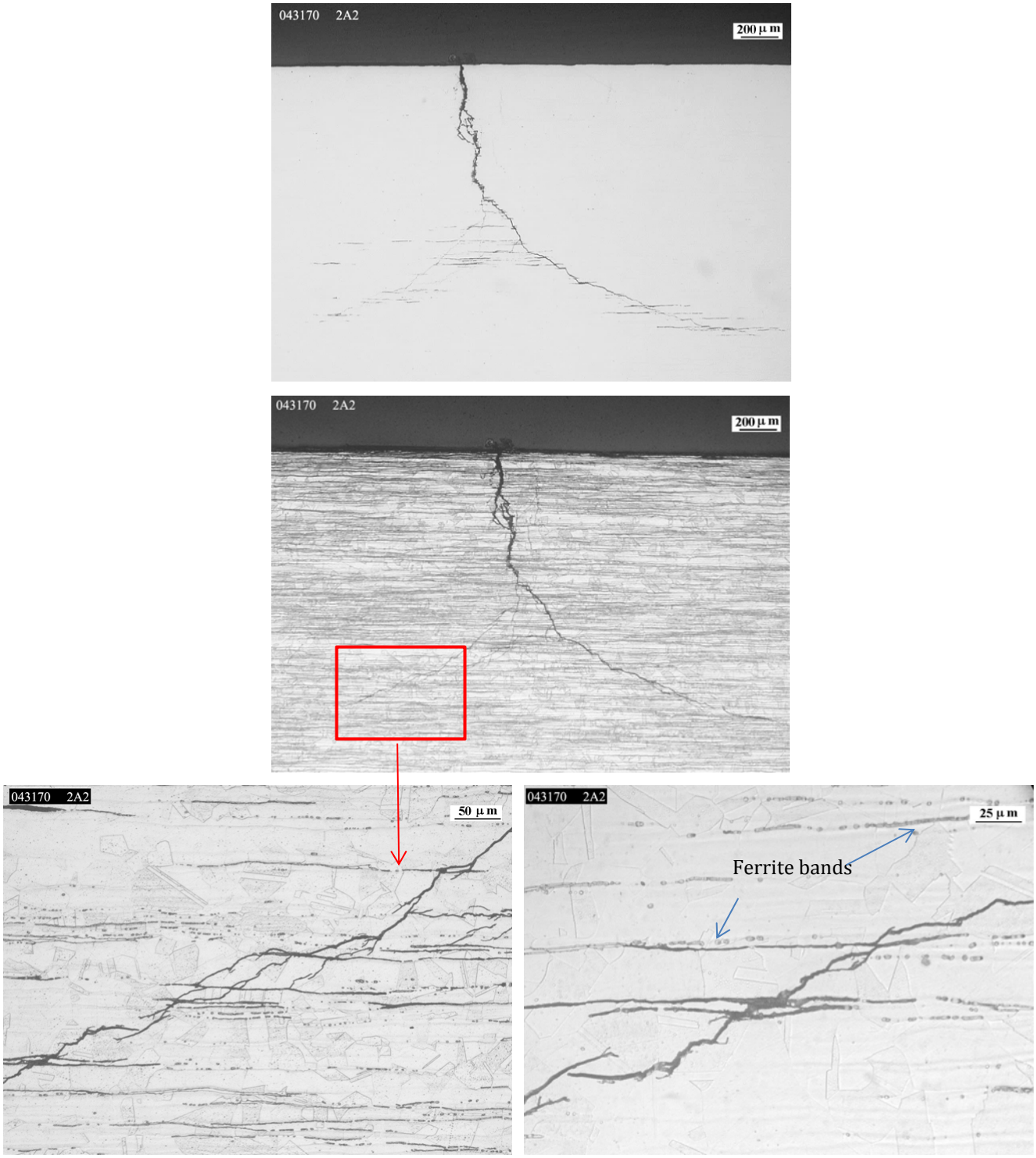

Figure 5.14: Optical micrographs of section of 316L stainless steel coupon ref. 2A2 showing transgranular cracking. Top unetched, middle and bottom with metallographic etching

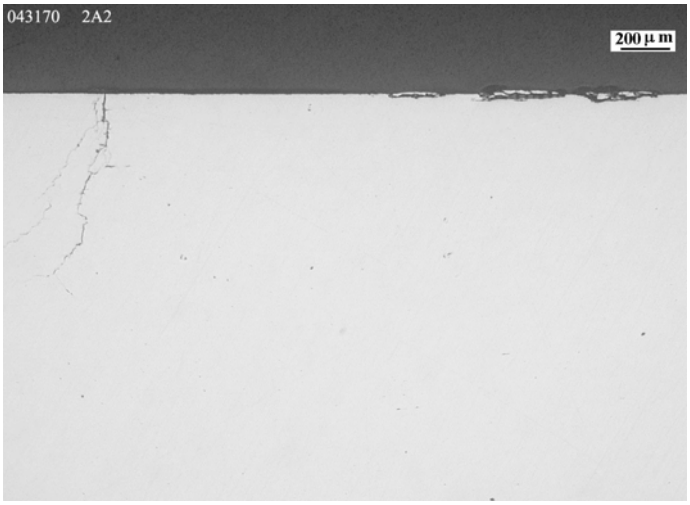

Figure 5.15: Optical micrograph showing cracking and shallow corrosion area for coupon ref. 2A2, unetched

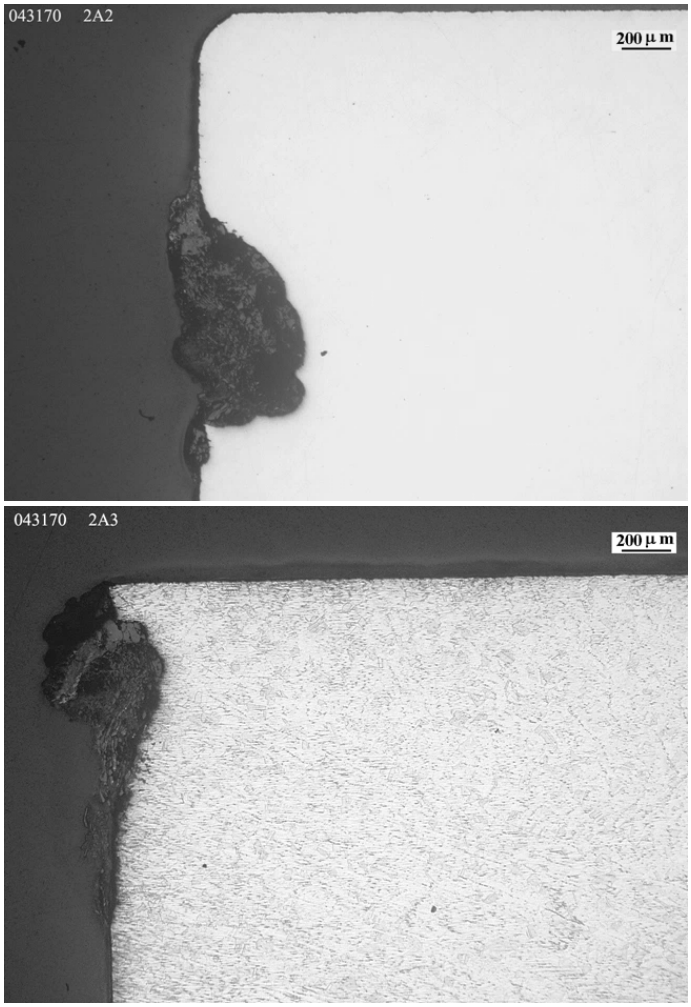

Figure 5.16: Optical micrographs of two sections of pits from coupons ref. 2A2 (top-unetched), and 2A3 (bottom - with metallographic etching)

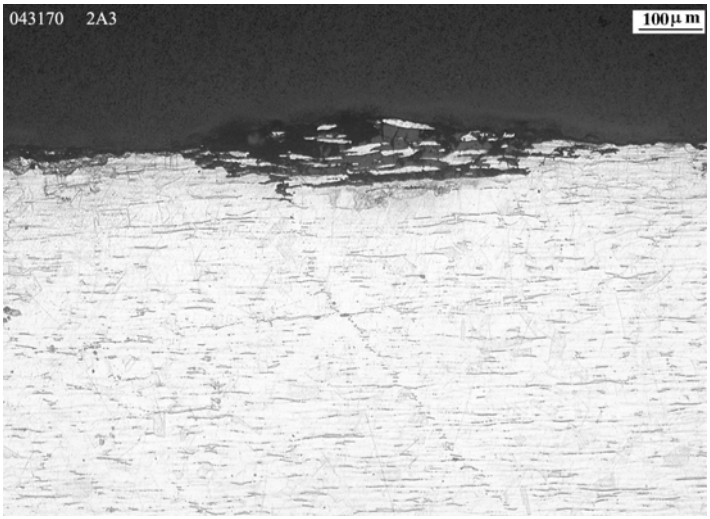

Figure 5.17: Optical micrograph of section of coupon ref. 2A3 (see Figure 5.6), with metallographic etching

5.3 Rack 3A: Titanium alloys coupons

5.3.1 Visual inspection

The aspect of the rack ref. A3 upon reception is shown in Figure 5.18. As it was indicated in the FEBEX-DP Extra Report No. 9, 04.07.2015, "Retrieving metallic coupons (Rack A) in the FEBEX experiment at Grimsel", Rack A3 was damaged and only partially recovered. Two titanium coupons were missing, and three of the recover titanium coupons were bent.

Initially a preliminary identification of the coupons was performed, based on their size. Once the coupons were weighted, the final identification was performed, according to Table 5.1.

Figures 5.19 to 5.24 show details of the 6 titanium alloys coupons. Visual inspection reveals little or no general corrosion. Reddish spots/particles are observed on the surface of almost all the titanium coupons. This is probably due to the corrosion of enriched iron particles. They appear to have been deposited or stuck on the surface of the samples.

Except for coupons ref. 3A2 and 3A3, used for metallographic analysis, the bentonite adhered in coupons ref. 3A4, 3A6, 3A7 and 3A8 has been removed with a plastic brush, as it can be seen in Figures 5.21 to 5.24.

No differences in corrosion behaviour are observed between welded and base material samples.

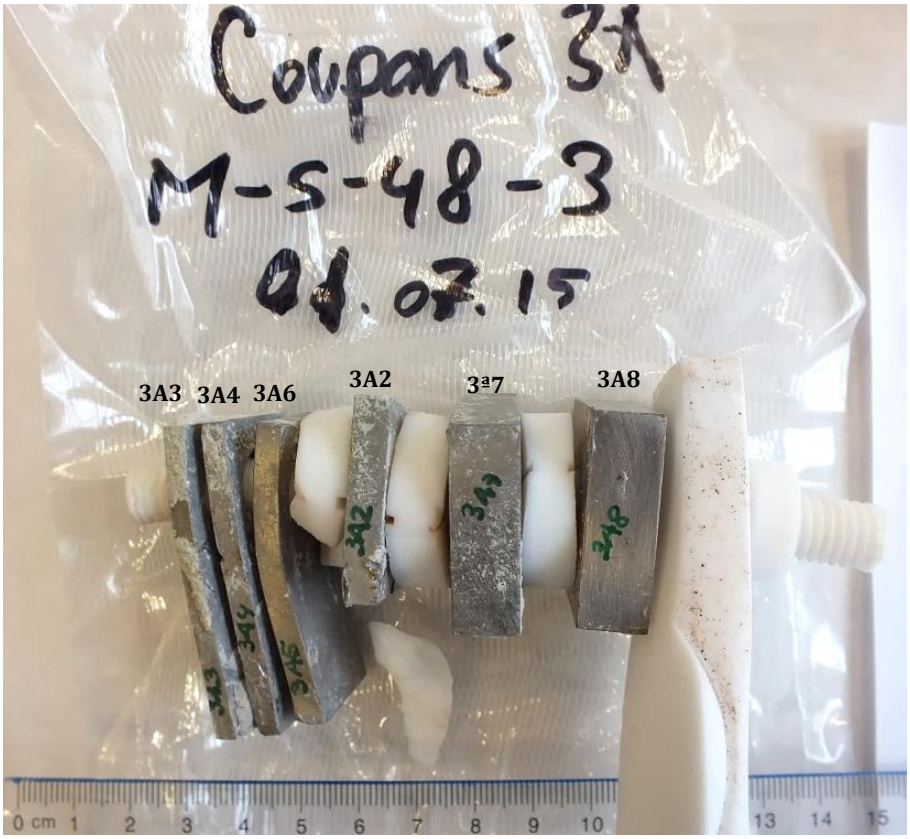

Figure 5.18: Macrographs showing general appearance on reception of rack ref. 3A (Titanium alloys)

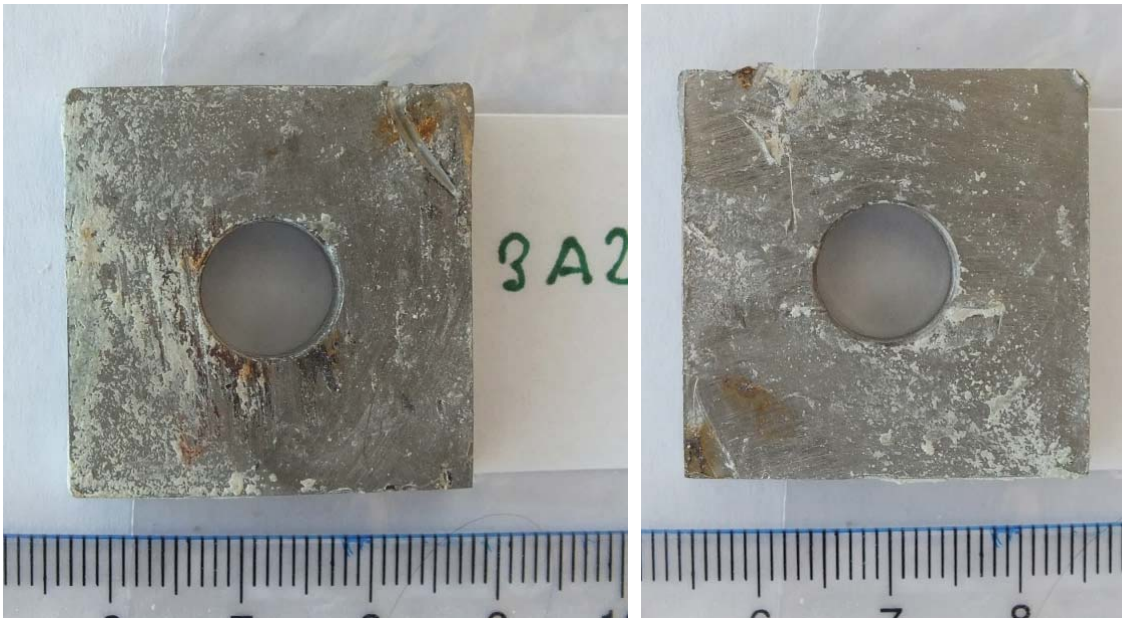

Figure 5.19: Photographs showing corrosion coupon ref. 3A2 (Ti2 EBW), one side and the other

Fig. 5.26

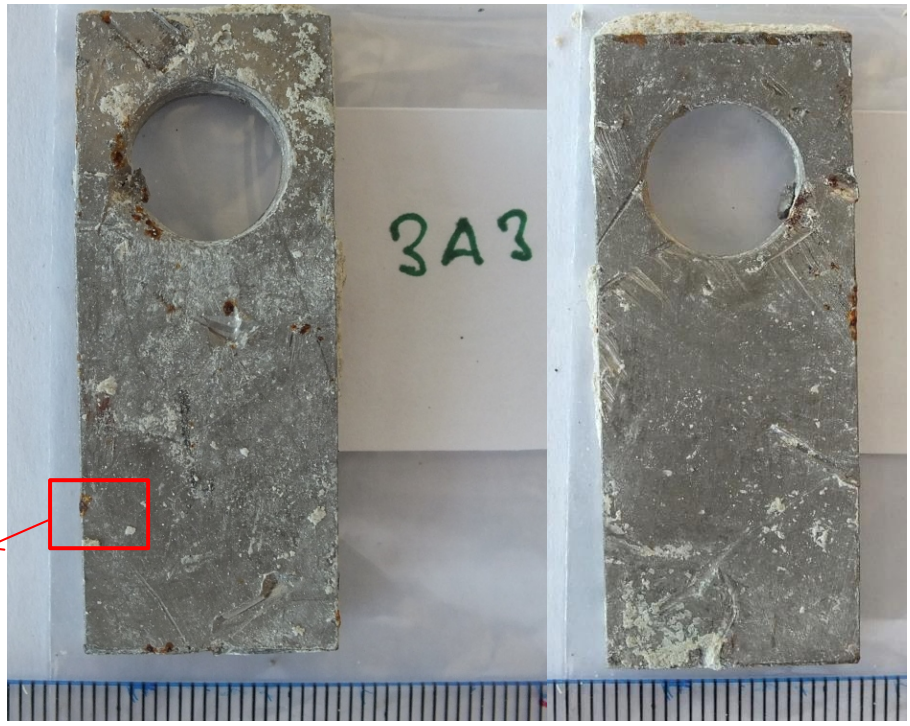

Figure 5.20: Photographs showing corrosion coupon ref. 3A3 (Ti7 base), one side and the other

Figure 5.21: Photographs showing corrosion coupon ref. 3A4 (Ti7 base), one side and the other

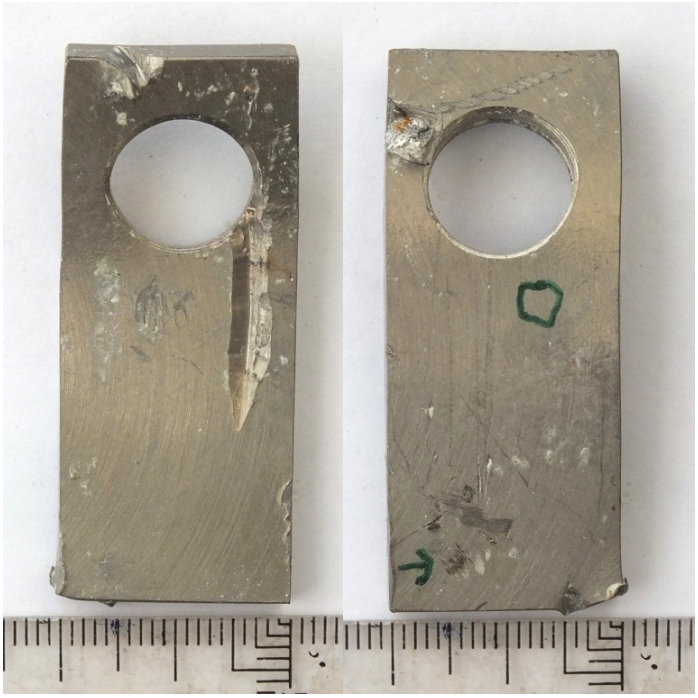

Figure 5.22: Photographs showing corrosion coupon ref. 3A6 (Ti7 PAW), one side and the other

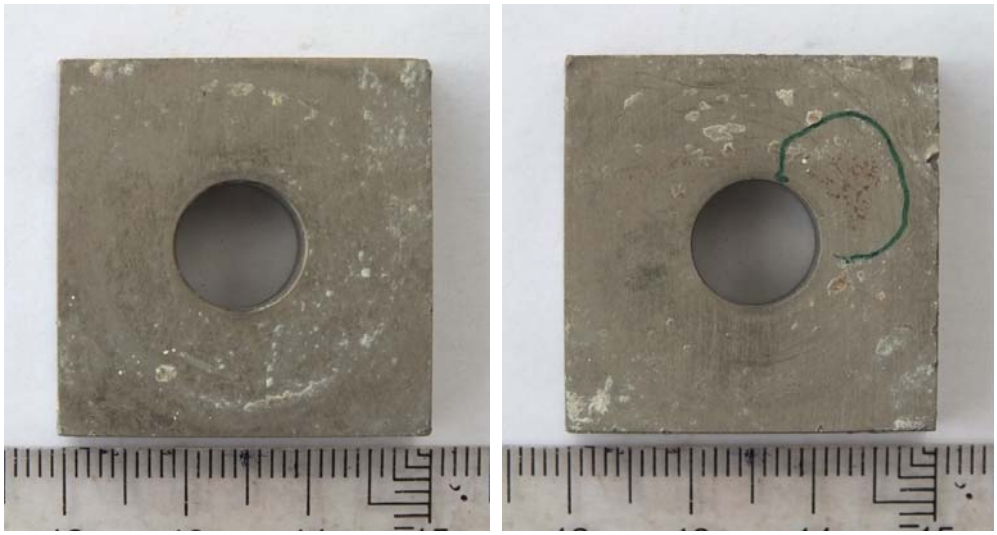

Figure 5.23: Photographs showing corrosion coupon ref. 3A7 (Ti12 Base), one side and the other

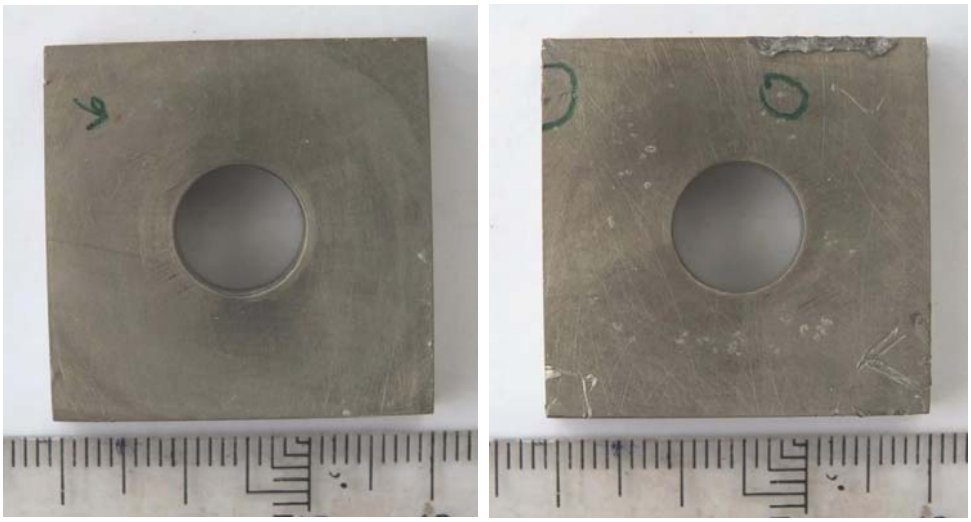

Figure 5.24: Photographs showing corrosion coupon ref. 3A8 (Ti12 Base), one side and the other

5.3.2 Corrosion products analysis: SEM/EDS and XRD

The SEM micrograph in Figure 5.25 shows a corroded "iron particle" on the surface of coupon ref. 3A3. EDS analyses indicate that these particles are composed principally of iron (Fe) and oxygen (O), as iron oxides.

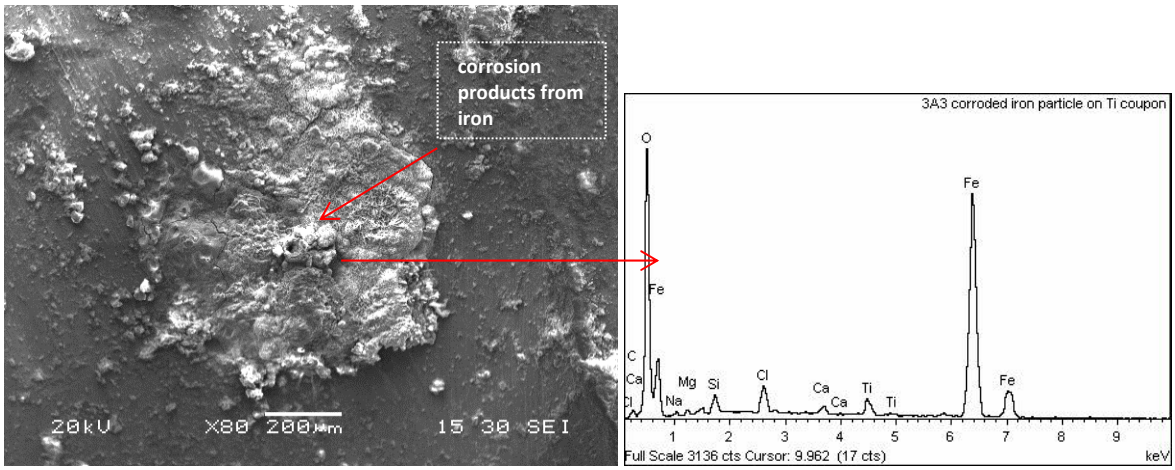

Figure 5.25: Electron micrograph showing detail of iron particle on the surface of coupon ref. 3A3 and the corresponding EDS spectrum

EDS analysis	Element (wt%)											
	C	O	Na	Mg	Al	Si	Cl	K	Ca	Ti	Fe	Total
3A3 corroded iron particle	2.12	39.91	0.59	0.52		1.22	1.97		0.58	1.75	51.33	100.00
3A2 corroded iron particle	9.24	47.01	0.74	2.33	4.22	12.03	1.57	0.34	1.75	1.46	19.30	100.00

Table 5.3: Semi-quantitative elemental chemical composition obtained in the EDS analyses carried out on titanium alloy coupons

No useful results were obtained in the XRD analysis. The XRD spectrum obtained for coupon ref. 3A3, only produces peaks for the substrate (titanium alloy).

5.3.3 Metallographic study

Optical micrographs in Figure 5.26 and 5.27 show two cross sections from coupons ref. 3A2, that contained iron particles. These particles are almost fully corroded.

Iron corroded particles seem to be associated to some kind of contamination of the coupons before testing or during the test.

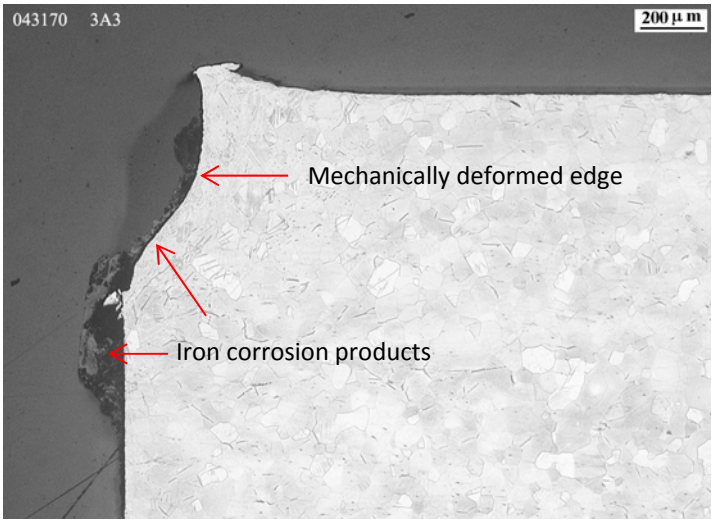

Figure 5.26: Optical micrograph of section of coupon ref. 3A3 (TiGr7), showing a mechanical deformed edge and iron corrosion products on its surface, with metallographic etching

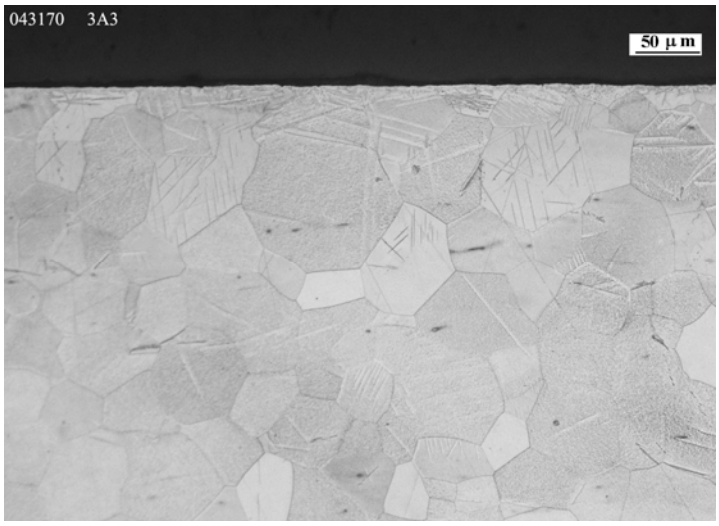

Figure 5.27: Optical micrograph of coupon ref. 3A3, with metallographic etching

5.4 Rack 4A: Copper alloy coupons

5.4.1 Visual inspection

This rack consists of 5 coupons: 2 of Cu-ETP copper (4A1 and 4A2), 2 of Cu10Ni cupronickel (4C3 and 4C4) and 1 of Cu30Ni (cupronickel (4C5). Figure 5.28 shows the appearance upon reception of rack ref. 4A.

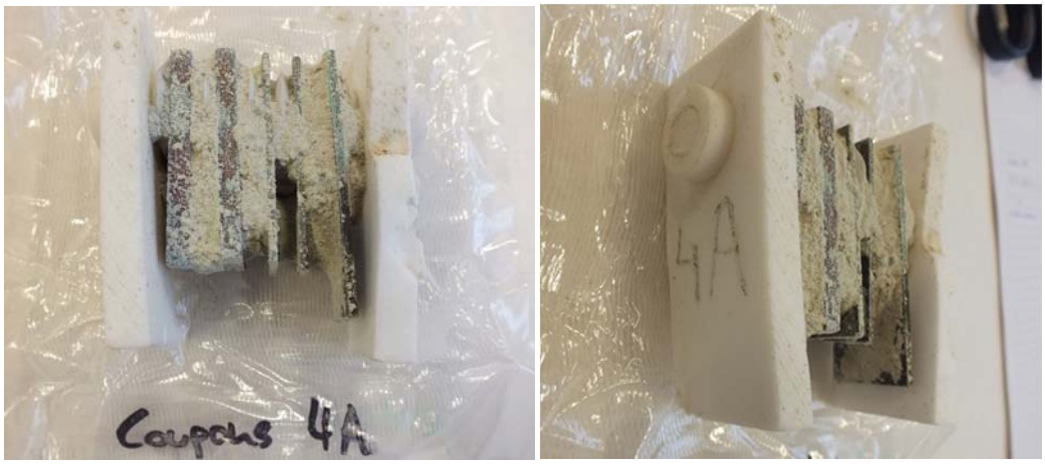

Figure 5.28: Macrographs showing general appearance on reception of rack ref. 4A

Cu-ETP coupons

The surface of the Cu-ETP coupons show a brownish-red color, with greenish areas mixed with bentonite, Figures 5.29 and 5.30. Uniform general corrosion appears to be the predominant mechanism observed, with a quite adherent oxide layer. Only when the adhered bentonite in coupon ref. 4A2 is removed with a plastic brush, there are observed small areas of localized corrosion in one edge of the coupon, Figure 5.30.

Figure 5.29: Photographs showing coupon ref. 4A1 (one side and the other)

Figure 5.30: Photographs showing coupon ref. 4A2 (one side and the other), and details of the corroded surface

Cu-10Ni and Cu30Ni coupons

The surface of the Cu-10Ni coupons shows a blackish-grey color, with greenish areas mixed with bentonite, Figures 5.31 and 5.32. Uniform general corrosion appears to be the predominant mechanism observed. There is no visible pitting or other types of localized corrosion.

With respect to the Cu30Ni, the test coupon examined shows a blackish-grey color, with greenish areas mixed with bentonite, Figure 5.33. Uniform general corrosion appears to be the predominant mechanism observed, with a quite adherent oxide layer generation. Of all copper coupons, this is the one that shows a smaller extension of the generalized corrosion.

Figure 5.31: Photographs showing corrosion coupon ref. 4A3 (one side and the other)

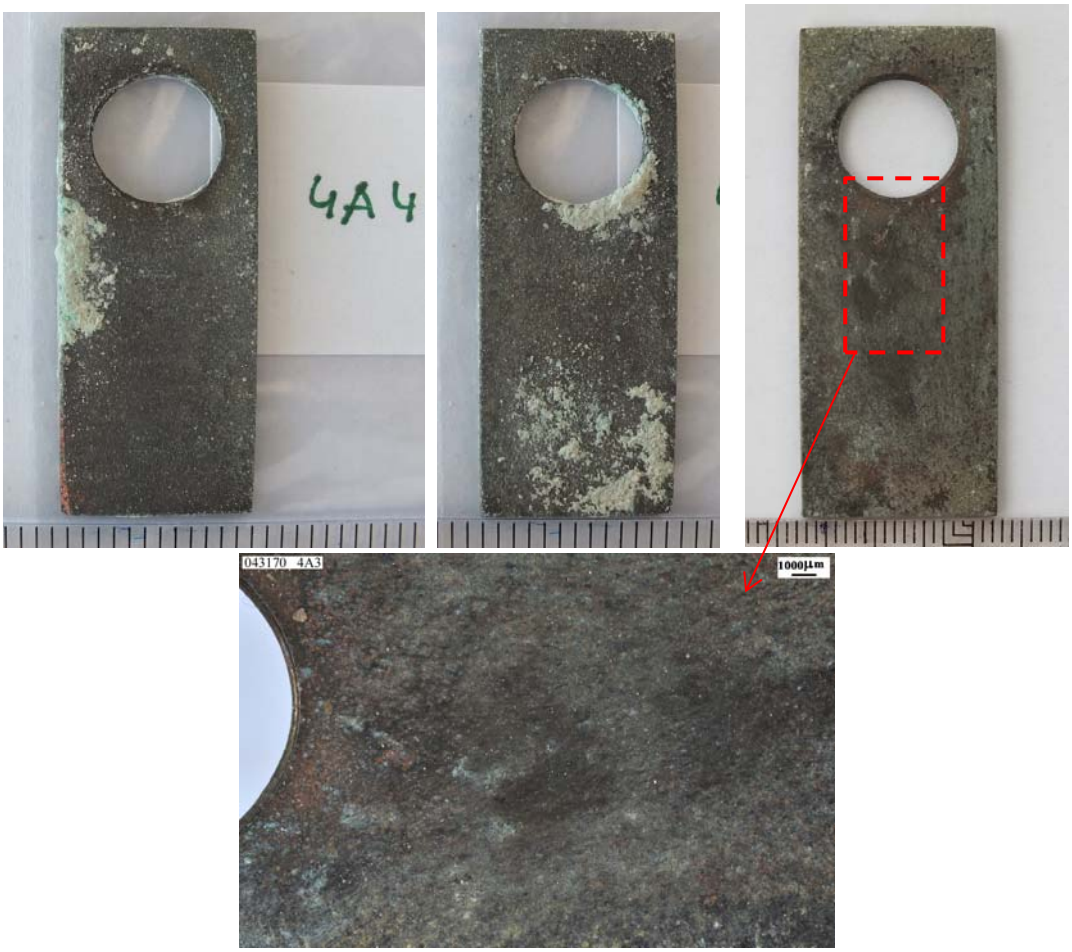

Figure 5.32: Photographs showing corrosion coupon ref. 4A4 (one side and the other)

Figure 5.33: Photographs showing corrosion coupon ref. 4A5, one side and the other

5.4.2 Corrosion products analysis: SEM/EDS and XRD

The SEM micrograph in Figure 5.34 shows a detail of the surface of coupon ref. 4A1. EDS analyses indicate that this surface is composed principally of copper and oxygen. Chloride is detected in all the corrosion products examined. The amount of chloride detected is higher for the blue greenish surface. Silicon, aluminum, magnesium and calcium proceeding from the adhered bentonite are also detected.

The XRD spectrum of the surface of coupon ref. 4A1 reveals that the oxide layer generated could correspond to the molecular cuprite Cu_2O, Figure 5.35.

EDS spectra from the cupronickel coupons, Figures 5.36 and 5.38, indicate oxide layers enriched in oxygen and nickel. Chloride peaks are also observed. In particular, a Cl peak is observed on a Cu-10Ni coupon (4A3), which could show the presence of the $CuCl_2$ phase; this phase has not been detected in the XRD analyses. A mercury (Hg) peak is also detected for both cupronickel alloys, probably coming from a damaged sensor/s.

The XRD spectrum of the Cu10Ni surface reveals that the oxide layer generated corresponds to cuprite Cu_2O, Figure 5.37. it is important to point out that in the XRD spectrum only the crystalline species (diffracting ones) are shown, and the height/width of the peaks are not dependent on the amount, but rather the degree of crystallinity of the compound.

SEM examination of the Cu30Ni alloy reveals a lesser extension of the generalized corrosion, Figure 5.38.

The semi-quantitative results obtained in the EDS analyses carried out on copper alloy coupons are given in Table 5.4.

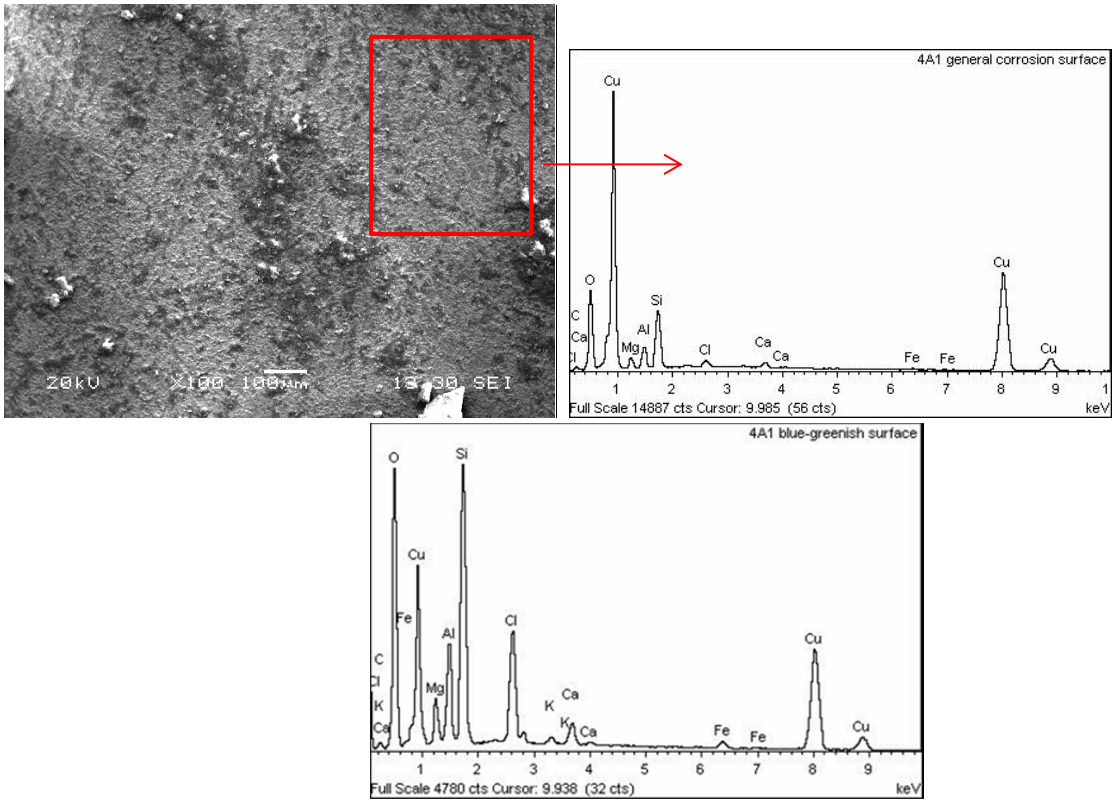

Figure 5.34: Electron micrograph showing detail of the surface of coupon ref. 4A1 and the corresponding EDS spectra

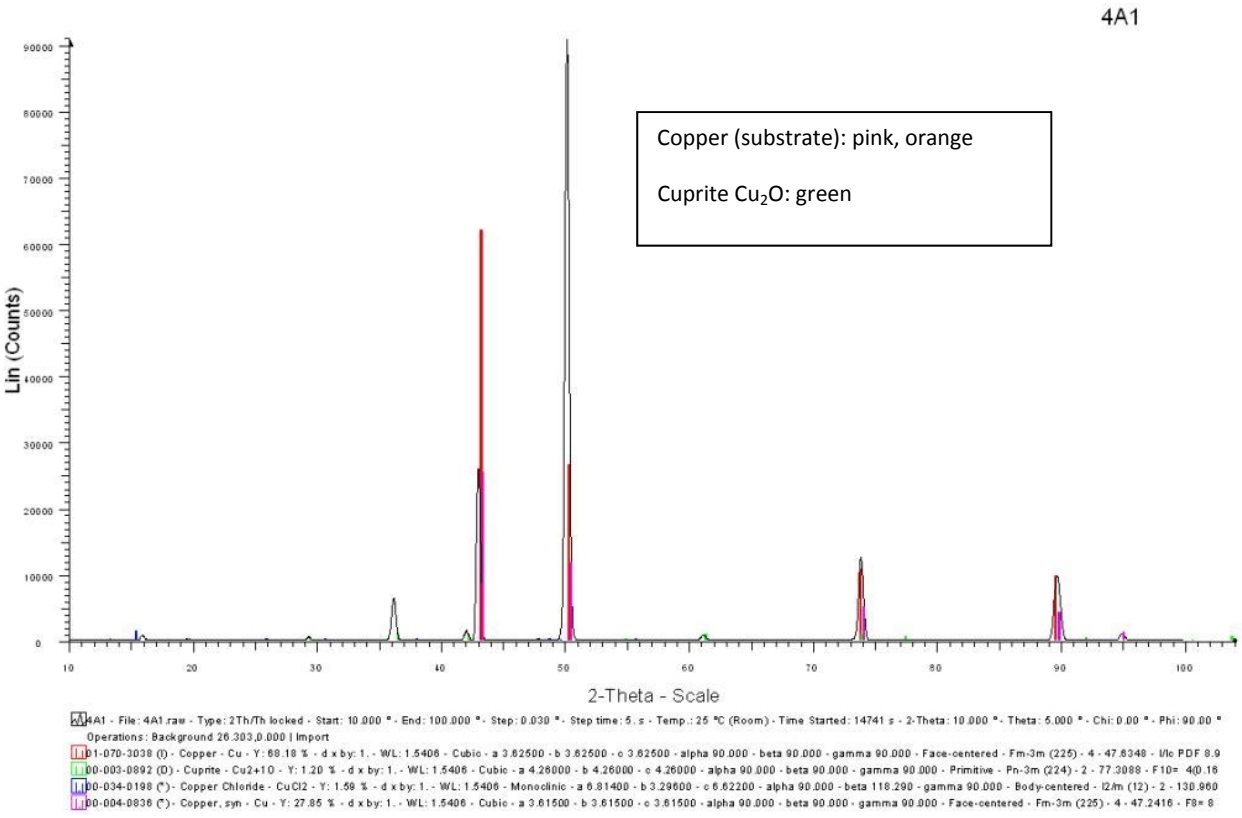

Figure 5.35: XRD spectrum of oxide layer on coupon ref. 4A1

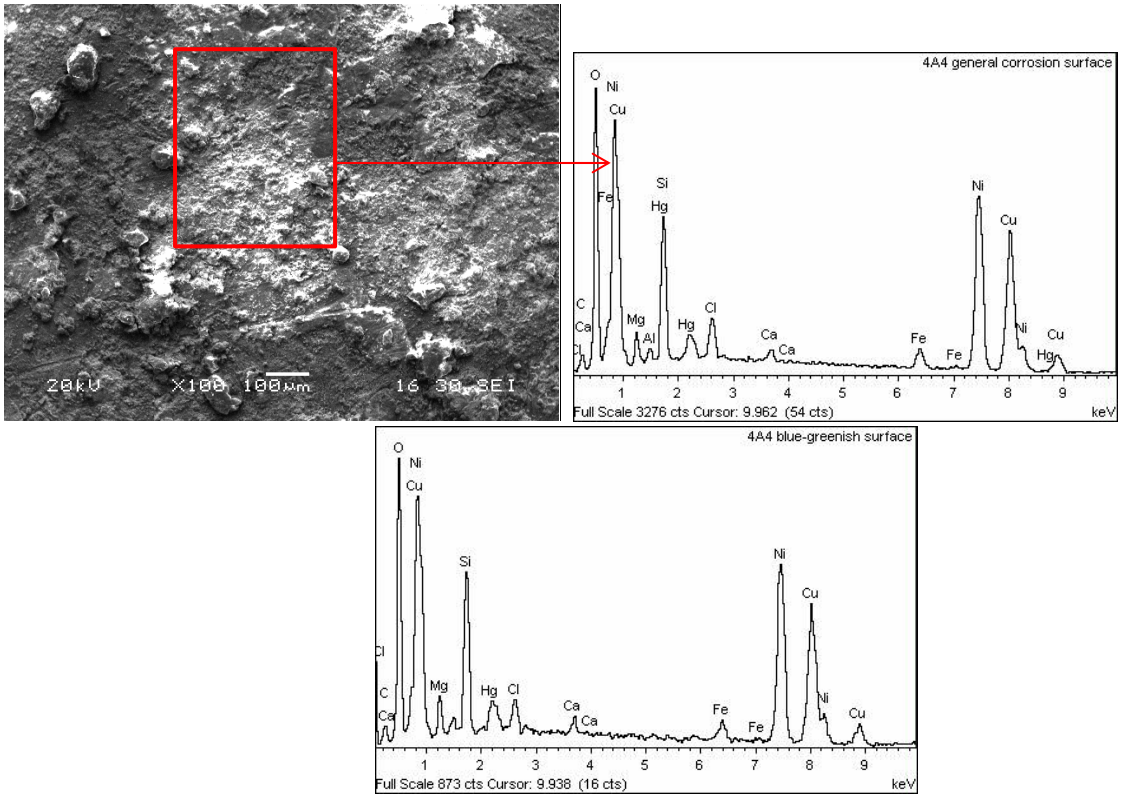

Figure 5.36: Electron micrograph showing detail of the surface of coupon ref. 4A4 and the corresponding EDS spectra

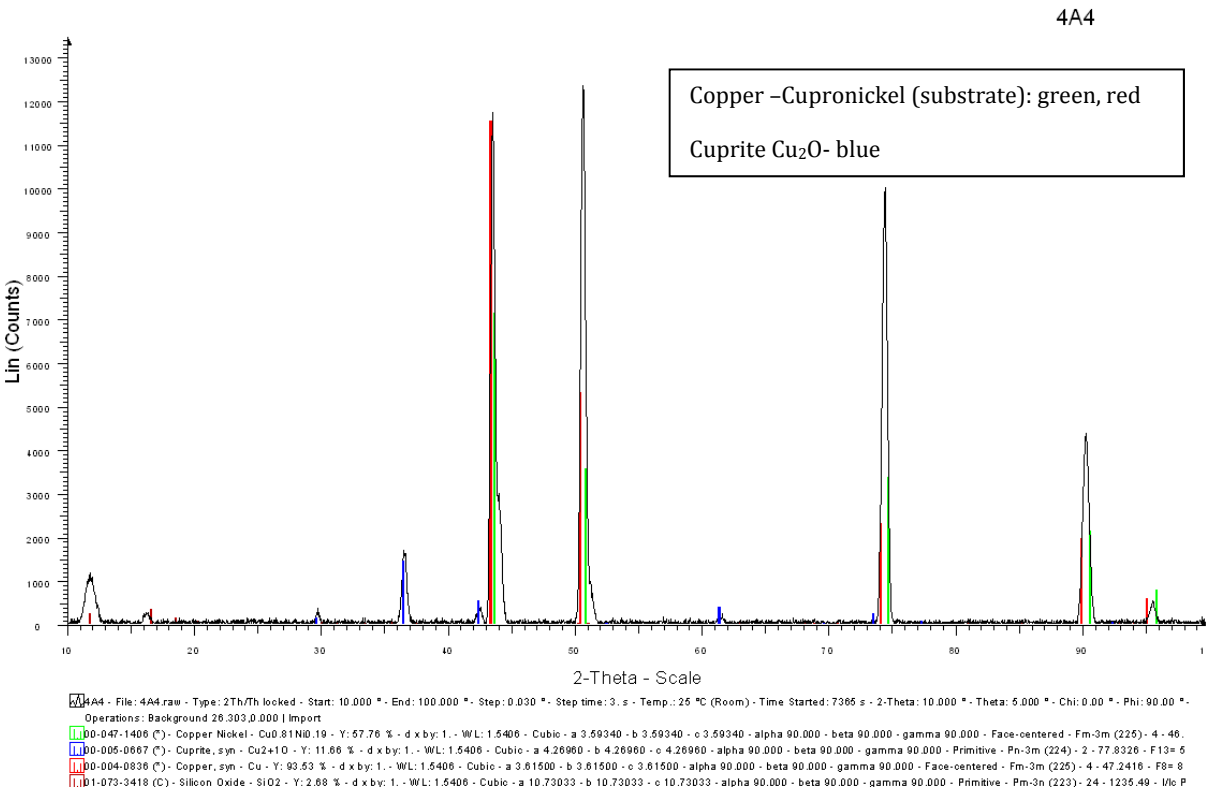

Figure 5.37: XRD spectrum of oxide layer on coupon ref. 4A1

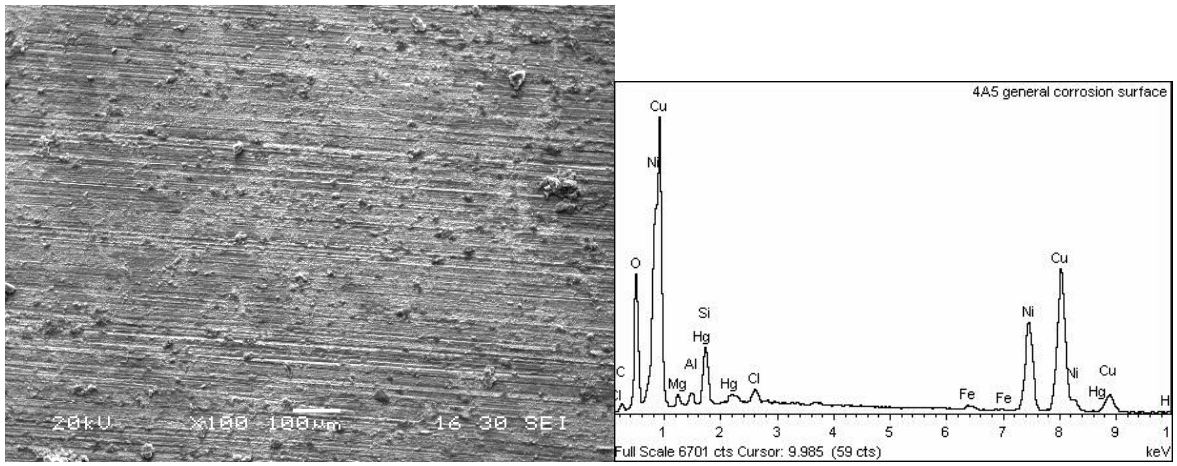

Figure 5.38: Electron micrograph showing detail of the surface of coupon ref. 4A5 and the corresponding EDS spectrum

EDS analysis	Element (wt%)													
	C	O	Mg	Al	Si	Cl	K	Ca	Mn	Fe	Ni	Cu	Hg	Total
4A1 general corrosion surface	2.16	22.77	1.97	2.99	7.06	0.75		0.61		0.39		61.29		100.00
4A1 blue-greenish surface	4.89	38.78	2.68	4.58	12.20	5.65	0.31	1.20		0.91		28.80		100.00
4A4 blue-greenish surface	4.58	25.45	2.50		6.08	1.27		0.63		1.63	27.76	26.67	3.41	100.00
4A4 general corrosion surface	4.25	25.75	1.81	0.57	5.41	1.57		0.48		1.82	27.92	27.82	2.61	100.00
4A3 general corrosion surface		24.47	1.58	0.59	5.01	1.60		0.50		1.15	24.94	35.14	5.03	100.00
4A3 general corrosion surface 2	2.13	32.03	2.18	1.41	7.33	8.04		0.78	0.33	1.36	11.80	29.86	2.77	100.00
4A5 general corrosion surface	3.01	19.59	1.28	0.97	3.83	0.84				0.47	22.28	46.20	1.54	100.00
4A5 blue-greenish surface		52.42	2.89	6.90	20.58	4.32	0.48	0.87		1.39	0.67	9.48		100.00

Table 5.4: Semi-quantitative elemental chemical composition obtained in the EDS analyses carried out on copper alloy coupons

5.4.3 Metallographic study

Optical micrographs in Figure 5.39 show a slight localized corrosion on one side of the copper coupon ref. 4A1. This small localized corrosion area was also observed in the visual examination of copper coupon ref. 4A2 (Fig. 5.30). The maximum penetration depth for this zone is about 100 microns. Apart from this, the copper coupon shows a generalized corrosion, with generation of a relatively uniform oxide layer, partially detached.

The cupronickel alloy ref. 4A4 shows a generalized corrosion mode. Few “micro-areas” of localized corrosion are observed in the embedded section of this coupon, with a maximum penetration depth less than 50 microns, Figure 5.40.

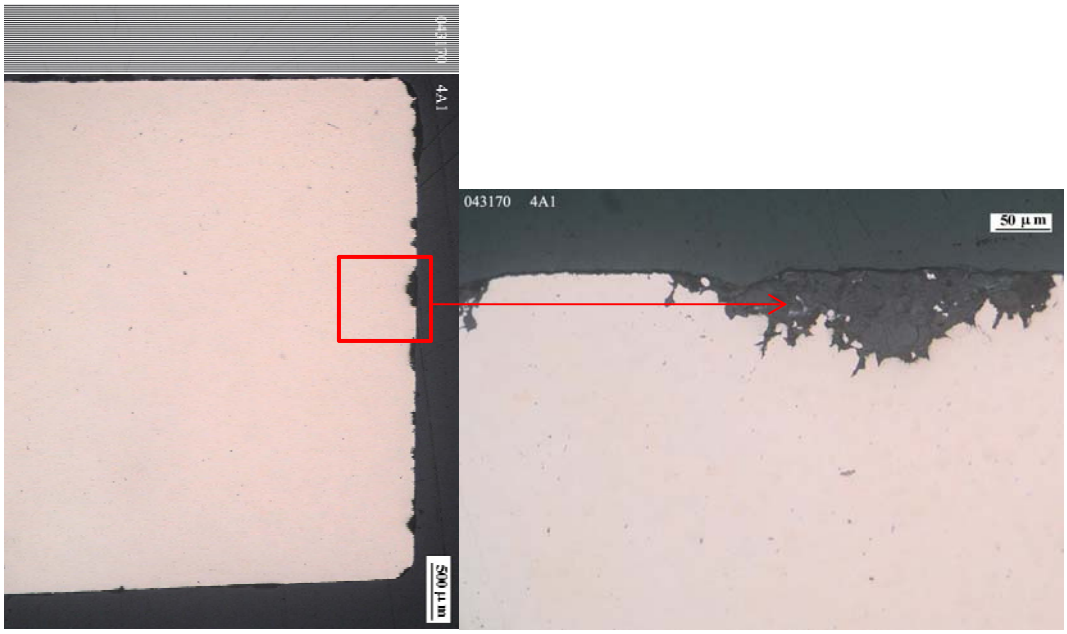

Figure 5.39: Optical micrographs of section of copper alloy ref. 4A1, unetched

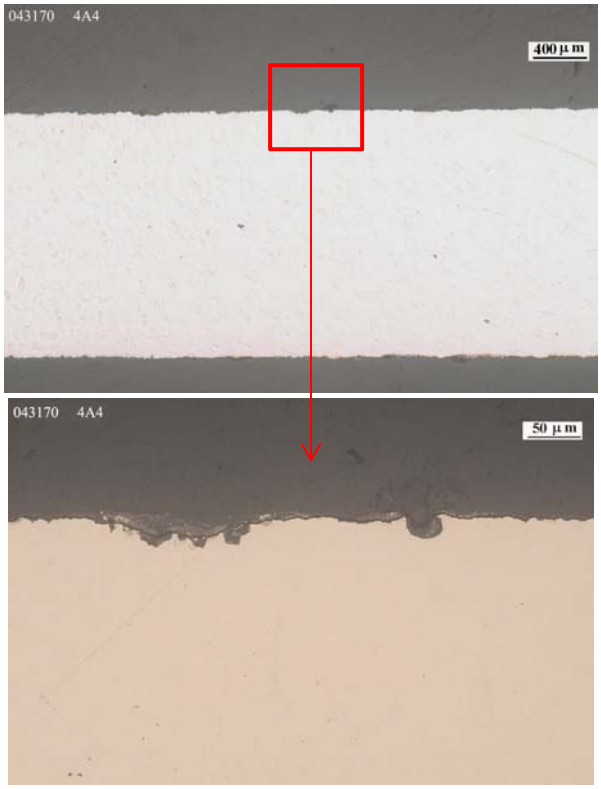

Figure 5.40: Optical micrographs of section of cupro-nickel alloy ref. 4A4, unetched

In order to obtain more information about the composition of the corrosion products inside copper pits, EDS analyses were conducted to determine the spatial distribution of the elements. Figure 5.41 shows the back-scattered electron micrograph obtained in a pit section from coupon ref. 4A1, together with the maps of the different elements. The obtained results indicate that the copper pit is filled with the elements making up the bentonite. Copper is not detected inside the pit.

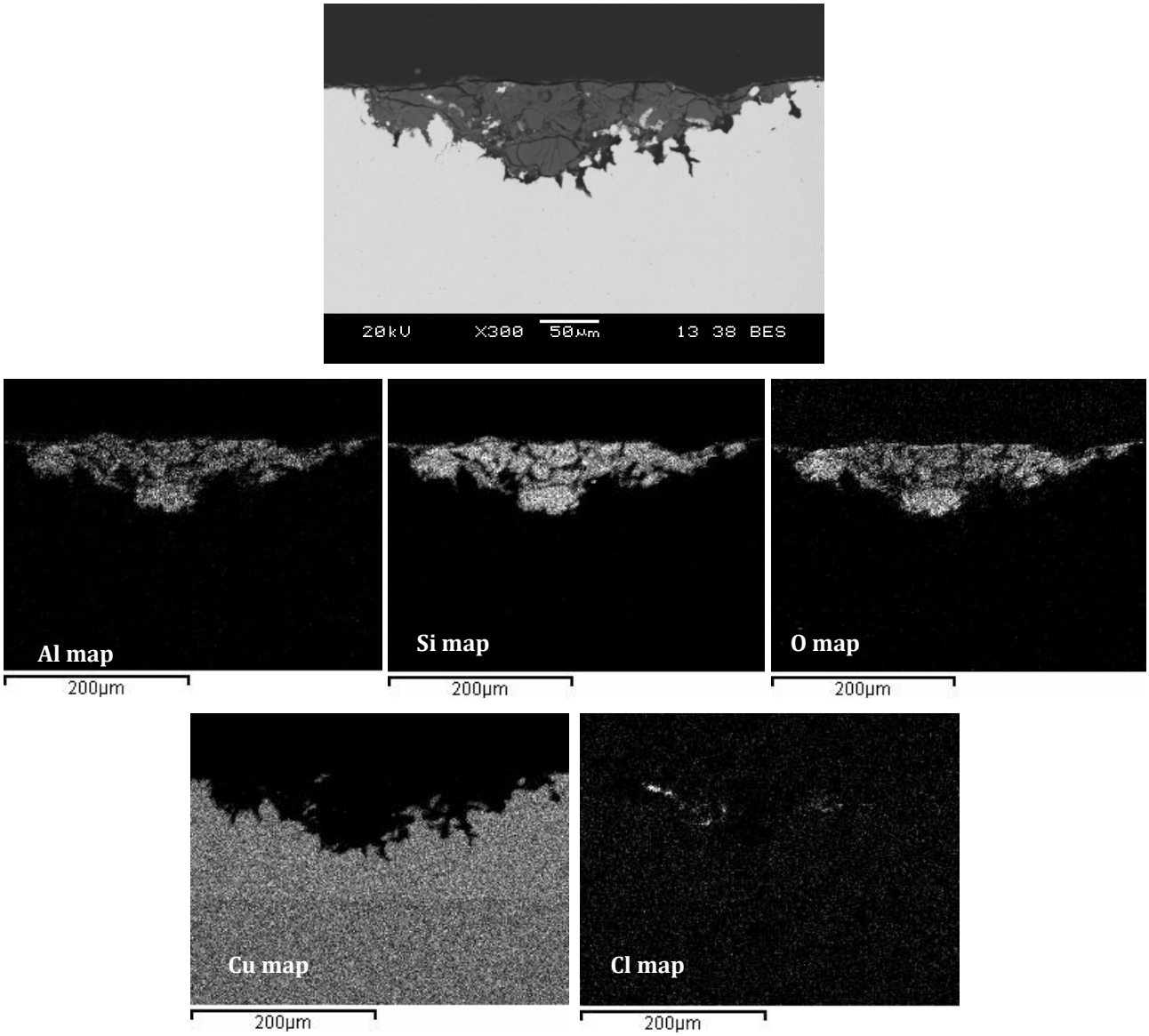

Figure 5.41: Back-scattered electron micrograph of pit section from coupon ref. 4A1 and associated element maps

6. LINER

The following liner samples were sent to TECNALIA:

ML-45-1, ML-45-2, ML-45-3 and ML-45-4
ML-52-1, ML-52-2, ML-52-3 and ML-52-4

All the liner samples were protected in vacuum pack (double aluminum foil). No vacuum loss was observed in any of the racks under study. Photographs showing the appearance of the liner quadrants on reception are given in Annex I of this document.

Figures 6.1 and 6.2 show the location of the liner samples in sampling section 45 and 52, respectively.

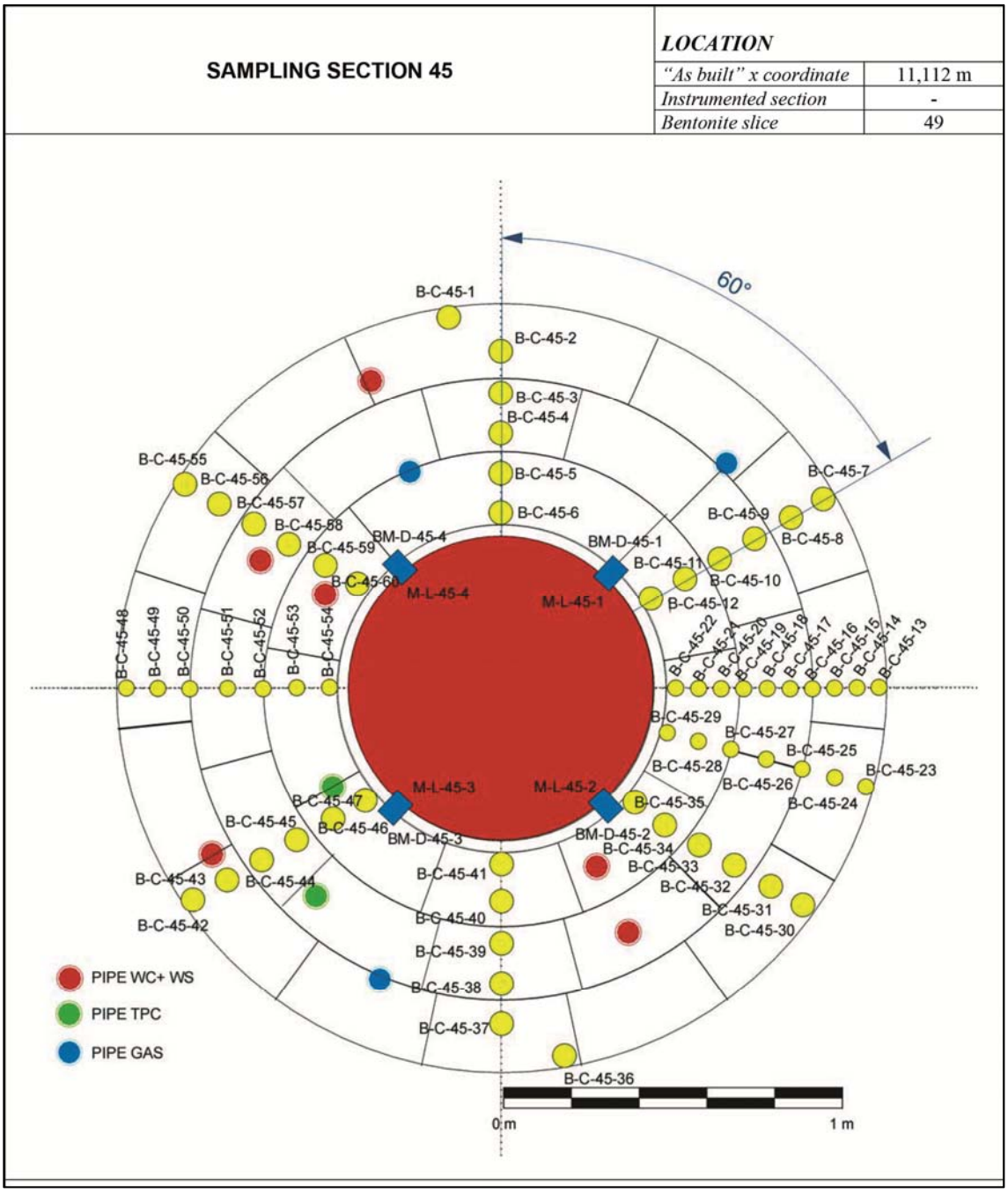

Figure 6.1: Location of liner quadrants in sampling section 45 (Bárcena & García-Siñeriz, 2015)

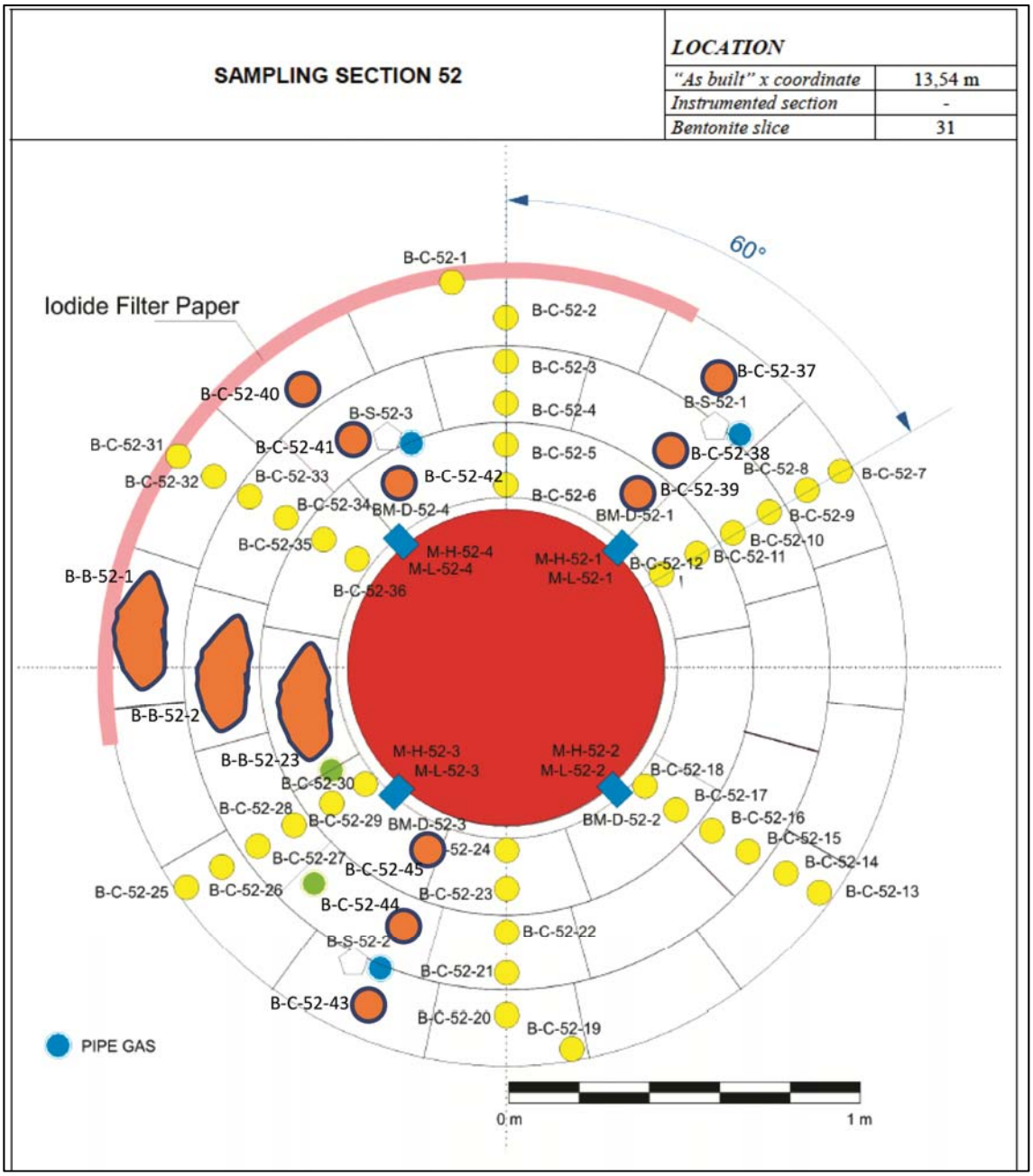

Figure 6.2: Location of liner quadrants in sampling section 52 (Bárcena & García-Siñeriz, 2015)

6.1 Section ML45

6.1.1 Visual inspection

The liner samples received at TECNALIA were visually inspected considering both the external and the internal side of the liner. Macrographs of the external and internal sides of the liner samples were systematically taken for all of the liner samples.

Figures 6.3 to 6.10 show different aspects of the corrosion generated on ML45 liner samples. A bentonite layer, compacted and apparently well adhered is observed in the four quadrants of the liner. A higher extension of the corrosion is detected in areas bordering the holes, or in areas that could correspond to the separations in the bentonite blocks. General corrosion is the predominant mechanism observed in both external and internal (underside) surface of the samples. There is no visible pitting or other types of localized corrosion.

Reddish-brown corrosion products are observed in the external surface, whereas more brownish-black corrosion products are observed in the internal surface, free of bentonite residues. The oxide layer generated in the internal surface seems somewhat more adherent and regular than that observed on the external surface. However the oxide generated in the internal surface of quadrants ML45-3 and ML45-4, is easily spalled.

Extension of corrosion is quite similar in the four quadrants. It is possible however to establish the following ranking (starting from the most corroded).

ML45-4 ≈ ML45-3 > ML45-2 > ML45-1

Framed areas in figures 6.3 to 6.10 correspond to areas with major corrosion damage. These areas are examined in detail in the SEM/EDS and metallographic analyses.

ML45-1

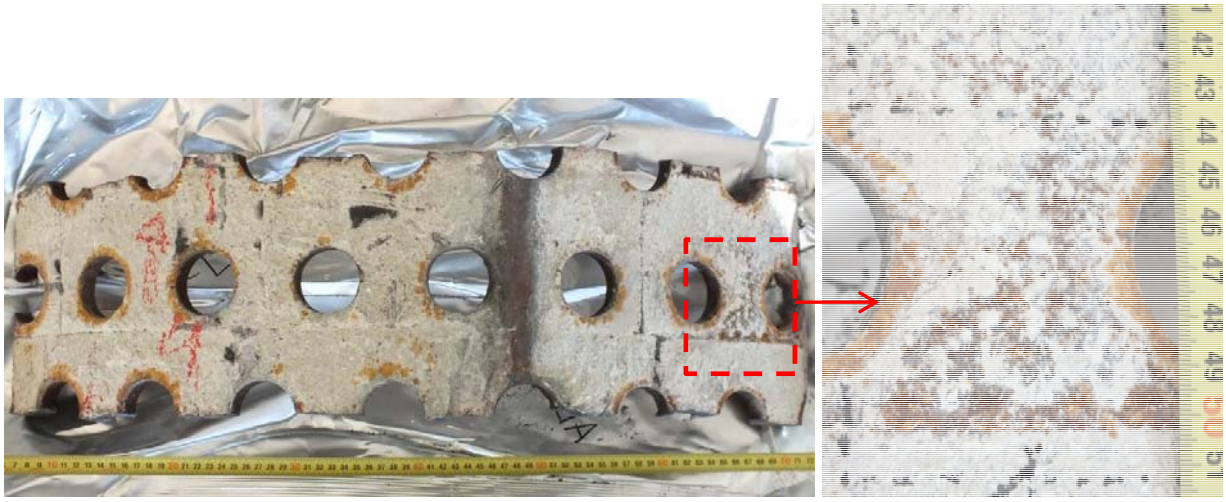

Figure 6.3: Photographs showing general appearance and detail of external surface of ML45-1 section

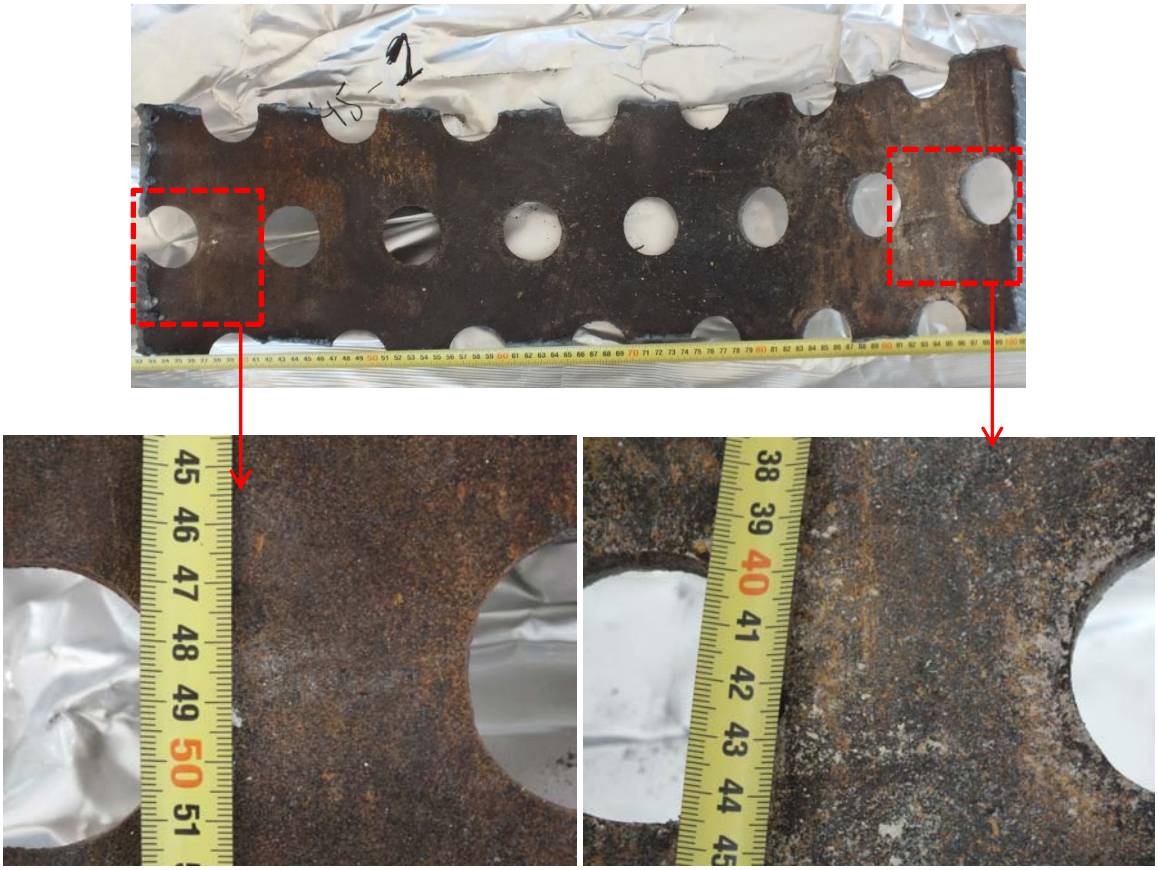

Figure 6.4: Photographs showing general appearance and detail of internal surface of ML45-1 section

ML45-2

Figure 6.5: Photographs showing general appearance and detail of external surface of ML45-2 section

Figure 6.6: Photographs showing general appearance and detail of internal surface of ML45-1 section

ML45-3

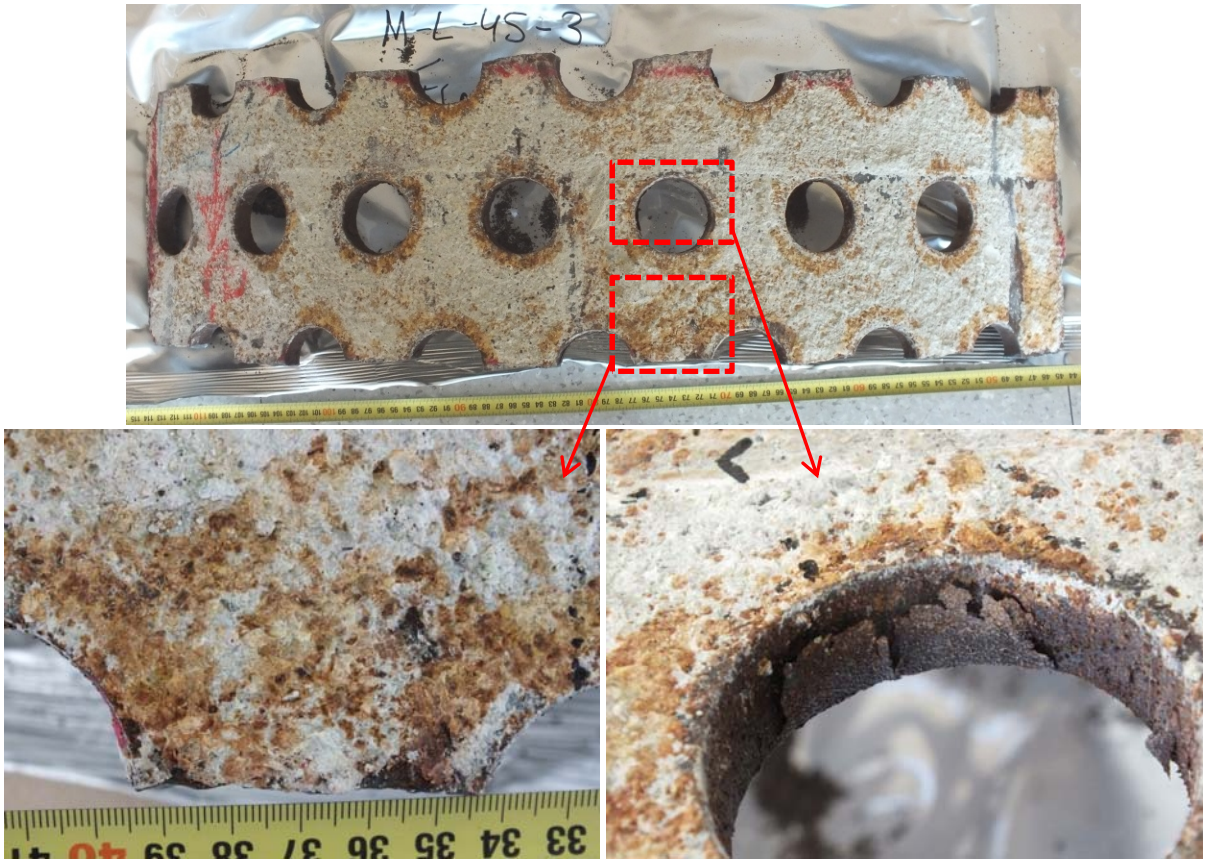

Figure 6.7: Photographs showing general appearance and detail of external surface of ML45-3 section

Figure 6.8: Photographs showing general appearance and detail of internal surface of ML45-3 section

ML45-4

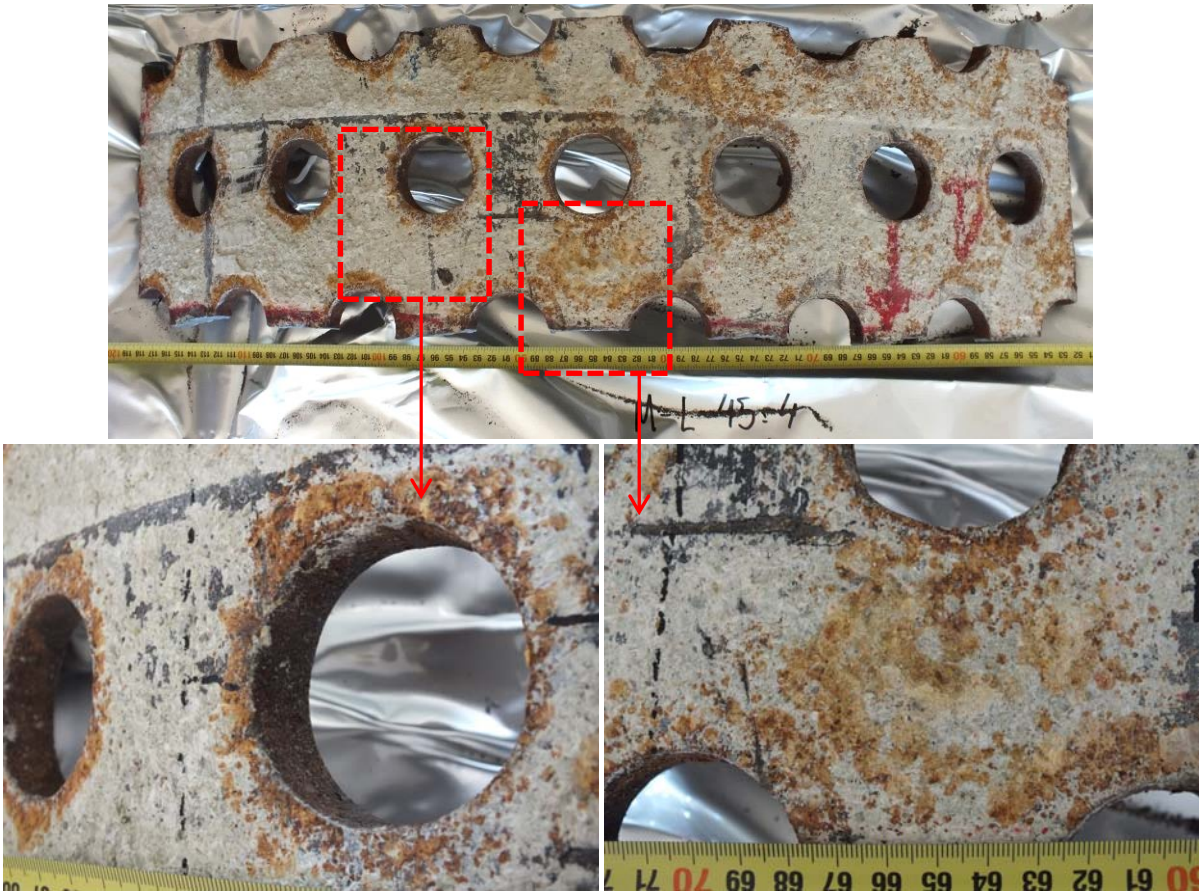

Figure 6.9: Photographs showing general appearance and detail of external surface of ML45-4 section

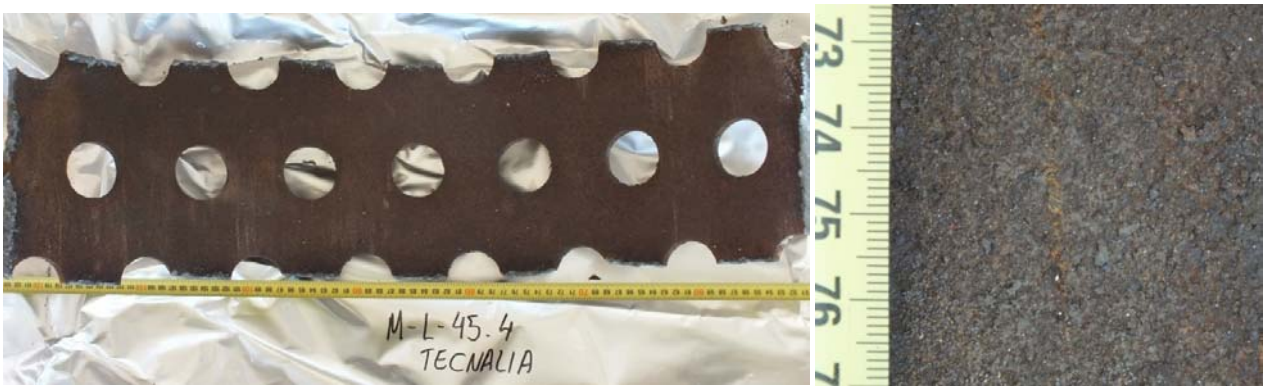

Figure 6.10: Photographs showing general appearance and detail of internal surface of ML45-4 section

6.1.2 Corrosion products analysis: SEM/EDS and XRD

Figure 6.11 includes photographs of liner sections from the different quadrants showing location of SEM/EDS analyses.

EDS analyses of the external corroded area in liner section ML45 indicate that the reddish corrosion products are basically comprised of Fe and O, Figure 6.12. A significant chloride peak is also detected in these areas, together with elements associated with the bentonite such as silicon and aluminum. The semi-quantitative results obtained in the EDS analyses are summarized in Table 6.1.

XRD analyses on the external surface of sections ML45-1 and ML45-2, shown in Figure 6.11, identify iron oxides as magnetite Fe_3O_4 in both XRD spectra (Figures 6.13 and 6.14). Other iron oxides/ hydroxides such as akaganeite (Fe^{3+} (O, OH, Cl), Fe_2O_3, are observed. Several peaks are also associated with iron carbonates such as siderite ($FeCO_3$). Halite (NaCl) is also detected in ML45-1 section.

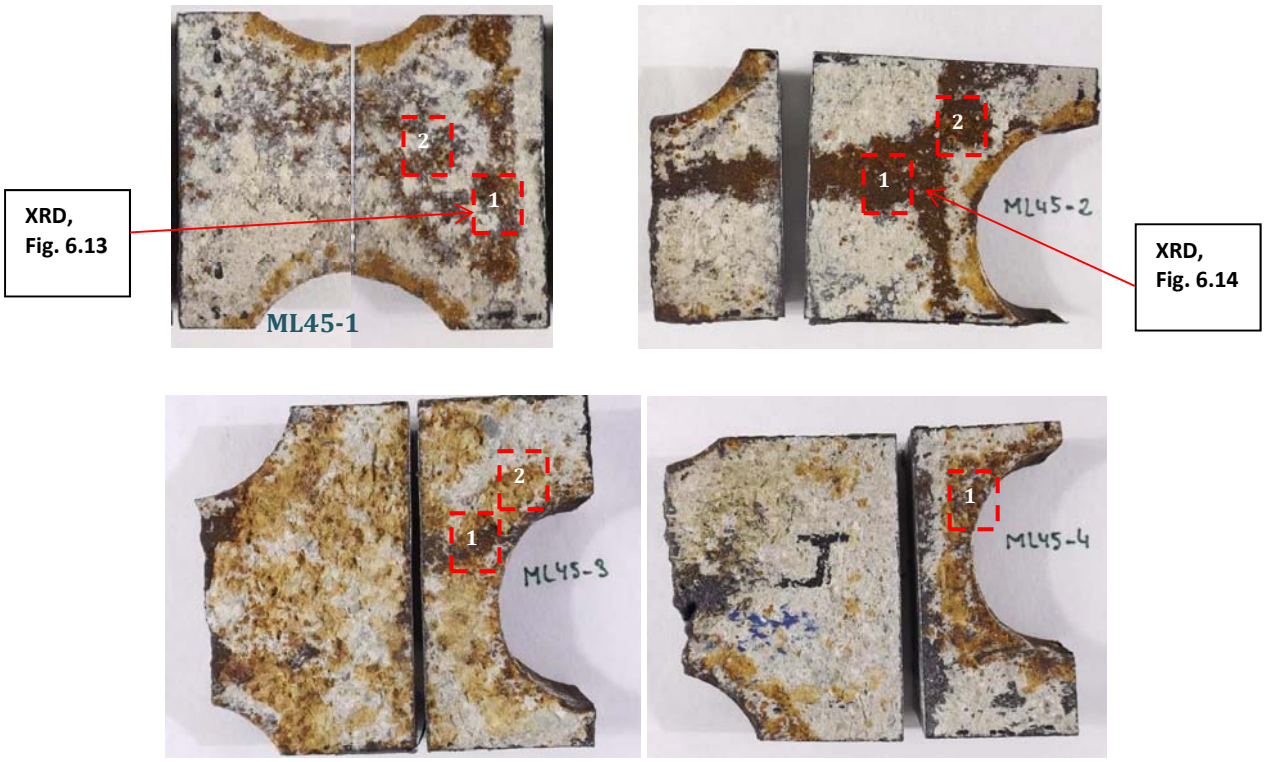

Figure 6.11: Photographs of different liner sections showing EDS analyses performed on ML45 section

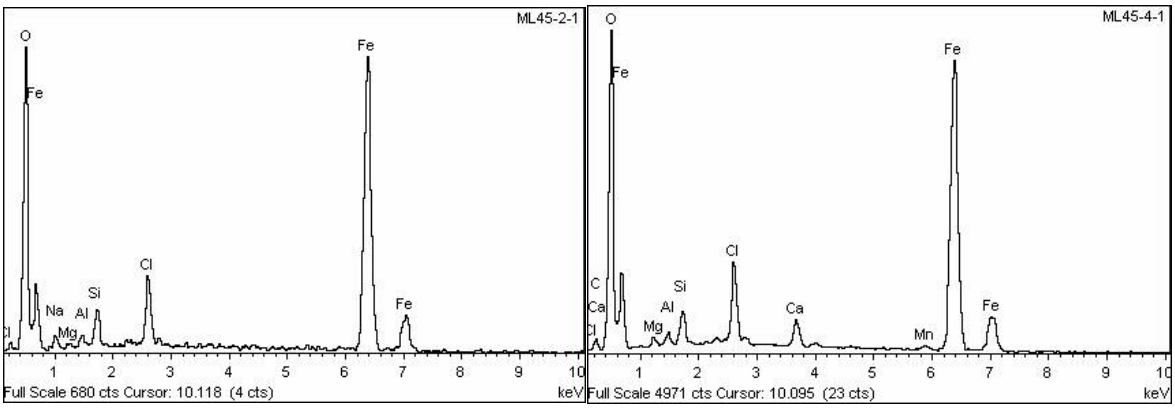

Figura 6.12: EDS spectra of ML45-2 and ML45-4 external surface

EDS analyses	Element (wt%)											
	O	Na	Mg	Al	Si	S	Cl	K	Ca	Mn	Fe	Total
ML45-1-1	39.80	6.39	1.40	2.36	5.69	0.32	3.52		0.52		40.00	100.00
ML45-1-2	40.56	1.60	1.64	2.94	7.75		3.67	0.28	0.39		41.18	100.00
ML45-1-E*	42.36	2.22	3.13	4.48	12.74		0.32	0.33	1.45	0.43	32.55	100.00
ML45-2-1	35.12	1.79	0.43	0.71	2.21		4.42				55.32	100.00
ML45-3-1	37.99	1.89	0.79	1.06	3.00		1.45		3.40	0.55	49.87	100.00
ML45-3-2	43.28	1.38	1.90	2.06	5.53		1.41		7.95	0.38	36.11	100.00
ML45-3-E*	36.02			0.63	1.51	0.30	0.93			0.52	60.10	100.00
ML45-4-1	37.81		0.67	0.71	1.78		4.61		1.80	0.54	52.09	100.00

Table 6.1 : Semi quantitative EDS analyses on ML45 section

*E: relates to the internal surface

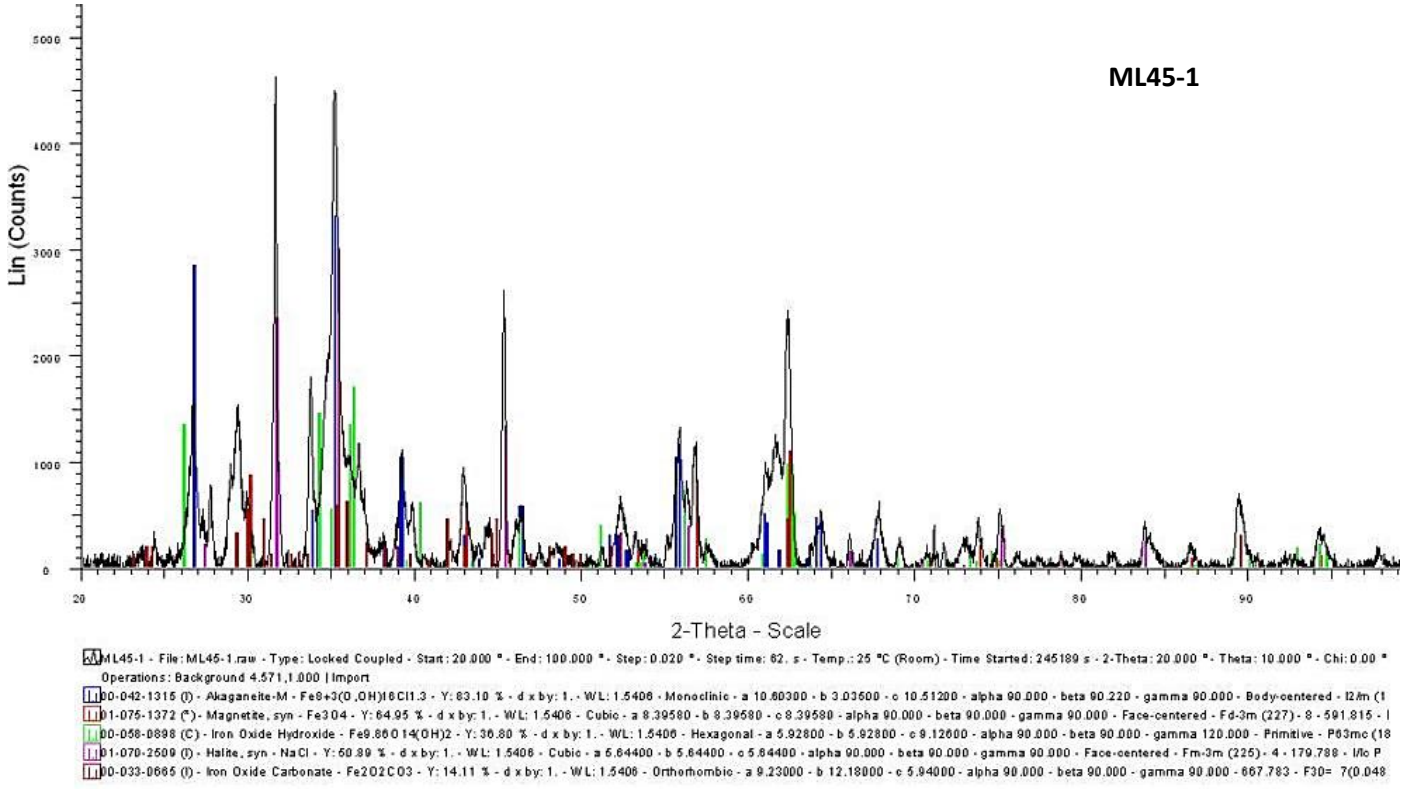

Figure 6.13: XRD spectrum on external surface of ML 45-1 sample

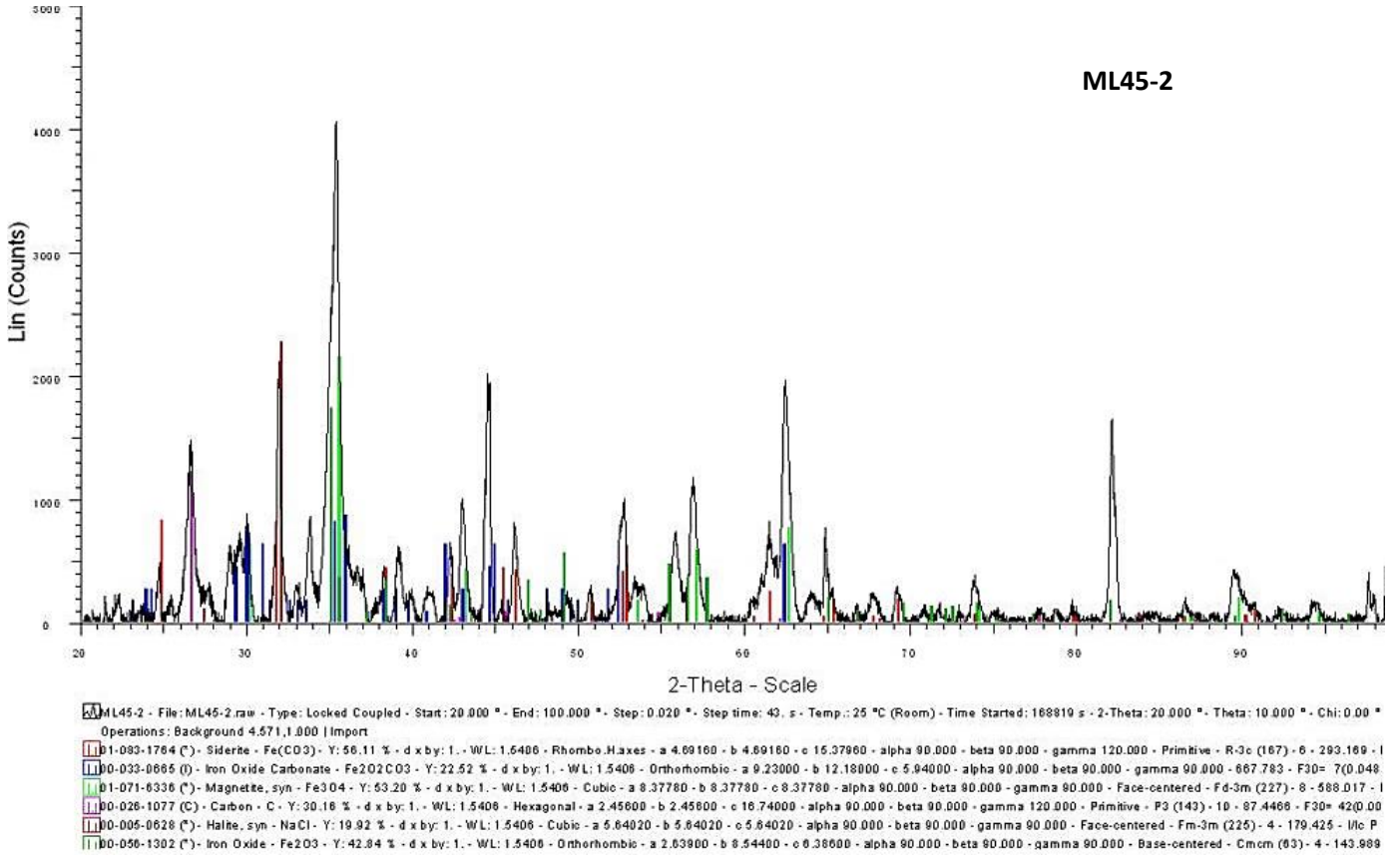

Figure 6.14: XRD spectrum on external surface of ML45-2 sample

6.1.3 Metallographic study

Cross sections transversals to the longitudinal axis of the liner were prepared metallographically, from each of the liner quadrants. These metallographic probes were further studied by optical microscopy.

The optical micrographs shown in Figures 6.16 show a quite compact and relatively uniform oxide layer in terms of thickness, and in general firmly attached to most part of the external surface of section ML45. The optical micrographs for the internal surface, Figure 6.17, show also a quite uniform oxide layer, somewhat thinner than that observed for the external surface. No pitting or other kind of localized corrosion is seen.

The remaining (un-corroded) wall thickness of section ML-45 is measured on the metallographic probes (Figure 6.15), using a measuring microscope. An average value of 14.7 ± 0.15 mm is obtained. Assuming that the liner was initially 15 mm thick, corrosion penetration values are in line with the maximum values measured on optical micrographs: approximately 200-250 microns on the external surface and up to 180 microns on the internal surface.

Chemical etching of metallographic probes reveal a ferrite-perlite microstructure for the steel constituting the liner, typical of carbon steels.

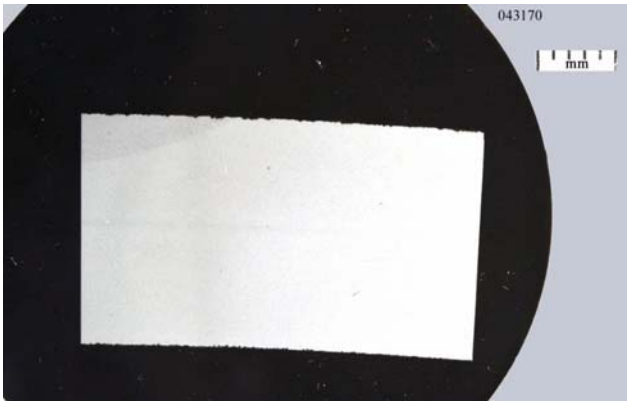

Figure 6.15: Metallographic probe of transversal section of liner sample ML-45, quadrant 2

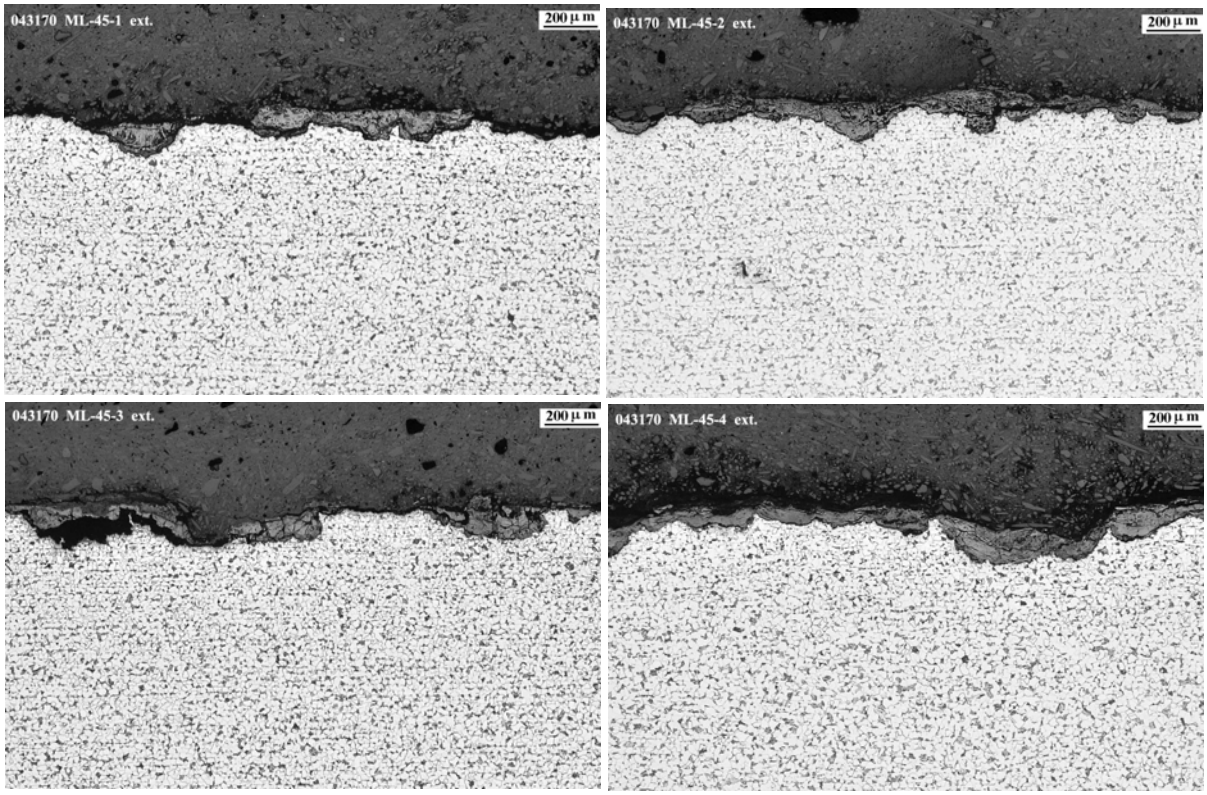

Figure 6.16: Optical micrographs of the external surface of section ML-45, quadrants 1, 2, 3 and 4, with metallographic etching

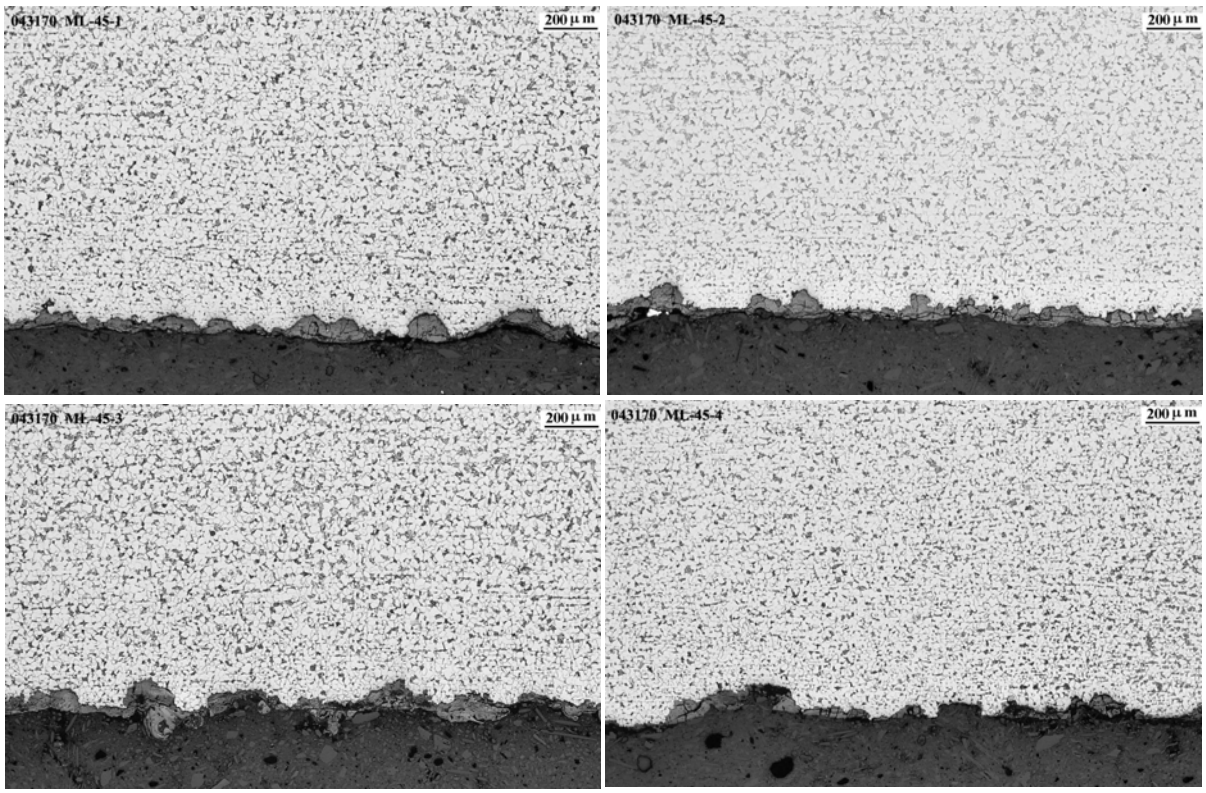

Figure 6.17: Optical micrographs of the internal surface of section ML-45, quadrants 1, 2, 3 and 4, with metallographic etching

6.2 Section ML52

6.2.1 Visual inspection

Figures 6.18 to 6.25 show different views of the liner section ML-52. As it was observed for section ML45, the extension of the corrosion is higher in areas bordering the holes, or in areas that could correspond to the separations in the bentonite blocks.

General corrosion is the predominant mechanism observed in both external and internal surface of the samples, with the formation of brownish-red corrosion products in the external surface, whereas more brownish-black corrosion products are observed in the internal surface, free of bentonite residues.

There is no visible pitting or other types of localized corrosion.

Several weld deposits are observed on the external surface of the liner.

Although corrosion extension is quite similar in the four quadrants, the following ranking, starting from the most corroded, could be established:

ML52-2 > ML52-4 ≈ ML52-1 > ML52-3

Visual inspection of liner section ML-52 indicates a higher extension of the generalized corrosion with respect to that observed for section ML-45. This aspect is corroborated in the metallographic examination.

ML52-1

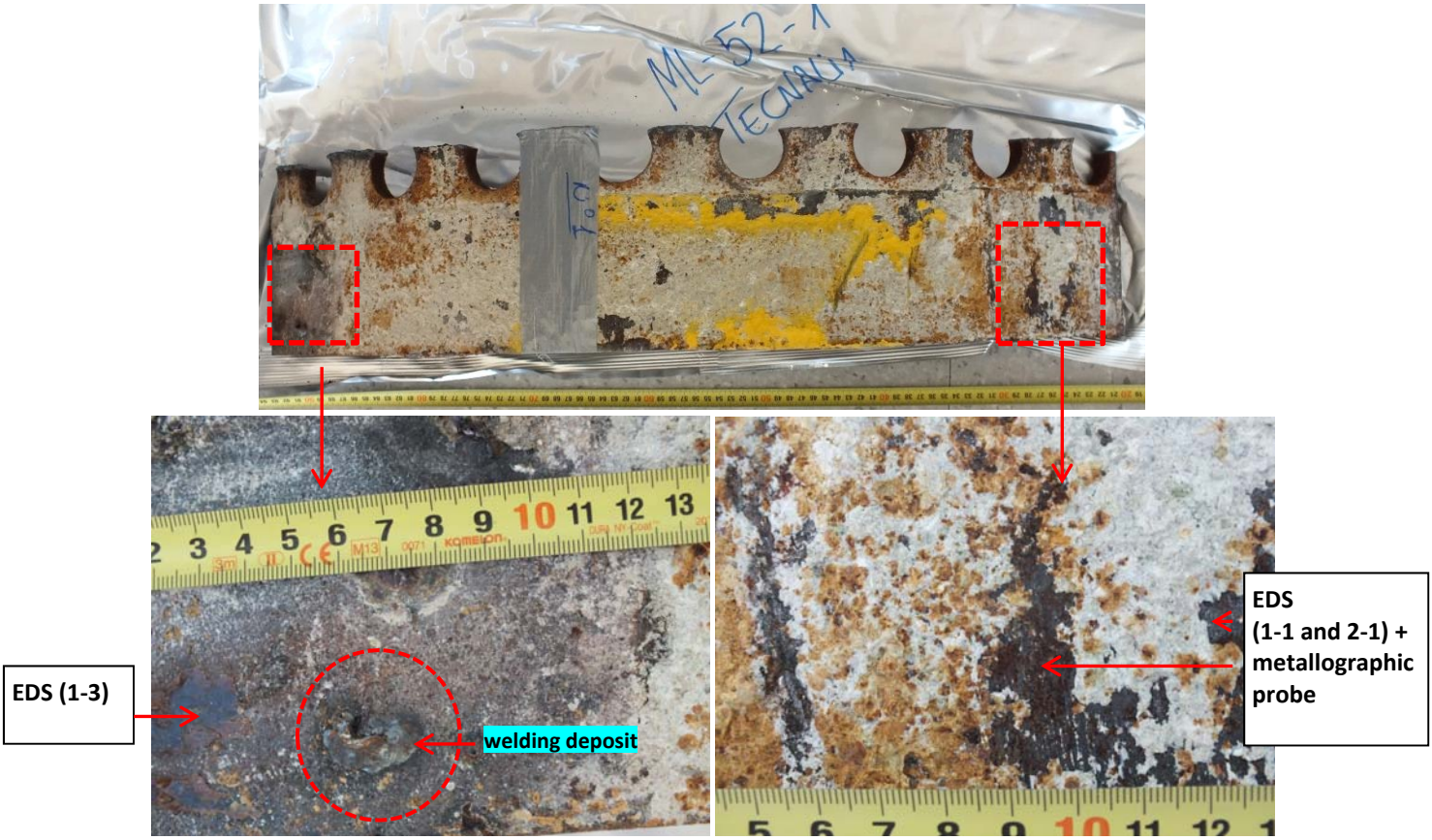

Figure 6.18: Photographs showing general appearance and detail of external surface in ML52-1 section

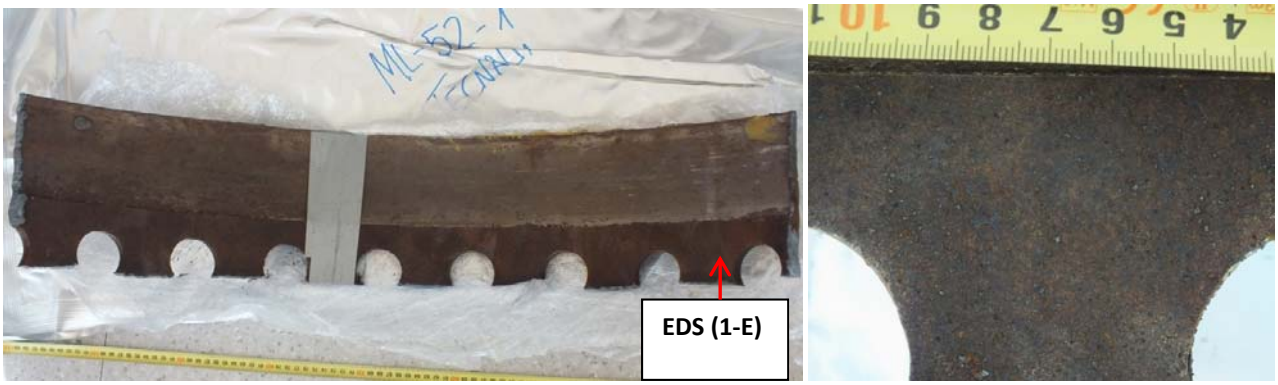

Figure 6.19: Photographs showing general appearance and detail of external surface of ML52-1 section

ML52-2

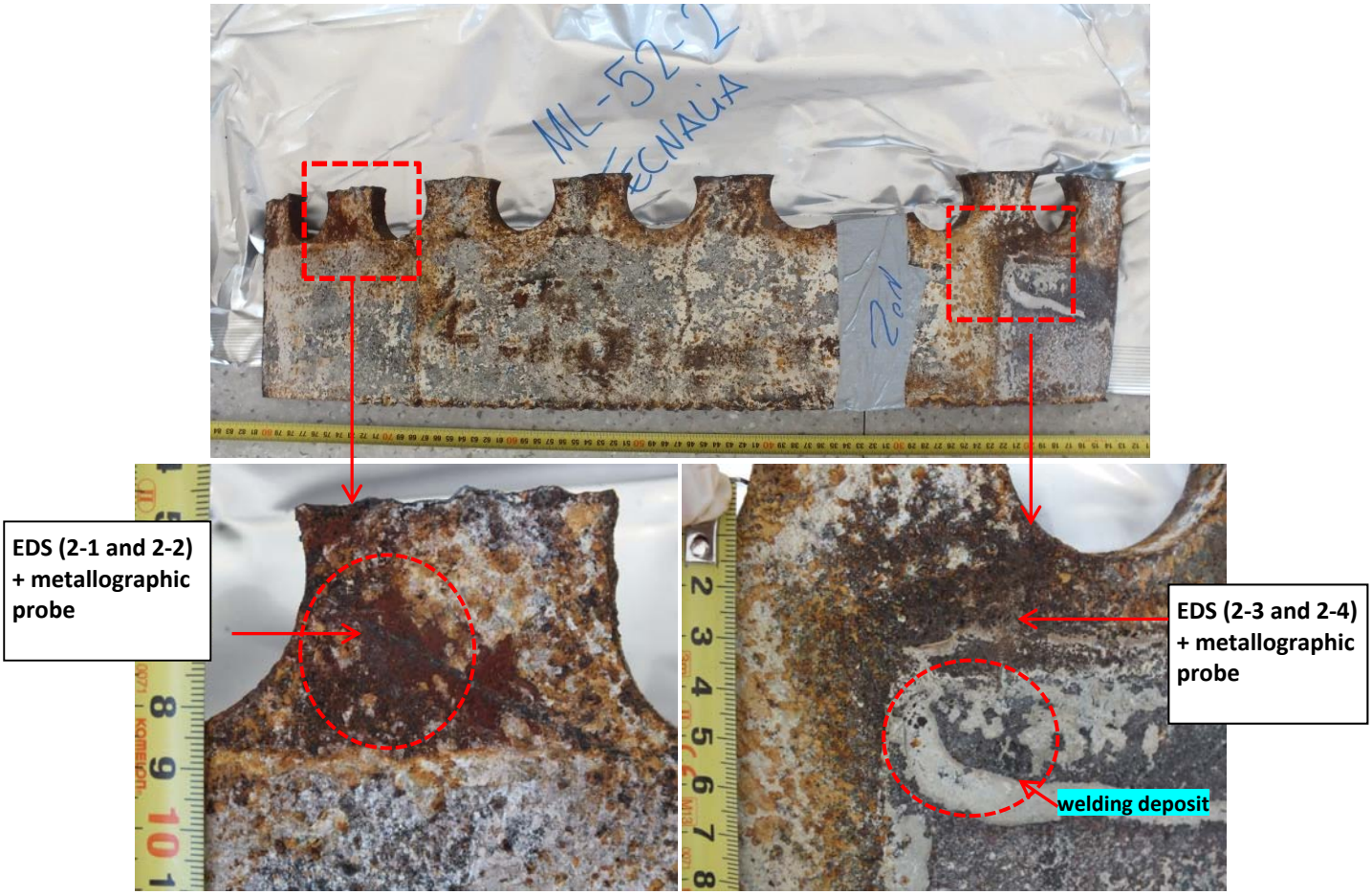

Figure 6.20: Photographs showing general appearance and detail of external surface of ML52-2 section

Figure 6.21: Photographs showing general appearance and detail of internal surface of ML52-2 section

ML52-3

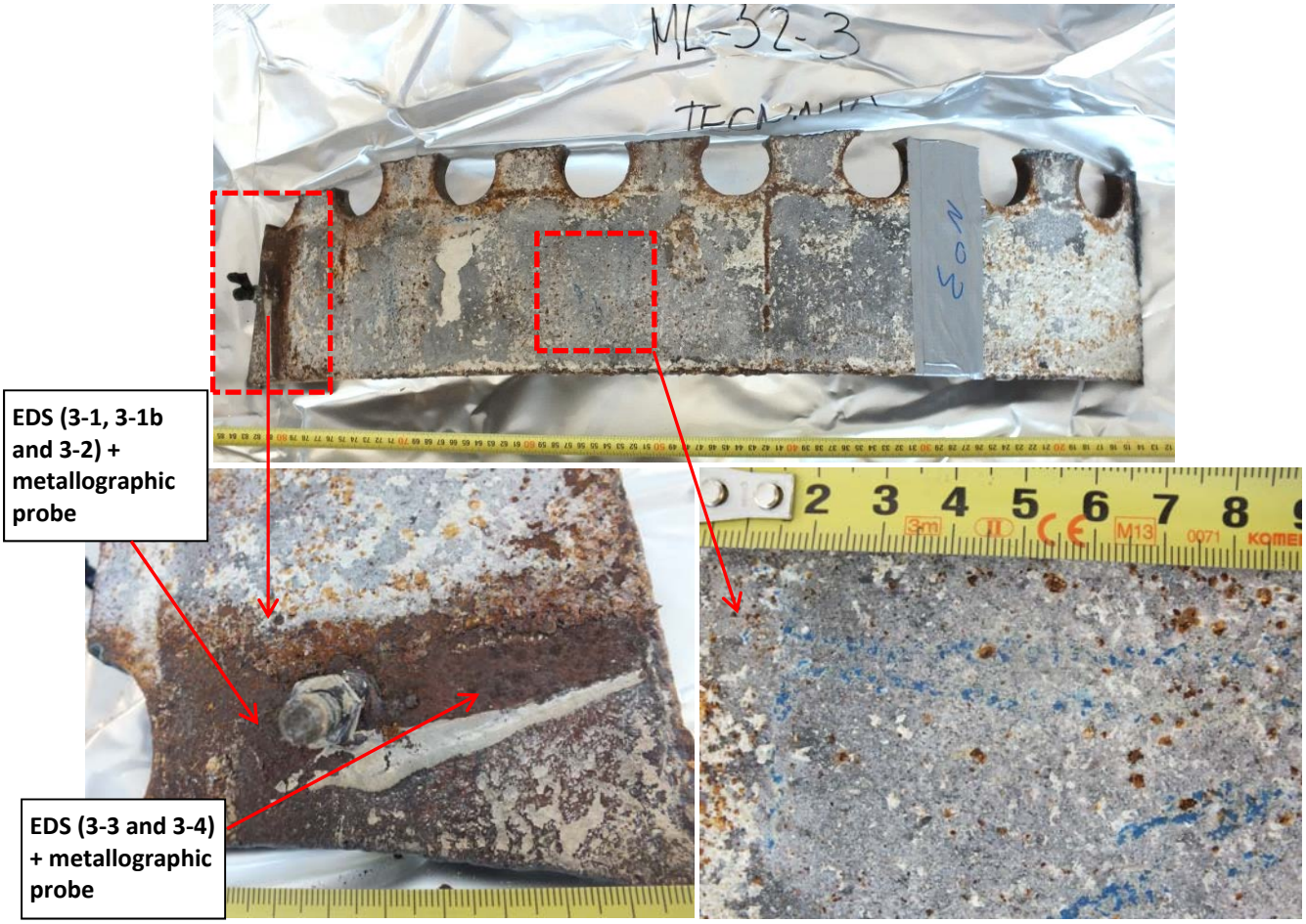

Figure 6.22: Photographs showing general appearance and detail of external surface of ML52-3 section

Figure 6.23: Photographs showing general appearance and detail of internal surface of ML52-3 section

ML52-4

Figure 6.24: Photographs showing general appearance and detail of external surface of ML52-4 section

Figure 6.25: Photographs showing general appearance and detail of internal surface of ML52-4 section

6.1.2 Corrosion products analysis: SEM/EDS

The EDS analyses of the reddish corroded area on the external surface of liner section ML52 mainly detect Fe and O as iron oxides, as well as elements constituents of the bentonite. Chloride peaks are detected in most of the spectra obtained. The amount of chloride obtained is somewhat smaller than that detected in section ML45. Sulphur is detected in the analyses of quadrant ML52-3.

The semi-quantitative results obtained in the EDS analyses carried out in section ML52 are summarized in Table 6.2.

EDS analyses	Element (wt%)											
	O	Na	Mg	Al	Si	S	Cl	K	Ca	Mn	Fe	Total
ML52-1-1	58.30		3.42	7.58	23.44		0.84	0.48	1.03		4.91	100.00
ML52-1-2	59.62		5.65	6.50	19.91			0.62	5.41		2.29	100.00
ML52-1-3	48.18		2.35	5.70	14.47		2.07	0.50	1.23		25.49	100.00
ML52-1-E*	34.44				0.73		1.76			0.97	62.10	100.00
ML52-2-1	35.78	2.11			1.25		2.60				58.26	100.00
ML52-2-2	44.77	1.73	3.66	3.51	11.63		1.18		1.41		32.11	100.00
ML52-2-4	53.47	14.06	2.48	3.31	8.97				4.42		13.28	100.00
ML52-2-E*	38.97						1.34				59.70	100.00
ML52-3-1	35.28				0.71	0.39	0.63	0.88			62.10	100.00
ML52-3-1b	39.52			0.98	2.67	1.82	1.30	0.71	3.72		49.28	100.00
ML52-3-2	37.31	1.77			1.36	0.71	0.79	1.64	10.04	1.39	44.98	100.00
ML52-3-3	56.90		6.89	7.01	21.74		0.71		3.46		3.30	100.00
ML52-3-4	39.78	2.40			1.87	1.52	0.68		3.16		50.58	100.00
ML52-3-E*	43.53	2.63	1.52	4.74	14.42				0.64		32.52	100.00
ML52-4-1	53.03	6.37	5.74	3.29	9.52				9.00		13.05	100.00
ML52-4-2	52.84		2.86	5.46	14.94		1.05	0.94	2.13		19.78	100.00
ML52-4-3	43.03		2.42	3.75	9.55		2.29		3.48		35.48	100.00
ML52-4-4	40.59	1.80	1.96	2.36	5.96	1.00			3.62		42.71	100.00

Table 6.2 : Semi quantitative EDS analyses on liner section ML52

*E: relates to the internal surface

6.1.3 Metallographic study

Metallographic probes were prepared from transversal cross sections from each of the liner quadrants and further studied by optical microscopy, Figure 6.26.

The optical micrographs shown in Figure 6.27 show a general non uniform corrosion morphology with an oxide layer in general firmly attached to most part of the external surface. The optical micrographs for the internal surface, Figure 6.28, show also a quite uniform oxide layer, thinner than that observed for the external surface and more uniform in terms of thickness.

As it was observed in the visual inspection, section ML-52 has a higher extension of the generalized corrosion, with respect to that observed for section ML-45. Maximum values of penetration of the corrosion of approximately 300-350 microns are measured on the external surface, and around 250 microns on the internal surface.

No pitting or other kind of localized corrosion is seen.

Chemical etching of metallographic probes reveals a ferrite-perlite microstructure for the steel constituting the liner, typical of carbon steels.

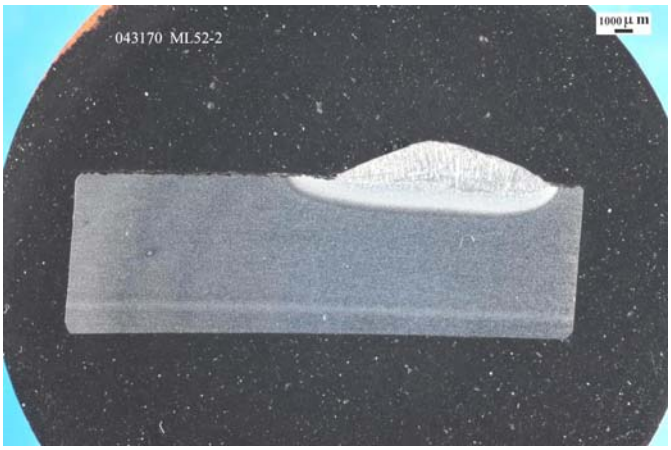

Figure 6.26: Metallographic probe of transversal section of iron welding deposit on external surface of sample ML-52-2, with metallographic etching

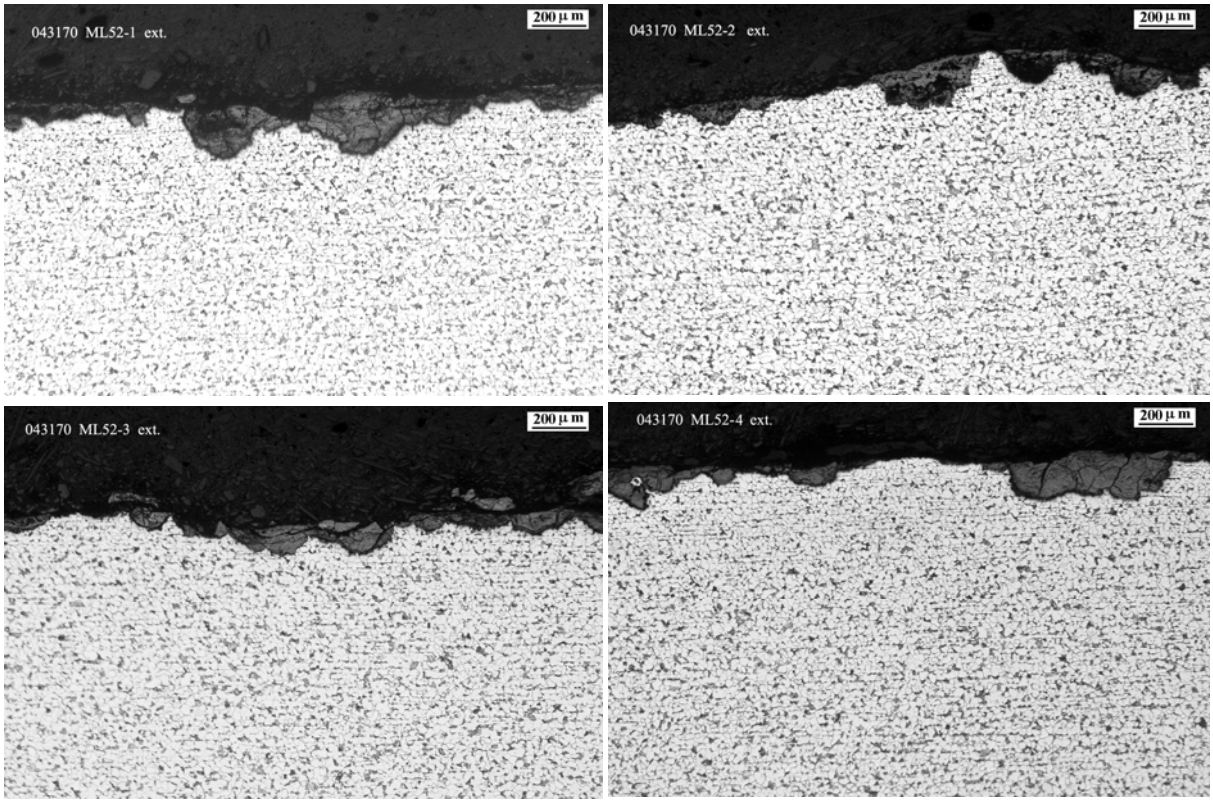

Figure 6.26: Optical micrographs of the external surface of section ML-52, quadrants 1, 2, 3 and 4, with metallographic etching

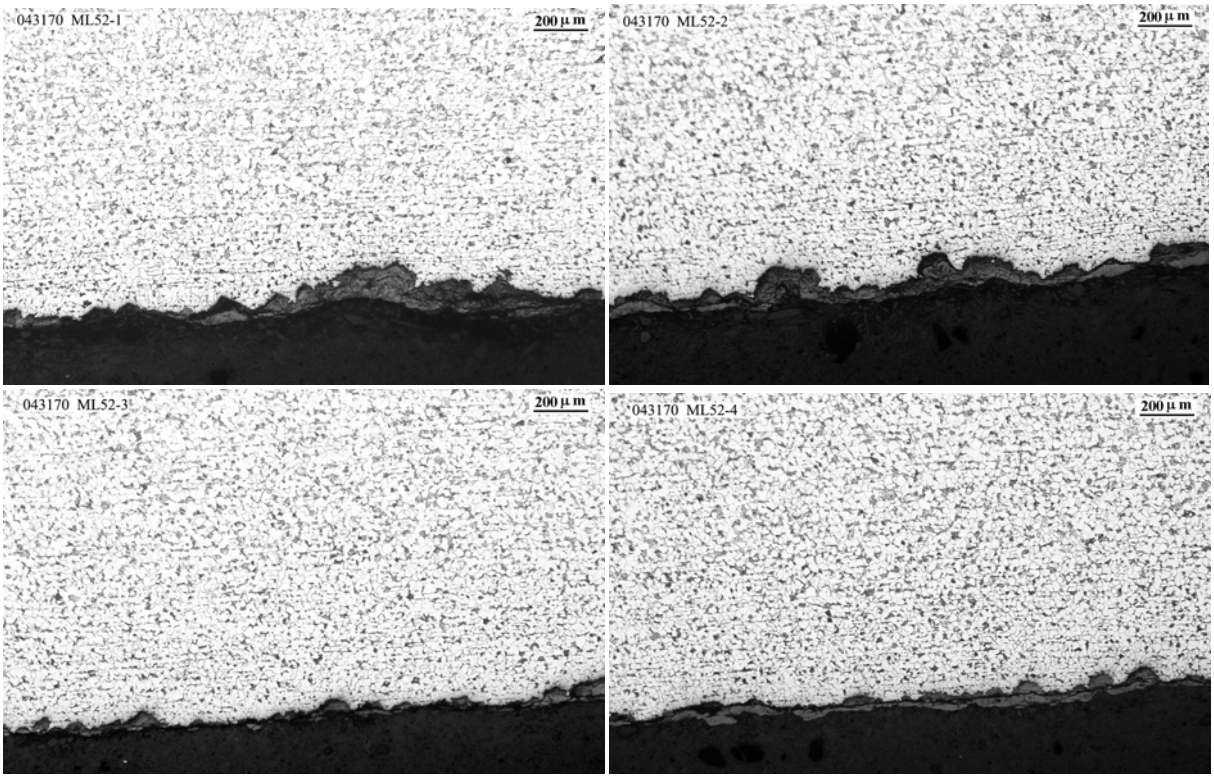

Figure 6.27: Optical micrographs of the external surface of section ML-45, quadrants 1, 2, 3 and 4, with metallographic etching

7. HEATER

7.1 Visual inspection at AITEMIN. Extraction of test samples

The heater reference MH was delivered from Grimsel to AITEMIN premises in Toledo (Spain). On November 24, 2015 a technician from Tecnalia carried out a visual examination of the heater and decided the cuts to be made. Three wedge-shaped sections were extracted from the heater with a radial saw, avoiding the use of cooling fluids.

It is important to point out that the heater has been in contact with the atmosphere since June 4, 2015. The corrosion damage observed at AITEMIN does not necessarily reflect the corrosion generated when the heater was retrieved from the gallery. Figures 7.1 to 7.16 show different views of the heater at AITEMIN premises. These photographs do not differ significantly, however, from those taken at Grimsel location (FEBEX-DP Extra Report No. 6, 04.06.2015).

Examination of the heater showed a quite uniform overall generalized corrosion of the surface. No visible pitting or other types of localized corrosion were detected. Reddish-brown corrosion products were observed in the external surface. The oxide layer generated in the surface of the heater was quite adherent and regular.

The front part of the heater showed a higher extension of the generalized corrosion damage. Bentonite deposits protruded through the liner holes were still stuck to the surface of the heater. The oxide layer generated in some zones of the front part (9 o´clock position), Figure 7.15, were more easily spalled.

The two lid-cylinder welded joints at the top and back side of the heater showed a good condition.

Figure 7.16 shows the location in the heater of sampling sites ref. MH-03-ET and MH-03-ET.

The three wedge-shaped sections extracted from the heater and identified with the references MH-01-F3C, MH-02-F9C and MH-03-ET are shown in Figures 7.17 to 7.19. F refers to Front; E to End; T to Top; 3C to 3 o´clock; and 9C to 9 o´clock. These photographs indicate the location of the EDS analyses carried out in these samples, as well as the location of the sections extracted for the metallographic study. Samples references MH-02-F9C and MH-03-ET include the lid, the welded joint and the cylinder.

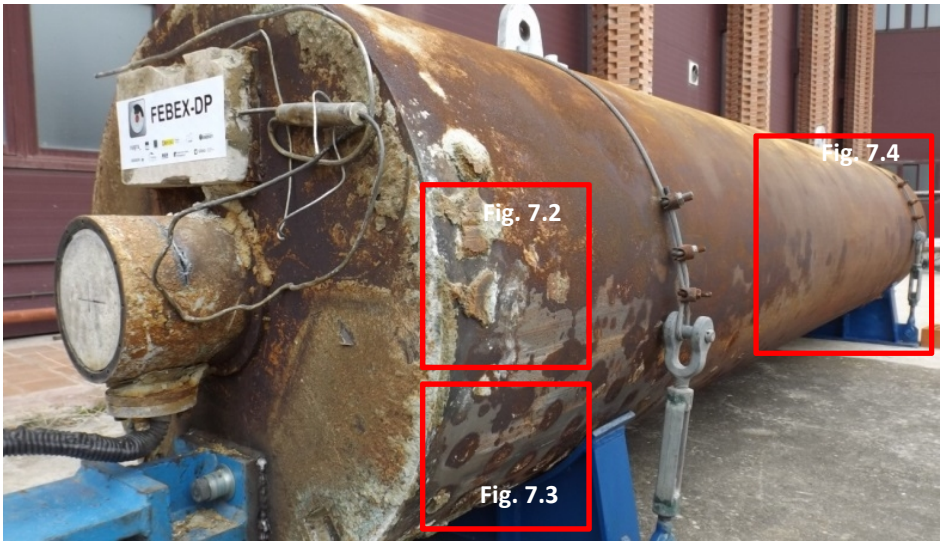

Figure 7.1: Photograph showing 3 o´clock view of the heater at AITEMIN premises

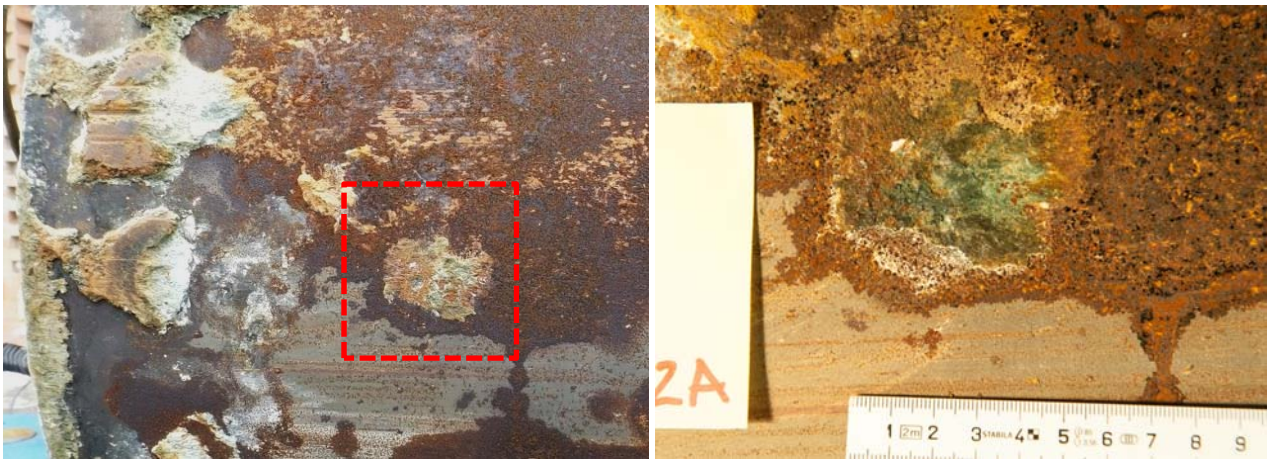

Figure 7.2: Detail of photograph shown in Fig. 7.1 (left). Photograph of the same zone taken at Grimsel (right)

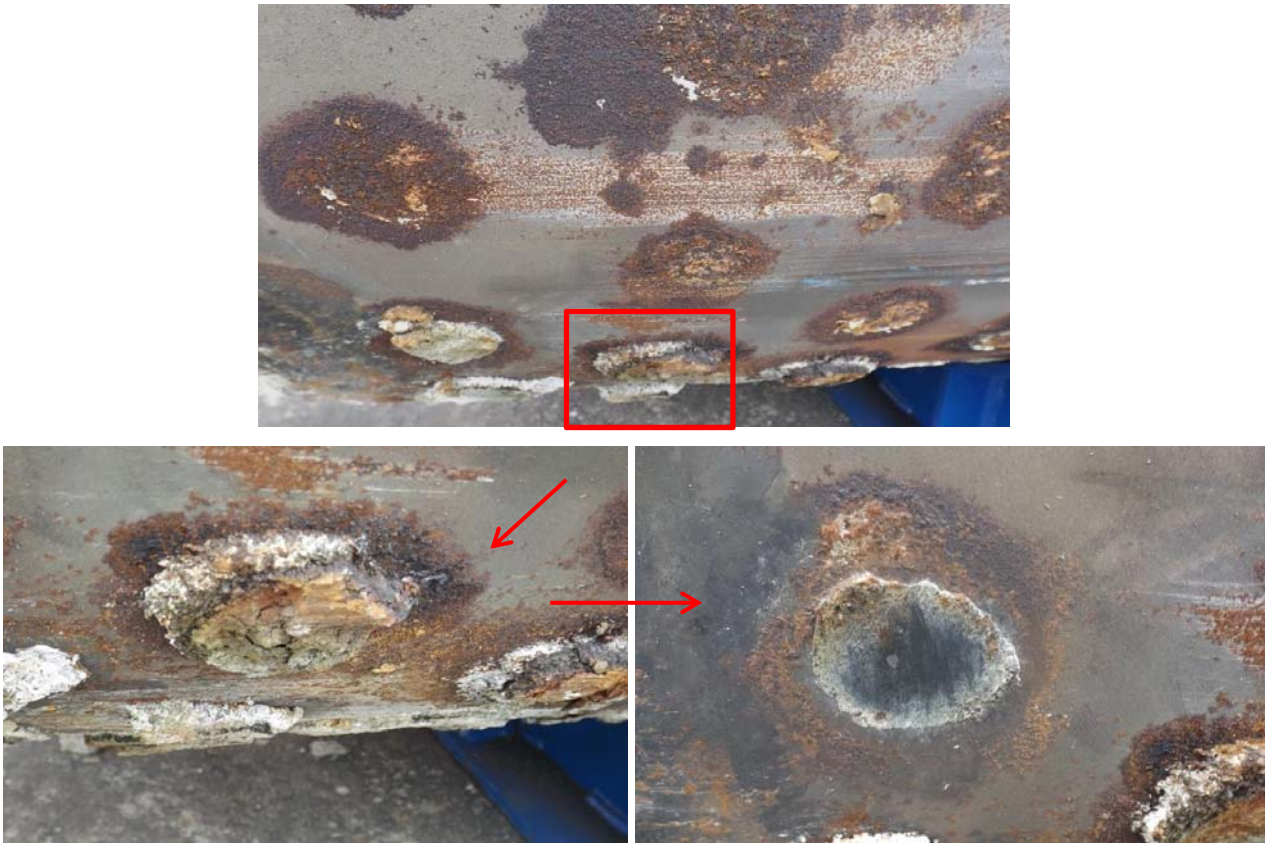

Figure 7.3: Detail of photograph shown in Fig. 7.1. Photograph of the bottom-right, shows this area after removing the adhered bentonite.

Figure 7.4: Photograph showing 3 o´clock view of the heater at AITEMIN premises

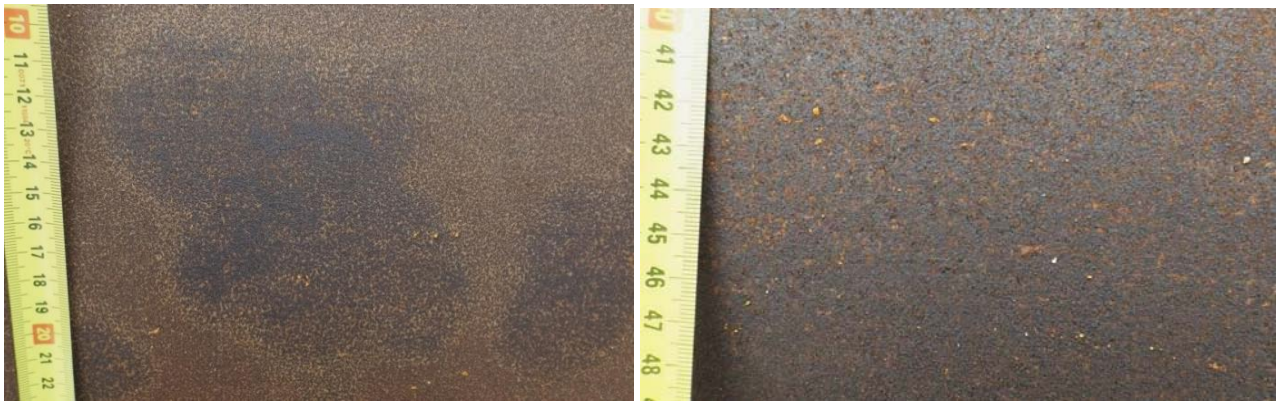

Figure 7.5: Details of photograph shown in Fig. 7.4

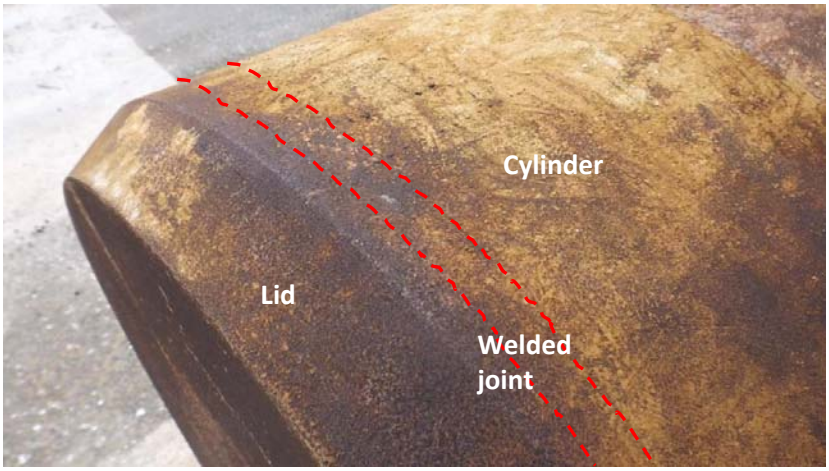

Figure 7.6: Photograph showing top end of the heater at AITEMIN premises

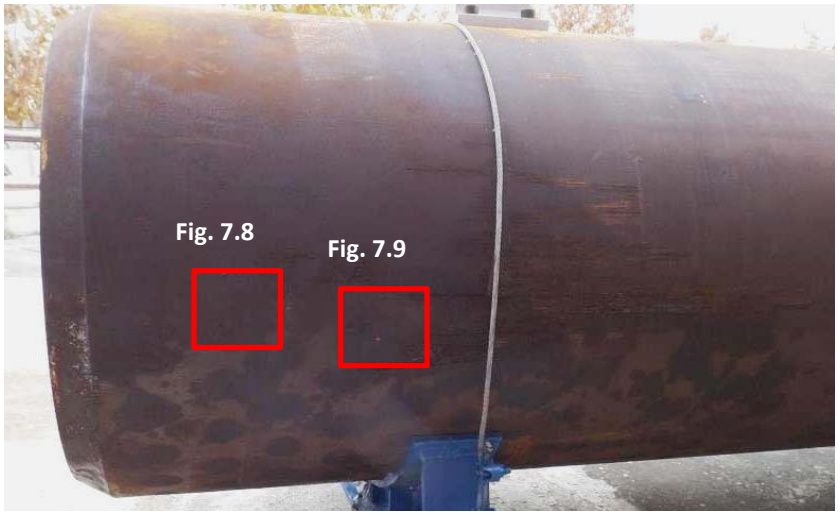

Figure 7.7: Photograph showing 9 o´clock view of the heater at AITEMIN premises

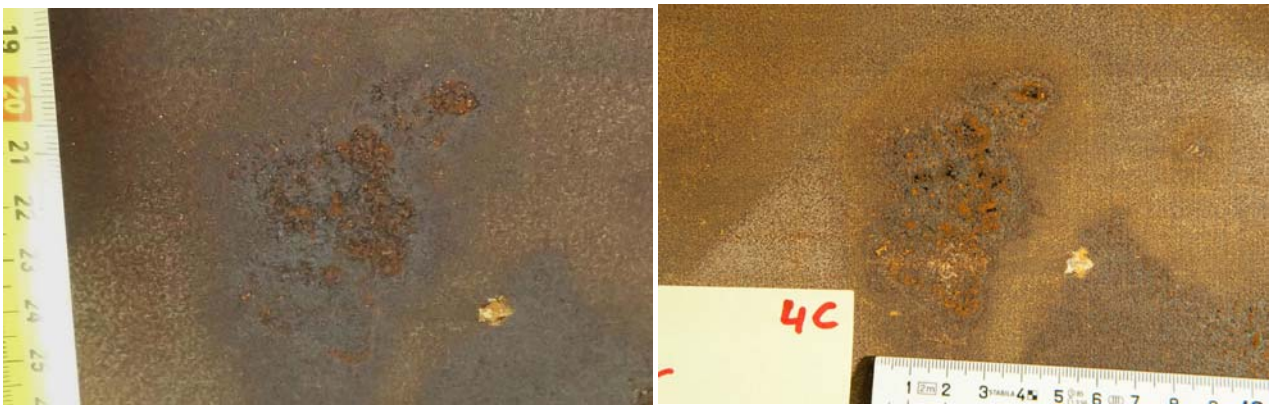

Figure 7.8: Detail of photograph shown in Fig. 7.7 (left). Photograph of the same zone in Grimsel (right)

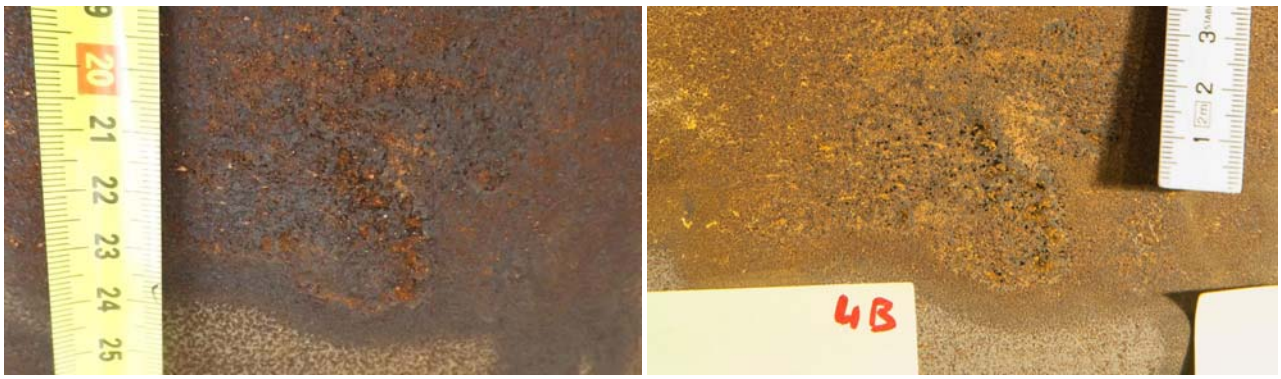

Figure 7.9: Detail of photograph shown in Fig. 7.7 (left). Photograph of the same zone in Grimsel (right)

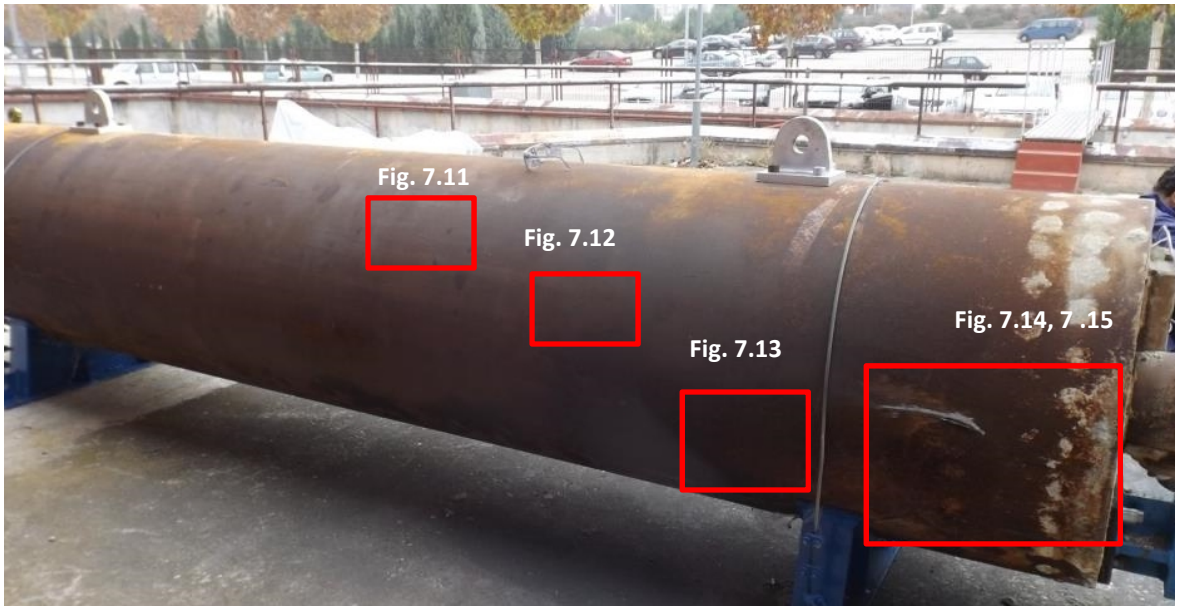

Figure 7.10: Photograph showing 9 o´clock view of the heater at AITEMIN premises

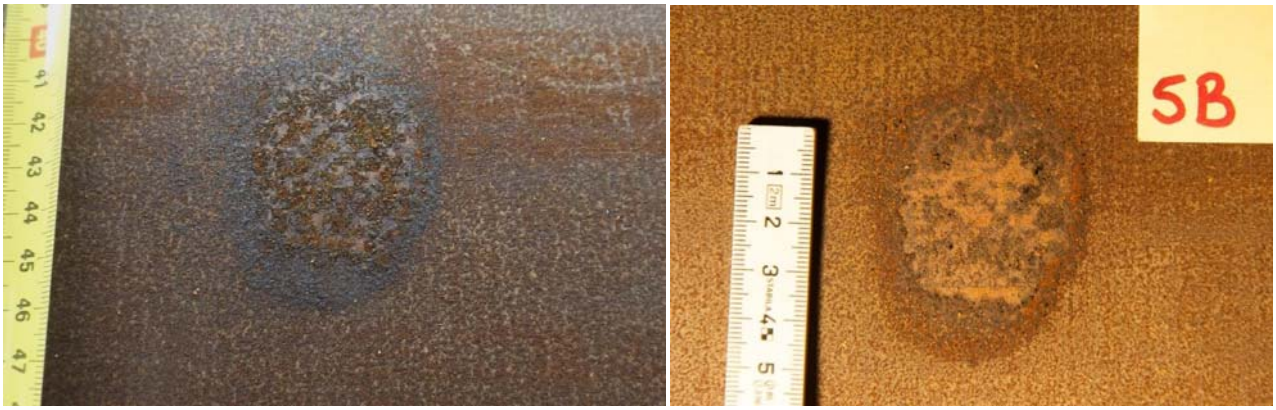

Figure 7.11: Detail of photograph shown in Fig. 7.10 (left). Photograph of the same zone in Grimsel (right)

Figure 7.12: Detail of photograph shown in Fig. 7.10

Figure 7.13: Detail of photograph shown in Fig. 7.10

Figure 7.14: Detail of photograph shown in Fig. 7.10. The red dotted line indicates location of heater sample ref. MH-02-F9C

Figure 7.15: Detail of photograph shown in Fig. 7.14

Figure 7.16: Photograph showing the location in the heater of samples ref. MH-03-ET (left) and MH-03-ET (right)

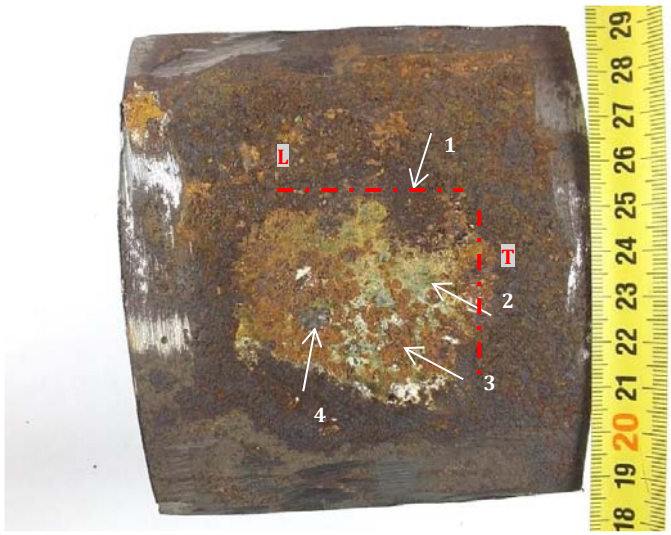

Figure 7.17: Photograph showing sample ref. MH-01-F3C. Arrowheads indicate location of EDS analyses shown in Table 7.1. Red dotted lines indicate the location of the metallographic probes (L=longitudinal, T=transversal)

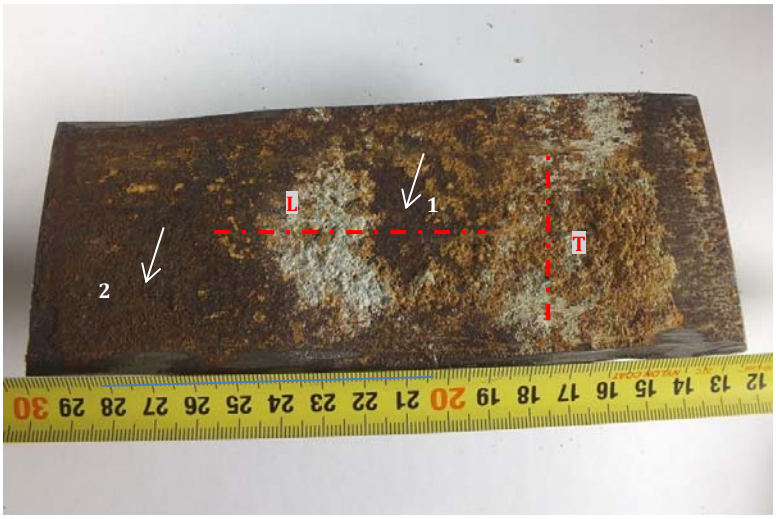

Figure 7.18: Photograph showing sample ref. MH-02-F9C. Arrowheads indicate location of EDS analyses shown in Table 7.1. Red dotted lines indicate the location of the metallographic probes (L=longitudinal, T=transversal)

Figure 7.19: Photograph showing sample ref. MH-03-ET. Arrowheads indicate location of EDS analyses shown in Table 7.1. The red dotted line indicates the location of the metallographic probe shown in Figure 7.23.

7.2 Corrosion products analysis: SEM/EDS and XRD

SEM/EDS analyses of the corrosion products generated on the surface of the samples from the heater were carried out. The photographs in Figures 7.17 to 7.19 show the location of the EDS analysis.

The results of the EDS analyses are summarized in Table 7.1. They indicate that the corrosion products are basically comprised of iron and oxygen, together with elements associated with the bentonite such as silicon, calcium, aluminum. A significant chloride peak is also detected for the three samples, Figure 7.20. Sulphur is detected in lesser quantities.

The corroded surface of samples reference MH-03-ET and MH-02-F9C is analysed by XRD. The spectra obtained are shown in Figures 7.21 and 7.22. In both samples the main iron oxide detected is akaganeite (Fe^{3+} (O, OH, Cl).

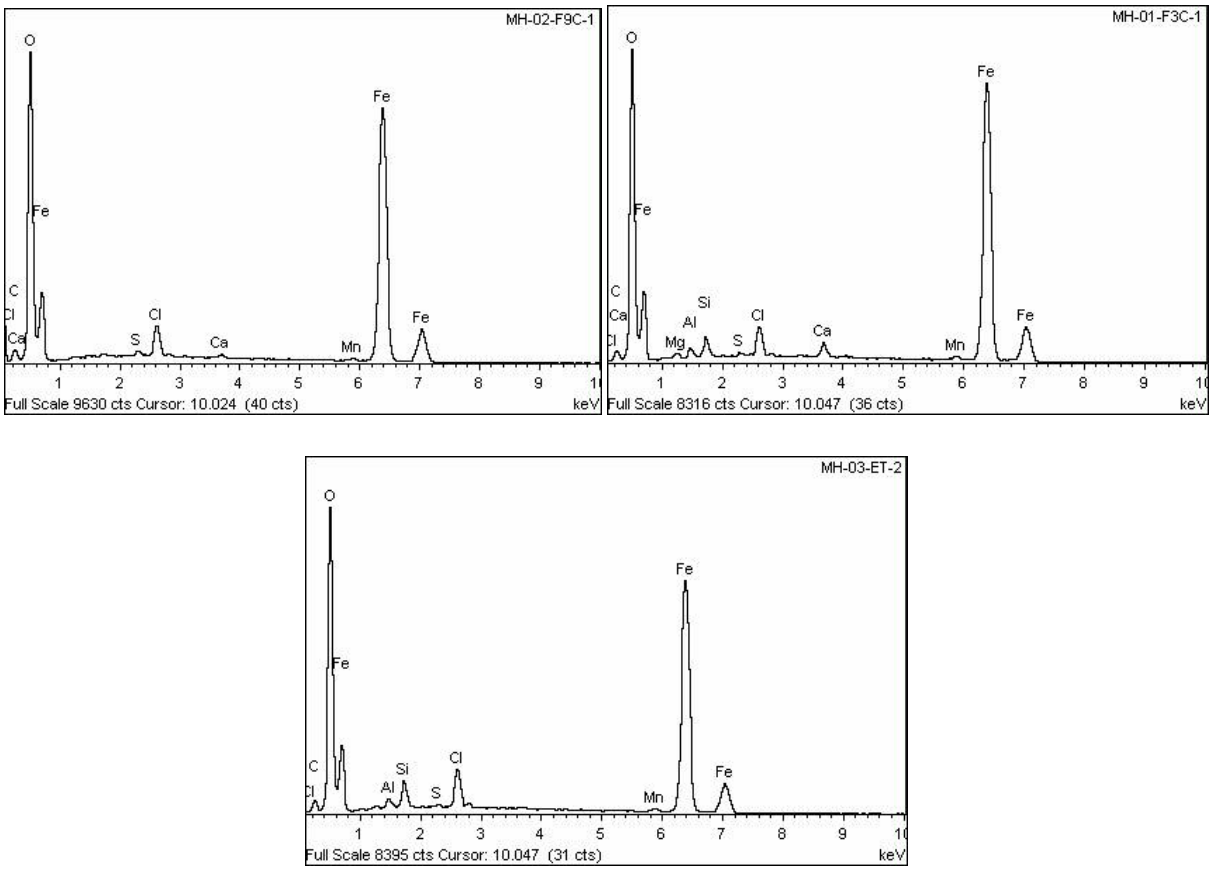

Figure 7.20: EDS spectra of the surface of heater samples ref. MH02-F9C, MH01-F3C and MH-03-ET

EDS Analyses	Element (wt%)												
	C	O	Na	Mg	Al	Si	S	Cl	K	Ca	Mn	Fe	Total
MH-01-F3C-1	3.34	37.27		0.45	0.60	1.08	0.19	1.80		0.94	0.48	53.85	100.00
MH-01-F3C-2	7.09	48.22		3.17	3.70	10.48		1.98	0.27	2.64	0.30	22.16	100.00
MH-01-F3C-3	2.34	39.96		0.90	1.63	4.43		2.38		1.09		47.26	100.00
MH-01-F3C-4	5.95	49.97	1.01	2.45	1.14	3.75			0.32	17.82	0.78	16.80	100.00
MH-02-F9C-1	3.93	39.16					0.28	2.08		0.25	0.39	53.91	100.00
MH-02-F9C-2	2.66	39.57		1.25	1.20	3.38	0.76	2.86		0.75	0.31	47.27	100.00
MH-03-ET-1	3.67	47.53		1.17	3.38	9.36		1.50				33.40	100.00
MH-03-ET-2	4.49	39.80			0.61	1.71	0.18	2.53			0.56	50.13	100.00

Table 7.1: Semi-quantitative results obtained in the EDS analyses performed on heater samples

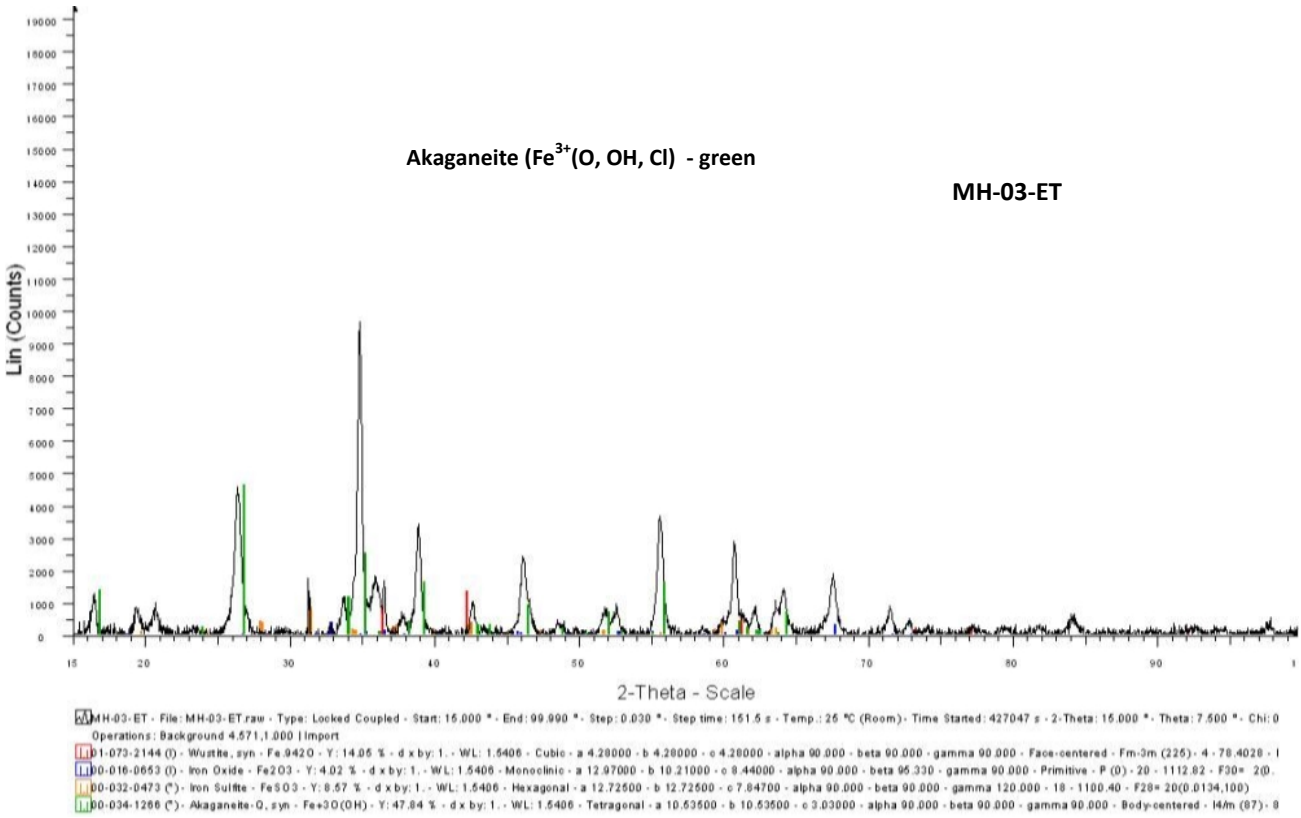

Figure 7.21: XRD spectrum on external surface of sample ref. MH-03-ET

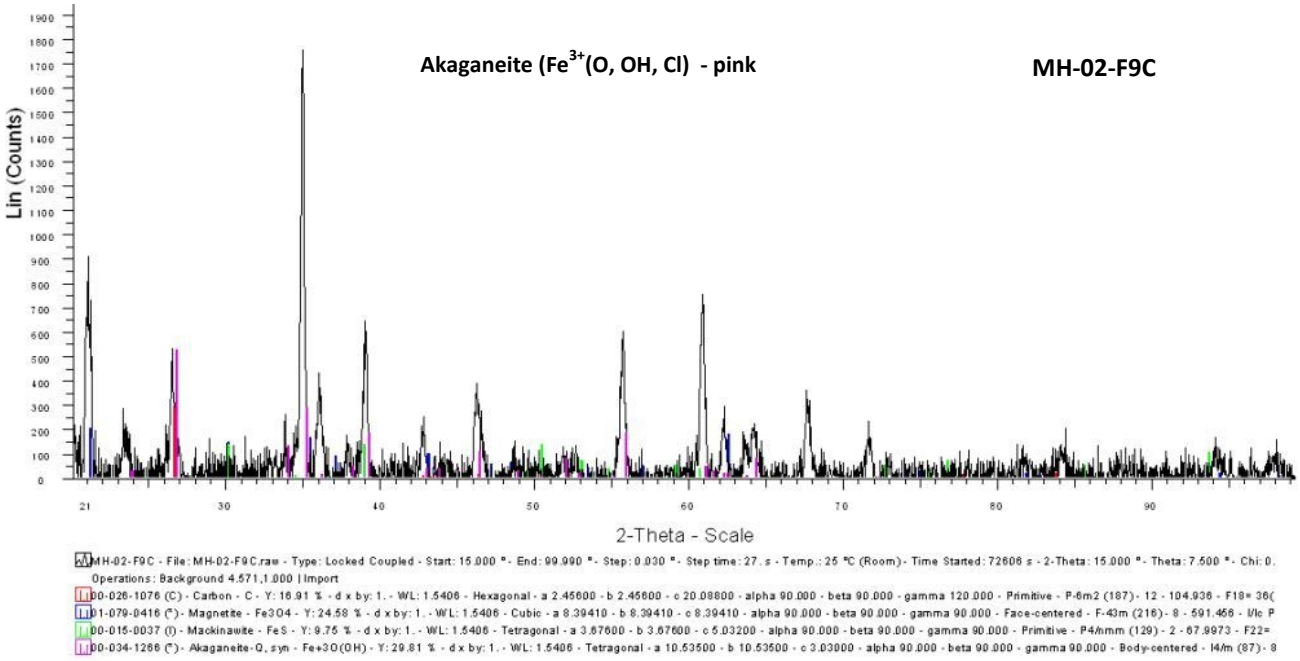

Figure 7.22: XRD spectrum on external surface of sample ref. MH-02-F9C

7.3 Metallographic study

Cross sections from each of the three heater samples were prepared metallographically.

The macrograph in Figure 7.23 shows a section of sample ref. MH-03-ET, including the welded joint between the lid and the cylinder.

Figure 7.24 shows a small localized corrosion area, which corresponds to the maximum corrosion penetration observed in the different embedded sections of sample ref. MH-01-F3C. The penetration depth for this area is about 400 microns. Apart from this area, no pitting or other kind of localized corrosion is seen. Optical micrographs in Figure 7.25 show a quite uniform generalised corrosion and a quite uniform oxide layer thickness for the transversal section of ref. MH-01-F3C.

Chemical etching reveals a ferrite-perlite microstructure for the steel constituting the cylinder, typical of carbon steels.

The metallographic analysis of the MH-02-F9C sample shows a quite uniform general corrosion of the external surface of the lid and cylinder components, Figure 7.26. A more localized corrosion is observed for the weld material and the heat affected zone (HAZ) of the cylinder joint, Figure 7.27. The penetration depth for this zone is less than 300 microns.

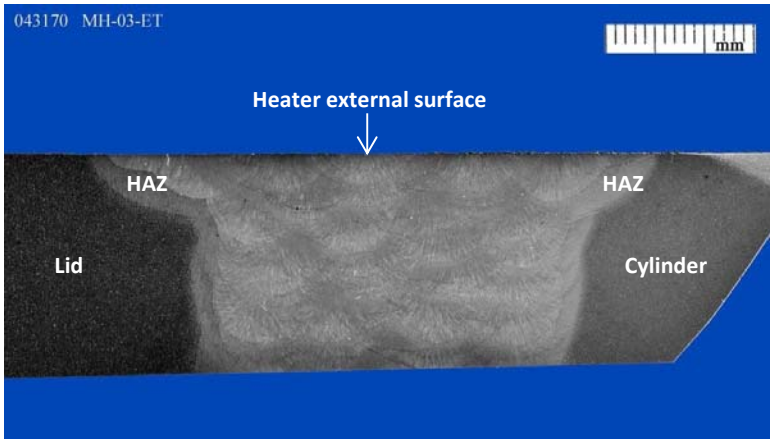

Figure 7.23: Photograph of the lid-cylinder welded joint of sample ref. MH-03-ET, with metallographic etching

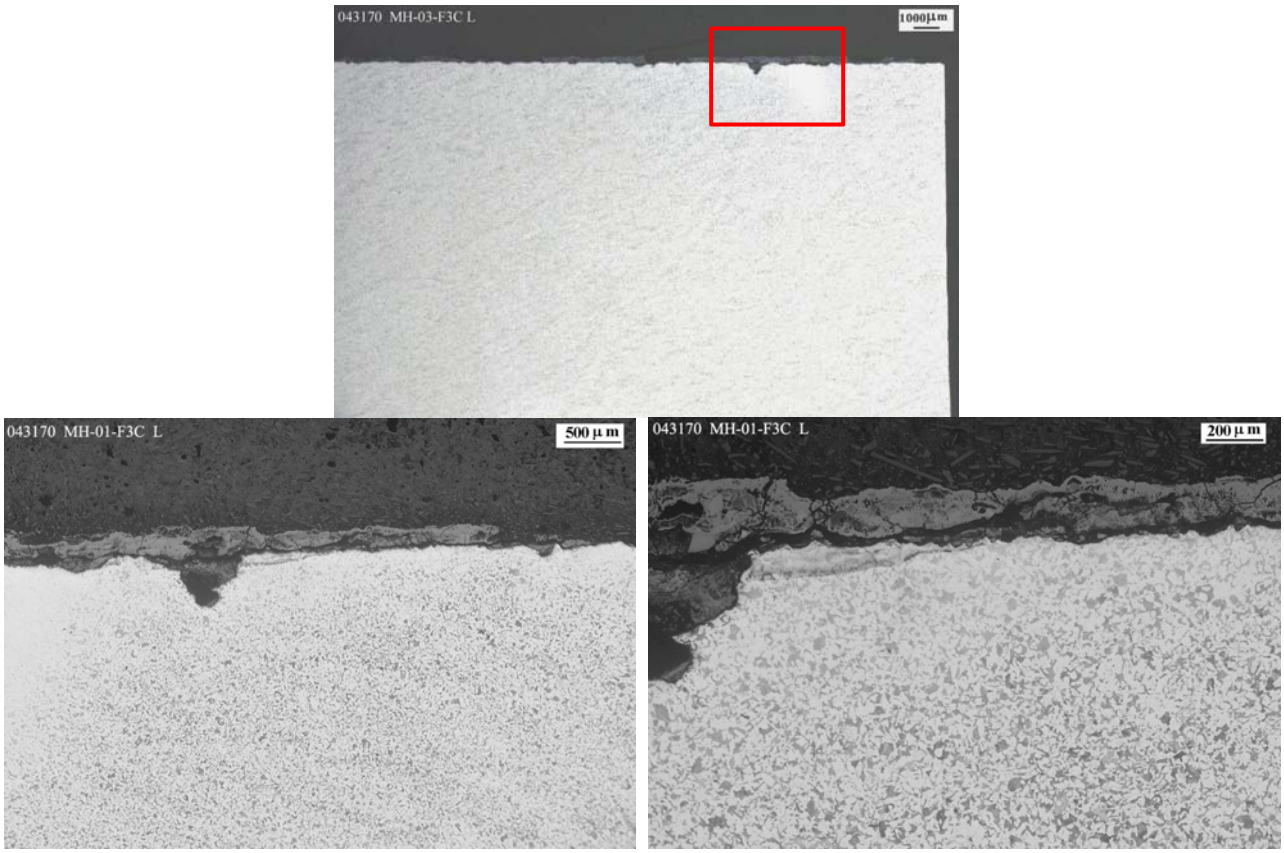

Figure 7.24: Optical micrographs of a longitudinal section of sample ref. MH-01-F3C, with metallographic etching

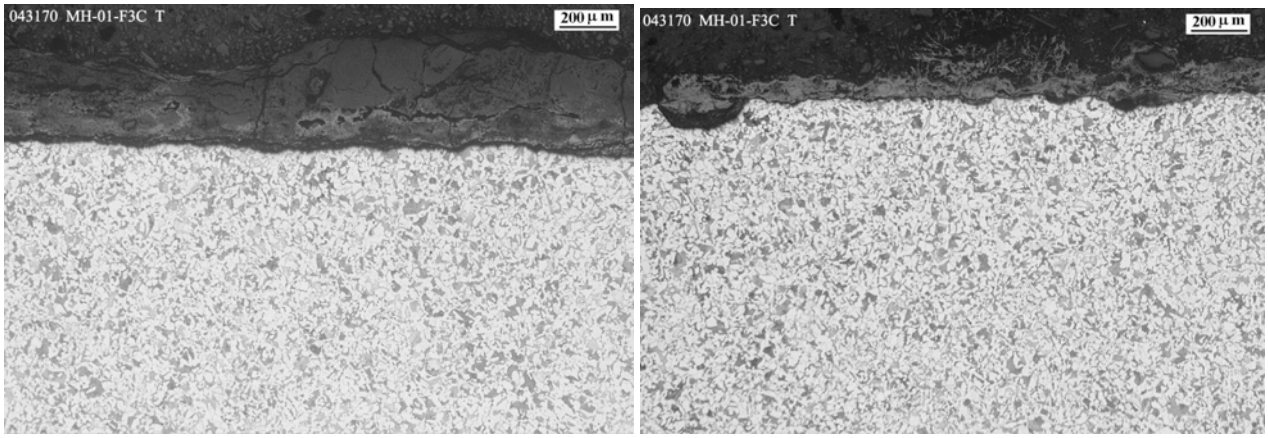

Figure 7.25: Optical micrographs of a transversal section of sample ref. MH-01-F3C, with metallographic etching

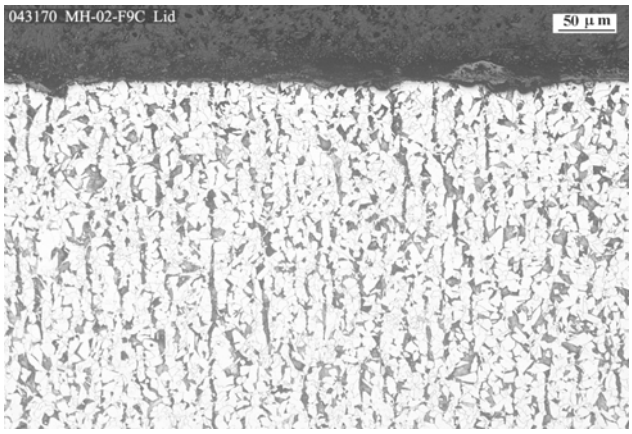

Figure 7.26: Optical micrograph of the external surface of the lid structure of sample ref. MH-02-F9C, with metallographic etching

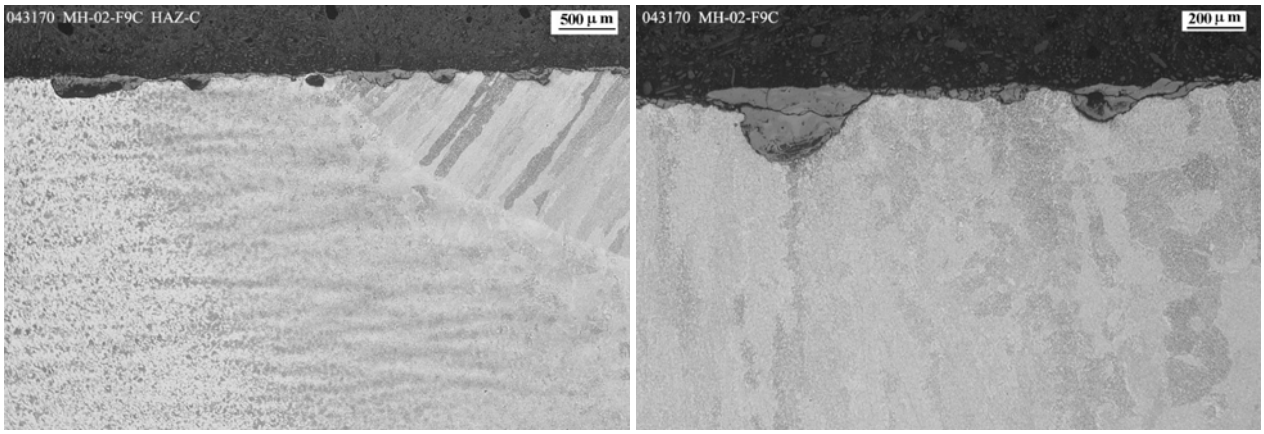

Figure 7.27: Optical micrograph of the external surface of cylinder (right) and HAZ (left) of sample ref. MH-02-F9C, with metallographic etching

8. CONCLUSIONS

The following conclusions can be reached on the basis of the results obtained:

SENSORS

- The corrosion damage observed on sensors ref. SHSD2-01, SHSD2-02 and SHSD2-03 is located on the carbon steel components for anchoring the sensors to the rock and to the liner. It is a generalized extensive corrosion mode, with an important generation of reddish corrosion products that correspond to haematite (Fe_2O_3), principally, and siderite ($FeCO_3$). Magnetite and siderite are commonly generated under reduced oxygen levels.
  No significant differences in the corrosion extension are observed between components close to the rock and those close to the liner.

- The corrosion damage observed in the stainless steel components of the anchoring devices is attributed to the corrosion of carbon or low alloyed steel particles/residues from the welding process. These particles corroded easily.

- No signs of localized or generalized corrosion are observed on the 316 stainless steel tubes sensors. Chemical etching reveals a non-sensitized austenitic microstructure.

- EDS analyses carried out on welded corroded joints close to the rock show a significant presence of sulphur. There is not detected sulphur in such significant way in other zones of the sensors. These joints show also a dendritic skeleton in the weld root. This corrosion morphology is sometimes associated with MIC. This dendritic corrosion can also be seen on chloride induced corrosion phenomena, although in this particular case, no chloride is detected in the analysis of the corrosion products.

    - Chloride is only detected in the EDS analysis carried out on the shallow “pits” observed on stainless steel components of the anchoring devices to the liner. Chloride is usually found in stainless steels in the bottom of pits, where it migrates in order to maintain electroneutrality. The higher chloride content of the bentonite surrounding the liner is probably a consequence of the advance of the wetting front.

- The corrosion damage in the sensors anchoring devices to the rock and liner is probably due to the high humidity, temperature and limited oxygen conditions surrounding these components.
  Although there were no bacteria detected in the bentonite housing the sensors, this corrosion mode cannot be totally discarded for certain areas close to the rock.

BENTONITE

- No viable bacteria were detected in the samples of bentonite surrounding sensors ref. SHSD2-01 and SHSD2-02. This result relates solely to these bentonite samples. Other studies on FEBEX

bentonite have shown the presence of micro-organisms (Bengtsson et al. 2016) at the time of dismantling.

316L STAINLESS STEEL COUPONS

- Corrosion damage observed in stainless steel coupons is localized, mainly manifested as pitting, observed for the four stainless steel coupons, and cracking detected on one base metal coupon, with no generalized corrosion.

- EDS analyses of corrosion products in cracks and pits reveal a quite significant amount of chloride. The 300 series austenitic stainless steels are very sensible to pitting and SCC in chloride containing environments.

- Cracks have a branched morphology with transgranular progression, typical of SCC of stainless steels. This localized corrosion phenomenon develops with the simultaneous interaction of a mechanical stress and a corrosive agent, normally chlorides in the case of stainless steels.

  316L stainless steel shows a non-sensitized austenitic microstructure (intergranular cracking is usually because of a sensitized microstructures). The main factors that influence the rate and severity of cracking are chloride content, oxygen content, temperature, and stress level.

- Pits generated on stainless steel coupons are filled with dark brown corrosion products, forming caps over the pit cavities. This pit morphology is observed in many cases of MIC, but also with non-MIC chloride induced pitting in stainless steel. Moreover, chloride is detected significantly in the pit corrosion products. Pit penetration, at least for the 316L metallographic coupons examined, is not very deep (about 300 microns). It seems that these pits have a slow propagation of the corrosion damage.

- No difference in corrosion behaviour is observed between the welded and the base parent material

- The corrosion damage observed in 316L coupons is mainly due to the relatively high concentration of chloride in the environment. Besides chlorides, the rate and severity of SCC and pitting increases with the oxygen content. Increased oxygen content decreases the critical chloride content for cracking to occur. The presence of corrosion products inside the cracks suggests that cracking has been produced during the partially aerobic periods during the FEBEX test. The effect of oxygen during the dismantling process cannot, however, be totally discarded in the cracking phenomenon

TITANIUM ALLOYS COUPONS

- No corrosion is observed on the titanium coupons examined, neither generalised, nor localized.
- No differences in corrosion behaviour are observed between welded and base material samples.

COPPER AND CUPRONICKEL COUPONS

- General corrosion is the predominant corrosion mode observed in copper and cupronickel coupons. Copper coupons show areas with very slight localized corrosion morphology, with maximum depth penetration of about 100 microns.

- A lesser extension of the generalized corrosion is seen for cupronickel alloys.

- The XRD analyses of the oxide layer generated in copper and cupronickel alloys could correspond to the molecular cuprite Cu_2O.

- A quite significant amount of chloride is detected in all the corrosion products examined.

LINER

- Liner sections ref. ML45 and ML52 show a non-uniform generalized corrosion, with a higher corrosion extension on section ML52. No localized corrosion, such as pitting or cracks, is detected.

- Little corrosion penetration is shown in the metallographic study. Thickness losses of 0.5-0.6 mm are found for section ML52 -the initial wall thickness for the liner was about 15 mm-.

- Corrosion products are mainly constituted by iron oxides and iron carbonates. A significant chloride peak is detected in all the EDS analyses carried out on the corrosion products.

- Availability of moisture, oxygen, and to a lesser extent, chloride, are responsible for the corrosion generated on the carbon steel liner sections.

HEATER

- Uniform generalized corrosion is the predominant corrosion mode observed for the heater. No pitting or other kind of localized corrosion is detected in the visual inspection. A higher extension of the general corrosion is observed in the front part of the heater. In this last zone, the metallographic examination shows areas with more localized corrosion morphology, with maximum penetration depth of 400 microns.

- The two lid-cylinder welded joints at the top and back side of the heater show a good condition.

- Corrosion products are mainly constituted by iron oxides associated to akaganeite (Fe3+ (O, OH, Cl). Chloride is detected in almost all the corrosion products analysed on the surface of the heater.

REFERENCES

Bárcena, I., García-Siñeriz, J.-L..(2015): FEBEX-DP (GTS) Full Dismantling Test Plan R7. Nagra Arbeitsbericht NAB 15-014

Bengtsson et al. (2016). FEBEX-DP: Microbiology in the FEBEX experiment. Nagra Arbeitsbericht NAB 16-015 (in prep.)

Kober, F.(2015): FEBEX-DP Sample Log Book. Nagra Aktennotiz. AN 15-578.

Kober, F.(2015): FEBEX-DP Summary of Extra Reports (1-13). Nagra Aktennotiz. AN 15-619.

ANNEX I: Photographs of the samples upon reception at TECNALIA

SAMPLES RECEIVED ON 25/08/2015

SAMPLES CODE	PHOTOGRAPHS ON RECEPTION	COMMENTS
BENTONITE + SENSORS		
BM-S-54-2 **S-S-54-14A** SHSD2-01	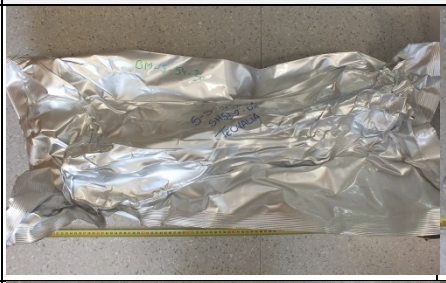 	- Double aluminium foil. - Bentonite included - No vacuum loss
BM-S-54-3 **S-S-54-15A** SHSD2-02	 	- Double aluminium foil. - Bentonite included - No vacuum loss.
SHSD2-03 **S-S-54-15**	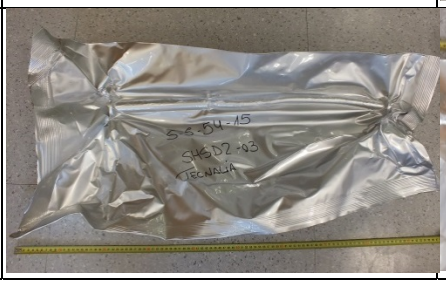 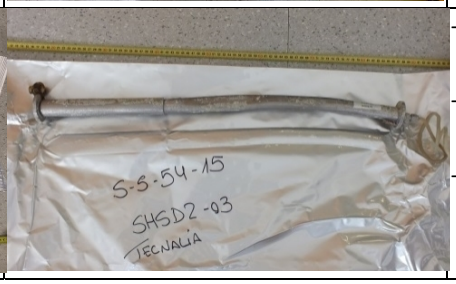	- Single aluminium foil. - No bentonite inside. - No vacuum loss.

LINER			
ML-52-1			- Double aluminium foil. - No vacuum loss
ML-52-2			- Double aluminium foil. - No vacuum loss
ML-52-3	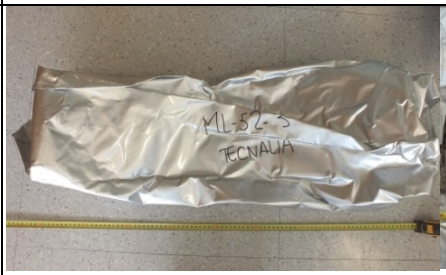		- Double aluminium foil. - No vacuum loss
ML-52-4			- Double aluminium foil. - No vacuum loss
ML-45-1			- Double aluminium foil. - No vacuum loss
ML-45-2			- Double aluminium foil. - No vacuum loss

ML-45-3			Double aluminium foil. No vacuum loss
ML-45-4			Double aluminium foil. No vacuum loss

SAMPLES RECEIVED ON 21/03/2016

SAMPLES CODE	PHOTOGRAPHS ON RECEPTION		COMMENTS
CORROSION COUPONS			
Coupons 2A M-S-48-2			- External aluminum foil + 2 plastic bags - Bentonite included - No vacuum loss
Coupons 3A M-S-48-3			- External aluminum foil + 2 plastic bags - No vacuum loss .
Coupons 4A M-S-48-4			- External aluminum foil + 2 plastic bags - Bentonite included - No vacuum loss